AED R-3440
Issued: April 21, 1969

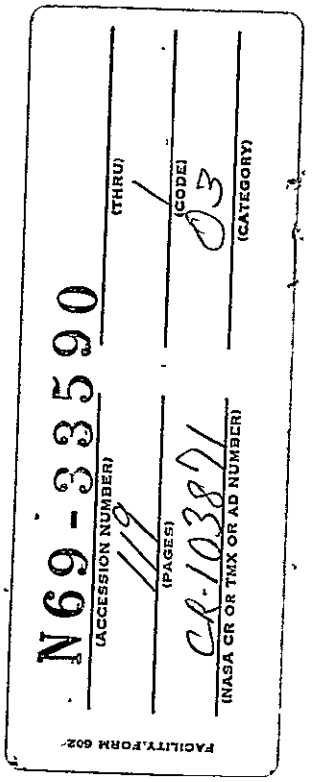

Final Report: Action Of Lithium In Radiation-Hardened Silicon Solar Cells

Prepared for:
Jet Propulsion Laboratory
California Institute of Technology
Pasadena, California
In Fulfillment of:
Contract No. 952249
April 23, 1968 through April 21, 1969

RCA

RCA | Defense Electronic Products
Astro Electronics Division | Princeton, New Jersey

AED R-3440
Issued: April 21, 1969

Final Report: Action Of Lithium In Radiation-Hardened Silicon Solar Cells

Prepared for:
Jet Propulsion Laboratory
California Institute of Technology
Pasadena, California
In Fulfillment of:
Contract No. 952249
April 23, 1968 through April 21, 1969

By

G.J. Brucker, T.J. Faith, and A.G. Holmes-Siedle

RCA | Defense Electronic Products
Astro Electronics Division | Princeton, New Jersey

This work was performed for the Jet Propulsion Laboratory, California Institute of Technology, as sponsored by the National Aeronautics and Space Administration under Contract NAS7-100.

NOTICE

This report contains information prepared by the Astro-Electronics Division of RCA under JPL subcontract. Its content is not necessarily endorsed by the Jet Propulsion Laboratory, California Institute of Technology, or the National Aeronautics and Space Administration.

ABSTRACT

This is the Final Report on a program to study and analyze the action of lithium in producing a recovery of radiation damage in silicon solar cells. This program had technical continuity with the work performed for NASA on Contract No. NAS 5-10239. The eventual goal of this effort is to understand the recovery mechanism so that realistic predictions of solar-cell performance can be developed and optimum designs of lithium cells for space use can be specified.

The test vehicles being used for this work are (1) small-area solar-cell model devices, (2) a group of solar cells supplied by NASA on the earlier contract, (3) solar cells supplied by JPL, and (4) silicon bars, usually in the "Hall-bar" configuration. The source of particle irradiation used was a 1-MeV electron beam, produced by the RCA Laboratories Van de Graaff generator.

The work performed on the present contract, by pursuing basic material studies and device studies in parallel, has produced significant advances in the understanding of the defect interactions, dynamics, and general prospects of lithium solar cells. The dynamics of lithium in silicon has been studied under conditions analogous to those which would be experienced in a practical lithium solar-cell array in a high-flux trapped space-radiation situation, namely in orbit near Earth, Jupiter or any other planet.

As a result of this, and the work of other contractors funded by JPL in 1968-69, the general confidence that we know what is happening in lithium cells has increased in many ways in the last year.

Tests on GFE cells irradiated to fluences from 10^{14} to 10^{16} e/cm^2 indicates that, to obtain good long-term stability in cells made from silicon of low oxygen content, the lithium density should be made as low as is compatible with maximum cell recovery for the fluence applied to the cells. Cells with high lithium concentration and steep gradients of lithium density near the junction show gross lithium motion near the junction over $\approx$ 1 year. Cells of this type have redegraded as much as 35 percent eleven months after bombardment to 10^{14} e/cm^2.

Redegradation in power output is due primarily to curve-shape changes and decreases in open-circuit voltage. Short-circuit current is, in general, constant during redegradation. Cells with smaller lithium-density gradient show better stability both before bombardment and after 10^{14} e/cm^2.

Preliminary measurements on Float-Zone cells indicate that the lithium-diffusion constant in these cells increases with increasing distance from the junction.

Hall-coefficient and resistivity measurements have been used to investigate the crystal growth and irradiation-temperature dependence of the introduction rate and room-temperature annealing of carrier-removal defects in lithium-doped silicon. Initial resistivity of the quartz-crucible silicon was 30 ohm-cm and of the float-zone silicon was $\geq$ 1500 ohm-cm. The silicon was doped with lithium to a density of 2×10^{16} cm^{-3}. Irradiations were carried out with 1-MeV electrons at bombardment temperatures ranging from 79°K to 280°K. Specimens were annealed to 200°K thereby separating intrinsic and impurity defects. Introduction rates of carrier-removal defects were exponentially dependent on the reciprocal of temperature for both types of crystal, but the slopes and limiting temperature values differed. The slope of the carrier-removal rate versus reciprocal temperature curve is 0.055 eV in crucible silicon and 0.09 eV in zone silicon. The temperature dependence was not consistent with a simple charge-state-dependent probability of interstitial-vacancy dissociation and impurity-vacancy trapping. Carrier concentrations measured at or near room temperature were increased in zone silicon, but were decreased in crucible silicon by isothermal annealing at room temperature. Crucible-silicon samples annealed to 373°K for 10 minutes exhibited complete recovery of mobility. Complete recovery of mobility in float-zone silicon took place in an annealing time $\leq$ 17 hours at room temperature. The time constant of the annealing kinetics at room temperature is consistent with the smaller lithium diffusion constant observed in oxygen-rich silicon compared to the lithium diffusion constant in oxygen-lean silicon. The mechanism of room-temperature annealing is attributed to neutralization of carrier-removal defects by lithium interaction in crucible silicon, and by both lithium interaction and defect dissociation in zone silicon. Results suggest that a lithium-oxygen-vacancy complex is produced by radiation in quartz-crucible grown silicon and a lithium-vacancy complex in float-zone refined silicon. The LiO-V defect is tightly bound compared to the oxygen-free Li-V defect. Measurements of carrier density as a function of reciprocal temperature located defect-energy levels near E_c-0.18 eV and E_c-0.13 eV, in irradiated-crucible silicon. The first defect level is the A-center and the latter is the reverse annealing center which is formed at a temperature of 250°K. A defect level located near E_c-0.08 eV formed after crucible-silicon samples were annealed at room temperature and lithium interacted with radiation defects.

The work during the latter part of the reporting period consisted of measurement of the physical properties and photovoltaic performance of a large number of JPL-furnished cells before irradiation and after recent irradiation to fluences of 1×10^{14}, 5×10^{14}, or 3×10^{15} e/cm^2. A total of thirty-two crucible-grown cells, irradiated to 1×10^{14} e/cm^2, have suffered no redegradation in a period extending to 69 days after irradiation. All except five cells (Lot C2) have shown significant recovery, one group of five having higher power than n/p control cells irradiated to the same level. This group of cells (Lot C2) were initially doped with antimony before diffusion with lithium. Analysis of doping density profiles near the depletion region indicates that there may be no lithium in this region. Float-Zone,

Quartz-Crucible, and Lopex cells irradiated more recently showed no redegradation in short-circuit current over a period extending to 11 days after irradiation. However, a Lot of Lopex cells with very heavy lithium doping (Lot T3) subsequently suffered short-circuit current redegradation of approximately 5 percent in the period from the 20th to the 60th day after irradiation. Measurements on five batches of Float-Zone cells (Lot C4) with different lithium diffusion and redistribution schedules indicate a decrease in lithium density and increases in minority-carrier diffusion length and photovoltaic response with increasing redistribution time.

The best possibility for stable, high performance, highly radiation-resistant lithium cells is (1) to fabricate the cells from silicon of moderate resistivity (phosphorus-doped ~ 10 ohm-cm), (2) to diffuse lithium into the cell with a concentration of 3 to 10 $\times$ $10^{14}/cm^3$ located at the edge of the depletion region, and (3) to distribute the lithium near the junction such that the density gradient is $\approx 10^{19}$ cm^{-4}. The choice of oxygen content will depend on the rate of recovery required by the space mission in question. Two preprints of technical papers arising from the project are included as appendices. Appendix A appeared in the Proceedings of the 1968 IEEE Photovoltaic Specialists' Conference. Appendix B will appear in Physical Review in Mid-1969. Appendix C collects all data on the lithium cells studied during this project.

PREFACE

This is the Final Report on a program to study the "Action of Lithium in Radiation-Hardened Silicon Solar Cells." This report was prepared under Contract No. 952249 for Jet Propulsion Laboratory, Pasadena, California, by the Astro-Electronics Division of RCA, Princeton, New Jersey. The period of performance covered by this report is from April 23, 1968 to April 21, 1969. The work reported here was conducted by the Radiation Effects group, a part of the Technology Development group of the Astro-Electronics Division, Manager, Martin Wolf. The Technology Development group is located at the RCA Space Center. The Project Supervisor was Dr. A. G. Holmes-Siedle and the Project Scientist was Dr. G. J. Brucker. The Technical Monitor of the program was Mr. Paul Berman of JPL.

TABLE OF CONTENTS

LIST OF ILLUSTRATIONS

LIST OF ILLUSTRATIONS (Continued)

LIST OF TABLES

SECTION I
INTRODUCTION

A. GENERAL

It has been shown that, at room temperature, electron, proton, and neutron-irradiated silicon solar cells spontaneously recover their electrical outputs following irradiation (Reference 1). Initially, the loss of electrical output is due to degradation of minority-carrier lifetime. The mobile lithium ion moves towards and combines with a defect-impurity complex, thereby changing its electrical properties. In solar cells, the interaction of lithium with radiation-induced defects ultimately produces a defect complex which appears to have little or no effect on the minority-carrier lifetime, the result being a near complete restoration of cell efficiency.

The contract effort reported here represents an experimental investigation of this phenomenon, by means of examining several of the physical properties of lithium-containing silicon bars and of p-on-n silicon solar-cells and by a study of the processes that occur in these devices after irradiation. The objectives of the effort are to identify the parameters which effect the recovery and long-term stability characteristics of the solar cell structure and to generate information which will lead to the optimization of these parameters. The eventual goal is to exploit this phenomenon for the production of solar cells for the space environment in quantity. In this direction, it is anticipated that (1) realistic predictions of lithium-cell performance can ultimately be developed, and (2) optimum designs of lithium cells for space use can then be specified.

B. TECHNICAL APPROACH

Stated briefly, the approach to the objectives involves the testing of bulk samples as well as government furnished (GFE)[1] solar-cells and in-house fabricated test-diodes[2]. Experiments on bulk samples include Hall and resistivity measurements taken as functions of (1) 1-MeV electron fluence,

---

[1] Government Furnished Equipment (by NASA under Contract No. NAS5-10239 and JPL under this contract).

[2] Test vehicles similar to solar cells in all but photovoltaic response, fabricated to be compatible with experiments which appear particularly promising in terms of information yield as well as the experiments which are regularly performed in the course of the work.

(2) sample temperatures during irradiation, and (3) isochronal anneals. Correlations of these tests have been made wherever possible with measurements on solar-cells and test-diodes. These measurements include minority-carrier diffusion length versus (1) fluence, (2) temperature, and (3) annealing schedule; photovoltaic I-V characteristics; and reverse-bias capacitance measurements. In addition, stability tests are being continued on test-diodes and solar-cells with post-irradiation histories dating back as far as December 1966.

C. SUMMARY OF PRECEDING WORK

A brief history is given here of the recent work performed on a predecessor contract[3] for purposes of continuity, and to provide the reader with a better understanding of the current technical approach, its problems and its objectives.

In the work of 1967 - 1968, in addition to continuing and extending a series of long-term stability tests on GFE[1] cells to in-house fabricated test-diodes[2] and to a new group of GFE[1] cells, extensive measurements of cell capacitance were made over a wide range of reverse biases. These measurements, which yield donor-density vs. distance from the junction, uncovered large lithium density gradients ($\sim 10^{19}$ cm^{-4}) near the junction and extending ≥ 10 μm from the junction. This gradient sets up a large internal electric field (> 100 V/cm near the junction edge) thereby creating a field-aided diffusion situation for minority-carriers. This effect invalidates the concept of diffusion length for small lifetimes, i.e., where the electric field effect is significant over a large fraction of the current-collection volume. This is the case after irradiation to fluences of the order 10^{15} to 10^{16} e/cm^2, making application of Waite's theory (Reference 2) very difficult. Accordingly, in the past year, some kinetic studies of damage recovery were made at lower fluences, in the range 10^{13} to 10^{14} e/cm^2. Waite's theory which reduces to a first-order kinetic equation at these fluences, was shown to describe the experimental recovery curves adequately for a large number of cells. These cells and cells irradiated to $\sim 10^{15}$ e/cm^2, as well as unirradiated cells, have since been undergoing long-term monitoring of their characteristics for (1) stability, (2) minority-carrier diffusion length, and (3) photovoltaic I-V characteristics. These stability tests have continued into the present contract and it is planned that they will continue throughout the duration of this effort. The cumulative results are presented and discussed in this report.

---

[3] "Radiation Damage in Lithium-Containing Solar Cells," Contract No. NAS5-10239, Performed for the National Aeronautics and Space Administration, Goddard Space Flight Center, Greenbelt, Md., Final Rept. Issued July 1968.

In 1967-1968, the first known used was made of capacitance techniques for direct measurement of the lithium-diffusion constant in a solar cell (Reference 3). Results obtained by using this technique have indicated the possibility that the lithium-diffusion constant at the edge of the junction, where the measurements are made, is often lower than that in the bulk of the current-collection volume. To clarify this question, which will have significant consequences in the understanding of cell stability, an attempt was made to probe further into the base region of the cell by use of the capacitance method.

In addition to the fabrication of many test diodes, some effort in 1967-1968 was directed toward modifying an existing apparatus for Hall measurements at liquid-nitrogen temperature and to the fabrication, lithium diffusion, and contacting of appropriate Hall samples. The purpose of these measurements is to obtain information on the defect formation and annealing processes occurring in the lithium cell and the band-gap energy levels occurring in these processes. Actual Hall measurements were started toward the end of the preceding contract.

SECTION II

TEST-DIODES

A. TEST-DIODE FABRICATION

In 1966 through 1968 under Contract No. NAS5-10239, several dozen test-diodes, both lithium-containing and non-lithium-containing "control" devices, were fabricated and subjected to irradiation and electrical measurements (Reference 3). In addition to continuing experiments on these diodes, a new set of test-diodes was fabricated under the present contract. The new group of devices will provide a close model of the junction structure used in solar cells. They are well-adapted for diffusion-length measurements at temperatures ranging from liquid-nitrogen to room temperature. The diodes, as shown in Figure 1, were made from high-resistivity (nominal 1900 ohm-cm) n-type Float-Zone silicon. The use of this material assures that the principal electrically active impurity in the base region is lithium. A p-n junction is made by diffusion of boron from a deposited 3000Å layer of 10-percent borosilicate glass at 1150°C for 15 minutes.

During lithium diffusion, the wafers were immersed in a 1-percent lithium-tin bath. Two different lithium-diffusion schedules have been used on different wafers. These are (a) an ~ 70-hour diffusion at 325°C and (b) a 2-hour diffusion at 375°C. Four-point probe measurements (Reference 5) on the back surfaces of each wafer indicated a resistivity of ≈ 1.5 ohm-cm, which is equivalent to a bulk lithium density of $\approx 4 \times 10^{15}$ cm^{-3}. The ≈ 0.025-inch thick wafers were cut into four 0.25×0.40-inch cells and solderable contacts were applied. The base contact was an alloyed Au-Sb contact; the contact to the p-skin was an ~3000Å chrome-gold evaporated layer. The cells were soldered onto a 0.020-inch thick metallized boron-nitride wafer. The boron-nitride wafer is soldered onto a cold finger which has been designed to fit onto the beam exit of the Van de Graaff generator. This apparatus permits capacitance, diffusion-length, and possibly pulsed-lifetime measurements on test-diodes and solar-cells as a function of electron fluence and temperature. The cold finger is described in the following paragraph.

B. VACUUM COLD-FINGER CONSTRUCTION

A cold-finger apparatus, for measurement of test-diode and cell parameters at temperatures ranging down to that of liquid nitrogren, has been designed to fit onto the electron-beam exit flange of the Van de Graaff generator. Briefly, the

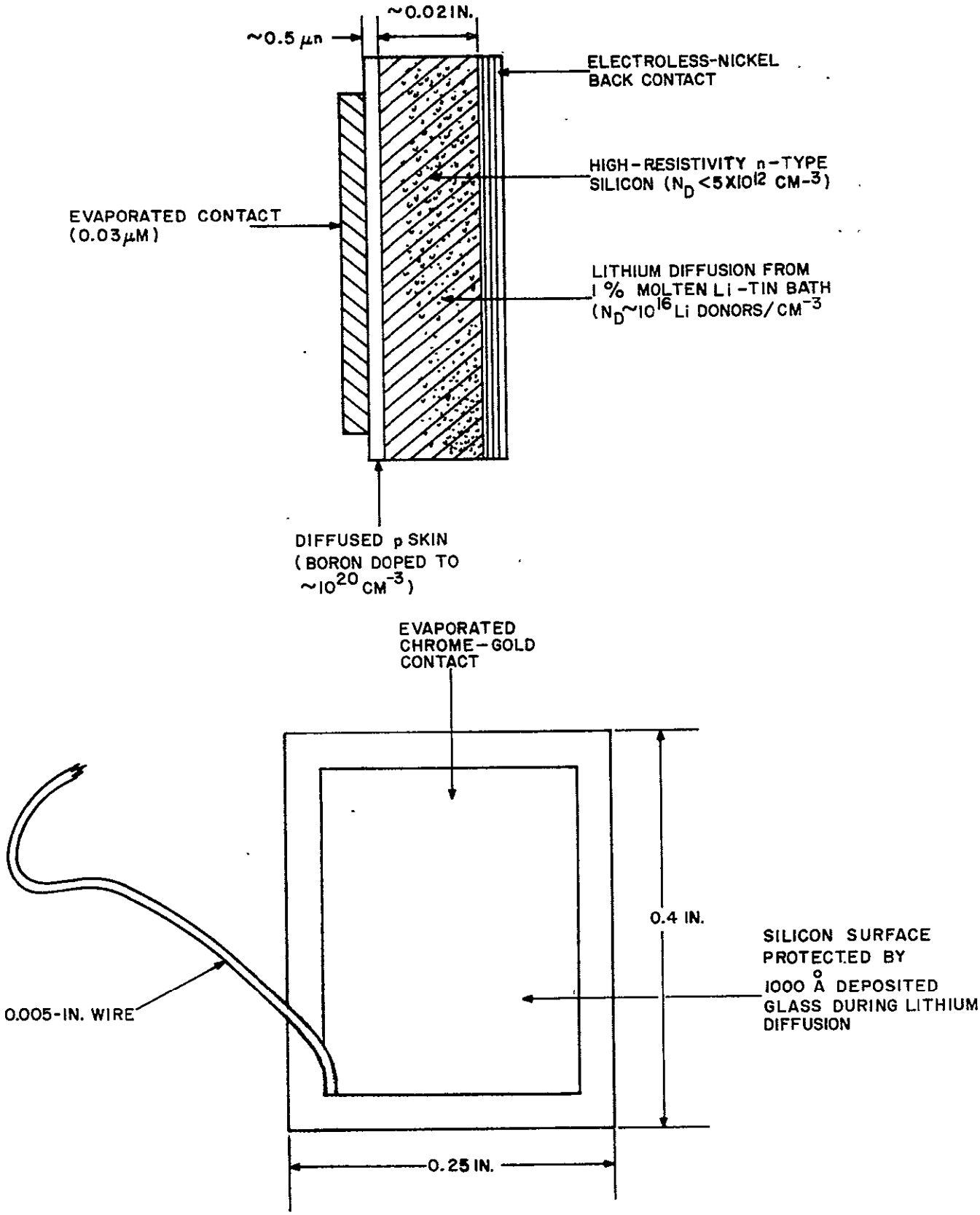

Figure 1. Construction of Test-Diode

apparatus, shown schematically in Figure 2, consists of a cold finger, F, enclosed in a vacuum-tight chamber, C. The finger consists of a rectangular 1- by 2-inch waveguide, W, 13-3/4 inches long; 12 inches have been milled off each of three sides, leaving a 1-3/4- by 1-inch extension which serves as the cold finger. Cells or test-diodes, D, are mounted at the end of this finger via the metallized boron-nitride wafer described in Section III. Metallized Alundum heaters are mounted on the back of the finger. The waveguide is closed by a brass plug, P, at either end; at the top, a stainless-steel tube, T, runs from the plug to a flange, F_1. Liquid nitrogen is poured into the waveguide through T_1. The flange has electrical feed-throughs for heater, cell, and thermocouple leads and a mechanical feed-through that enables vertical movement of a 0.012-inch aluminum moderator, M_1, used in electron-voltaic diffusion-length measurements. The cold finger fits into a larger, 3- by 1-1/2-inch waveguide; a vacuum (O-ring) seal is made between W_1 and W_2, the latter being the flange on the larger waveguide. The large waveguide contains a Faraday cup, FC, for electron flux measurements, and a mechanical feedthrough, M_2, which enables horizontal movement of a 0.095-inch aluminum plate which shields the cell from the beam when desired. A tube, T_2, connects with the vacuum pump. The entire assembly is attached to the beam exit flange through a mating flange, F_2, on the large waveguide. A hole in the shape of a "T" was milled in the large waveguide near the center of F_2 to permit access of the electron beam to the sample and Faraday-cup areas. Vaccum seals to the beam exit flange are made by two neoprene gaskets and a 0.001-inch aluminum window. The apparatus was tested at liquid-nitrogen temperature and was found to operate satisfactorily at this temperature.

C. TEST-DIODE EXPERIMENTS

Because of financial limitations, low-temperature experiments on the test-diodes were temporarily deferred. However, room-temperature experiments were performed on a set of lithium-doped test-diodes made from Lopex* and Float-Zone silicon with starting resistivities of 1, 10, and 30 ohm-cm. The diodes were irradiated to a fluence of 1×10^{13} e/cm^2 after which their minority-carrier diffusion lengths (Reference 5) were monitored as a function of time. This type of experiment had been performed previously (References 6 and 7). This previous work showed that the recovery kinetics are best described by a formulation of Waite (Reference 2) which reduces to first order kinetics for low electron fluences. The purpose of the present experiments was to search for differences in recovery kinetics between cells with different starting resistivity, i.e., with different phosphorus doping.

---

*Trademark of Texas Instruments, Inc.

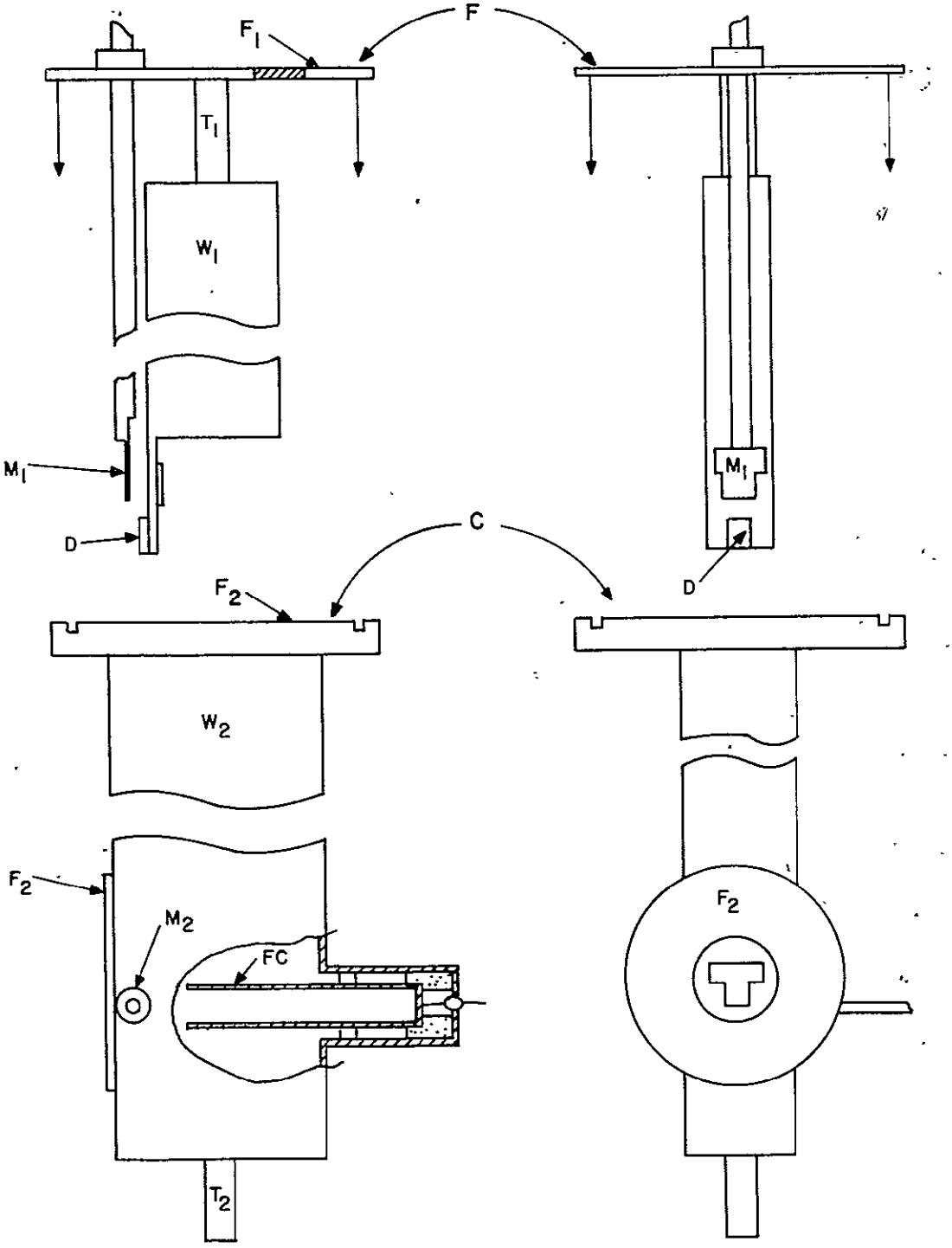

Figure 2. Cold-Finger Apparatus, Schematic Diagram

The results of the experiments confirmed the first order nature of the recovery kinetics at the low electron fluence of 10^{13} e/cm^2, where the density of radiation-induced defects is much less than the lithium-doping density. This confirmation was obtained from the observed linear increase of the inverse fraction of unannealed defects, $(f_r)^{-1}$, with time after cessation of bombardment. The quantity $(f_r)^{-1}$ is given by:

$$f_r^{-1} = \frac{\frac{1}{L_1^2} - \frac{1}{L_0^2}}{\frac{1}{L_2^2} - \frac{1}{L_0^2}} \qquad (1)$$

where L_0, L_1, and L_2 are the minority-carrier diffusion lengths before bombardment, immediately after bombardment, and at a time, t, after bombardment.

The recovery curves (f_r^{-1} vs time) for all three starting resistivities showed similar behavior. However, slight differences were observed between the high and low starting resistivity cells. This is illustrated in Figure 3, where recovery curves for test-diodes D-2-4 (1 ohm-cm F. Z.) and F-1-2 (30 ohm-cm F. Z.) are given. It is seen that the curve for D-2-4 is approximately linear with a single slope up to $f_r^{-1} \sim 100$ whereas that for F-1-2 "breaks-off" to a shallower slope at $f_r^{-1} \sim 10$. The two linear regions on either side of the break may represent regions in which recovery of different types of centers predominate, for instance: for $1 < f_r^{-1} < 10$ $(P\text{-}V)^- + (Li)^+ \rightarrow$ P-V-Li predominates and for $10 < f_r^{-1}$ $(Li\text{-}V)^- + (Li)^+ \rightarrow$ Li-V-Li predominates. At this point this is only a speculative hypothesis however, and further recovery experiments would be required to establish the significance of these results.

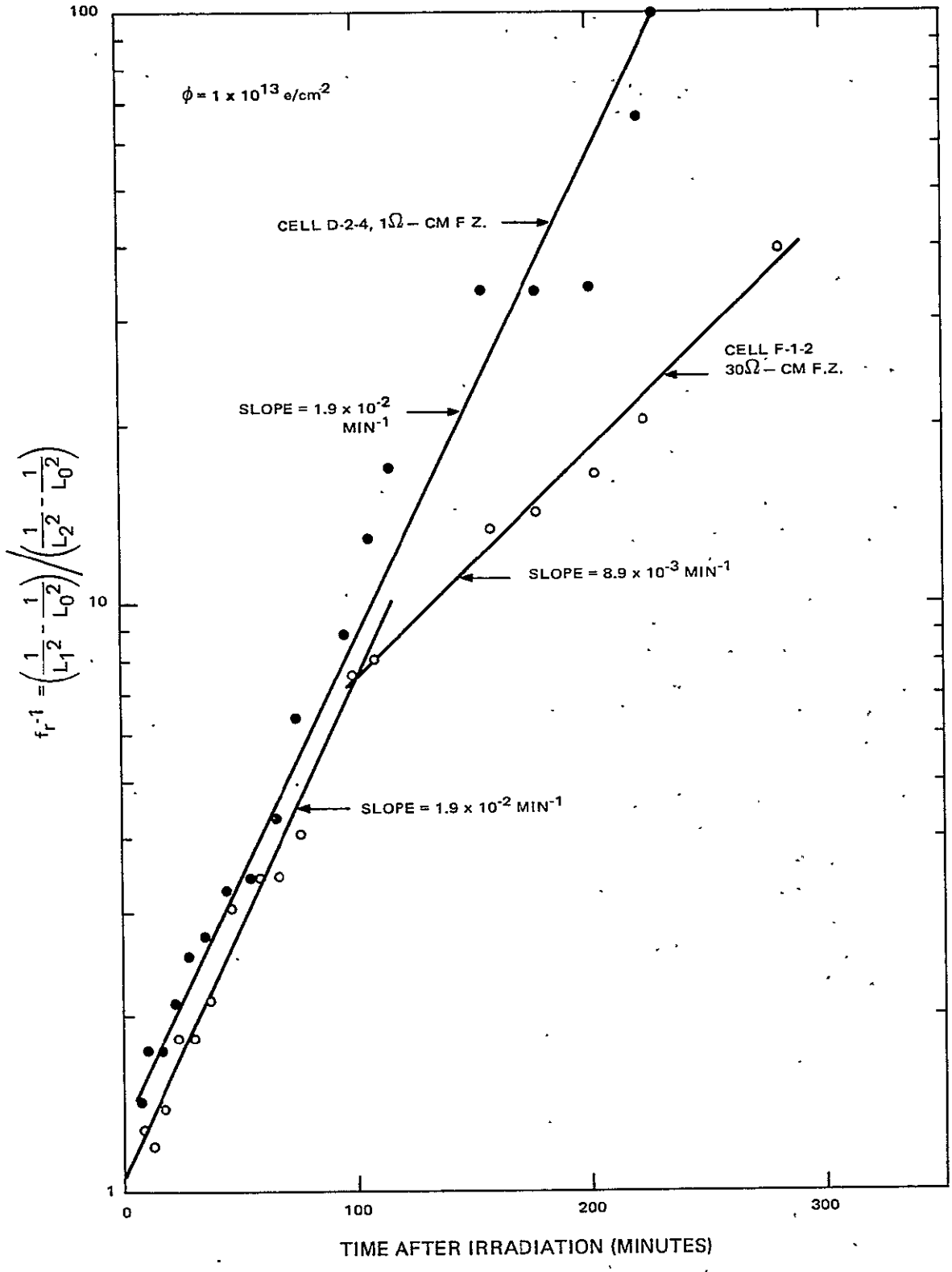

Figure 3. Recovery Curves for Two Test-Diodes Made From Float-Zone Silicon After a Fluence of 1×10^{13} e/cm^2 of 1-Mev Electrons

SECTION III

STABILITY OF NASA-FURNISHED CELLS

A. GENERAL

A large group of lithium-containing p/n silicon solar cells furnished under contract No. NAS5-10239 (Reference 3) had been irradiated in 1967-68 with 1-MeV electrons. Measurements of cell parameters have been made, including photovoltaic I-V characteristics under illumination by a filtered-tungsten source at 100 mW/cm^2 and minority-carrier diffusion length (Reference 5) both before irradiation and at periodic intervals after irradiation. From the results of these and pre-irradiation capacitance measurements, information has been obtained on the stability of irradiated and unirradiated lithium-containing cells over a wide range of cell types and for values of electron fluences ranging from 10^{14} to 10^{16} e/cm^2. As of early 1969, the duration of these tests ranges from 12 to 19 months. Stability tests have been made on unirradiated cells for a period of 16 months. The cells in all the tests, both irradiated and unirradiated, were stored at room temperature, under fluorescent illumination and under open-circuit conditions except for brief intervals (~hours) when photovoltaic, electron-voltaic, or reverse-bias capacitance measurements were being made.

The irradiations of these and all other cells in this report were carried out in air. A vacuum Faraday cup was used to measure the fluence. The electron beam energy as it left the exit window of the machine was 1 MeV. The air path to the cells introduced negligible losses. Thus in all cases, except where otherwise indicated, the electron energy was 1 MeV. During irradiation, the cells were mounted on the periphery of a rotating wheel with 20-cell positions. The wheel has openings at 3 other positions on the periphery through which the beam is transmitted to the Faraday cup positioned behind the wheel for beam current measurement. Beam currents were maintained low enough to keep the sample temperature at approximately 25°C during the irradiation.

B. EXPERIMENTAL TECHNIQUES

Testing was done on cells irradiated at several dates to varying fluences: (1) cells irradiated to 1×10^{16} e/cm^2 in February - March 1967, (2) cells irradiated to 1.4×10^{15} e/cm^2 in November 1967, (3) cells irradiated to 1×10^{14} e/cm^2 in November 1967, and (4) cells irradiated to 1×10^{14} e/cm^2 in March 1968. The main body of results from these experiments was reported

at the Seventh Photovoltaic Specialists Conference (Reference 8). This report is included here as Appendix A. More recently, tests have been continued on the unirradiated cells and on all the electron irradiated cell groups except those irradiated to 1×10^{16} e/cm^2. These results are presented below.

C. EXPERIMENTAL RESULTS

Cells were tested for short-circuit current on the 100 mW/cm^2 tungsten source used in obtaining the results in Appendix A. All the cells tested (including all of the TI cells irradiated to 1.4×10^{15} e/cm^2, all of the TI and He cells irradiated to 1×20^{14} e/cm^2, both unirradiated TI cells, and eight unirradiated He cells) had the same short-circuit current, within experimental error, as in the last reading (October 1968) reported in Appendix A. Testing was then transferred to the (more reproducible) 140 mW/cm^2 source used for tests on the JPL-furnished cells (see Section IV) for photovoltaic characteristic measurements. All of the He cells were seen to remain stable with respect to all photovoltaic properties. The TI cells irradiated to 1.3×10^{15} e/cm^2 had also been stable since October 1968 as had TI 976, one of the unirradiated cells. The other unirradiated cell, TI 979, and the four TI cells irradiated to 1×10^{14} e/cm^2, all of which had previously displayed marked instability relative to open-circuit voltage and p/n junction characteristic, showed only small additional decreases in open-circuit voltage of approximately 3 percent since October 1968. Capacitance-voltage measurements indicate that the lithium donor density profiles in the He cells have also remained stable, and that in the TI cells have stabilized at values approximately equal to those reported for October 1968. In addition, the photovoltaic curve shapes of the TI cells are similar to those obtained in October 1968. The relatively good stability of these TI cells since October (disturbed only by the 3-percent voltage drop), coinciding as it does with the stabilization of the lithium density profile in these cells, substantiates the hypothesis, forwarded in Appendix A, that the instability of the TI cells was in large measure due to the high lithium density gradient and could be correlated with a gross motion of lithium in the junction region of these cells.

In order to illustrate the relationship of junction characteristics to cell redegradation (or degradation) in these particular cells, recently plotted dark I-V curves are given for the unirradiated TI cells in Figure 4. In plotting these curves from the raw dark current, the cell series resistance, as obtained from photovoltaic characteristics (Reference 9), was eliminated. The marked difference in junction characteristics between Ti 976, the stable cell, and TI 979, the unstable cell is immediately evident. TI 976 has a rather high, but uniform empirical A-factor throughout the voltage range, whereas TI 979 has a low A-factor at low voltages but an extremely high A-factor of ≈ 4.8 beginning at ≈ 0.35 V which actually suggests obliteration of the junction at these biases. Similarly, anomalous behavior was observed in some of the JPL-furnished cells of lot T3 to be discussed in Section IV. Since T3 cells also have very high lithium densities, this factor could be a key to the p/n junction behavior.

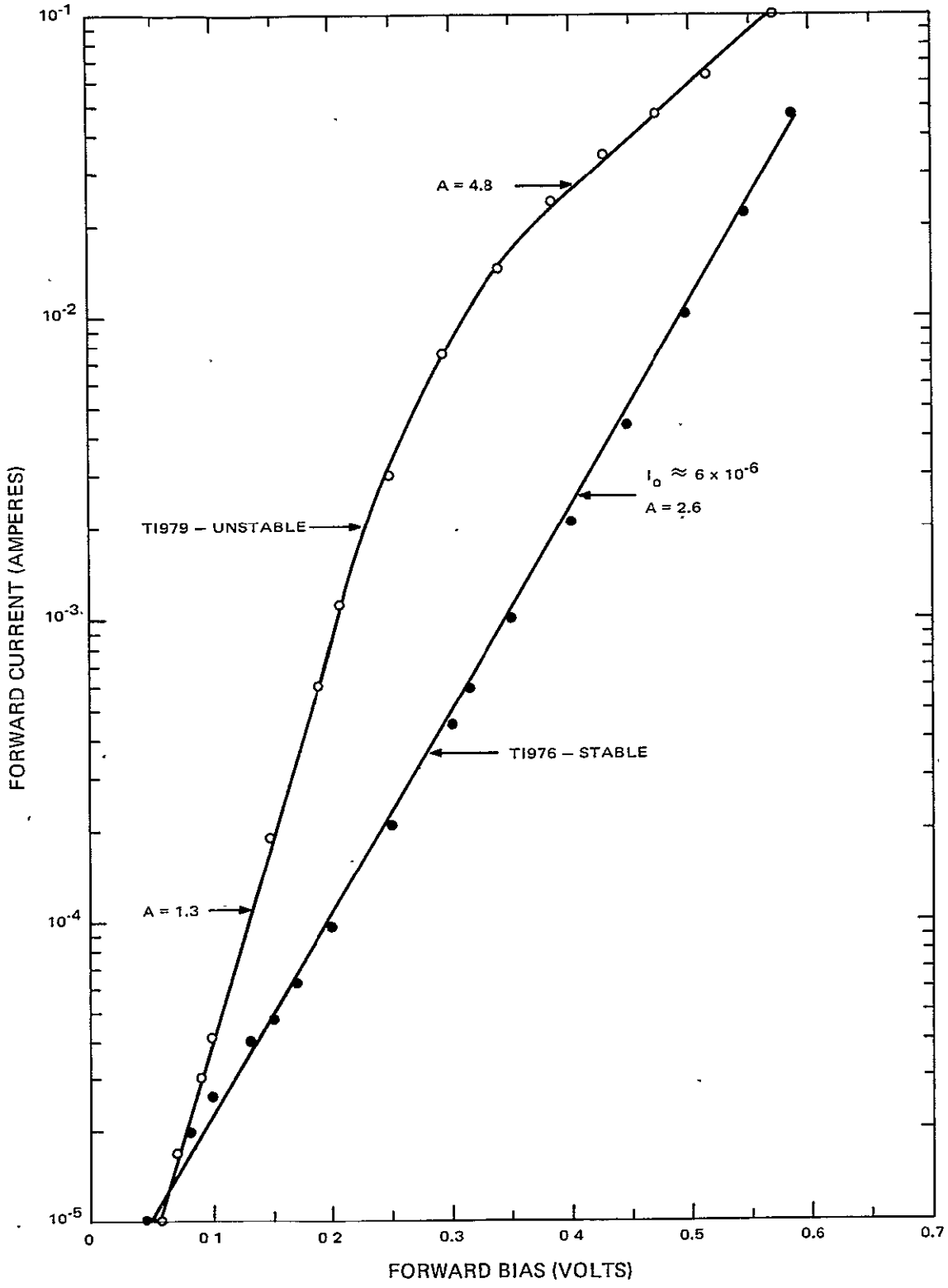

Figure 4. Comparison of p/n Junction Characteristics of a Stable Cell, TI 976, and an Unstable Cell, TI 979

SECTION IV
PERFORMANCE OF JPL-FURNISHED CELLS

A. INTRODUCTION

One objective of the present contract was to evaluate a large number of lithium-diffused p/n solar cells, supplied by JPL. The cells were delivered in four shipments and included lithium cells fabricated by T.I., Heliotek, and Centralabs from a wide variety of silicon stock and with varying lithium introduction conditions. No p/n non-lithium controls were supplied but several competitive 10 ohm-cm n/p commercial solar cells were supplied for comparison purposes. Tests performed on the cells included measurements of photovoltaic response under unfiltered tungsten illumination and air-mass-zero short-circuit current predictions, extrapolated from filter-wheel measurements (Reference 10), measurements of p/n junction characteristics in the dark, reverse-bias capacitance measurements to obtain donor-density profiles, and minority-carrier diffusion-length measurements. The tungsten I-V characteristics were measured with a power density of 140 mW/cm^2 incident on the cell surface. The cell temperature was maintained at 28°C by water and forced-air cooling. The measurements have long-term reproducibility of approximately 2 percent. In addition to the measurements at 140 mW/cm^2, comparative I-V characteristics were frequently taken at a number of light levels. Measurements of this type provide information on cell series resistance and junction characteristics (Reference 9). Cells were irradiated by 1-MeV electrons to one of three fluence values:[5] 1×10^{14}, 5×10^{14} or 3×10^{15} e/cm^2. All irradiations were made at a rate of approximately 3×10^{13} e/cm^2/min. Several cells, however, were left unirradiated, in order to provide a test of whether or not the redegradation phenomenon is induced by radiation.

Measurements after irradiation have consisted mainly of taking I-V characteristics under 140 mW/cm^2 tungsten light. Measurements were repeated periodically, to determine the recovery and stability properties of the test cells. Wherever appropriate, such as when some cell redegradation was observed, multilevel tungsten I-V measurements, and capacitance and dark I-V measurements were made in order to determine the relationship between changes in I-V characteristics and the cell's physical properties. In all the cells of this section the first post-irradiation photovoltaic reading was taken within 30 minutes after irradiation.

---

[5] In one of the irradiations, due to an error, cells were exposed to $\approx 8 \times 10^{14}$ e/cm^2 of ≈ 0.7 MeV electrons instead of the intended 5×10^{14} e/cm^2 of ≈ 0.7 MeV electrons instead of the intended 5×10^{14} e/cm^2 of 1-MeV electrons.

In this section the lithium-containing cells will be discussed in separate paragraphs according to shipment number. However, for convenience of the reader, much of the data on these cells is collected in Appendix C, along with data on cells fabricated as far back as 1965. Each shipment is separated into cell-lots, e.g., shipment No. 1 consists of C1 cells and H1 cells. Cells from each lot are separated into several groups according to the fluence to which they have been exposed. These groups are indicated by the numbers in parentheses, e.g., lot C2 is in three groups; C2 (1) exposed to 1×10^{14} e/cm^2 C2 (2) exposed to 5×10^{14} e/cm^2; and C2 (3) exposed to 3×10^{15} e/cm^2. In discussing cell performance, the average for a given group will be presented. Individual cells will be discussed only when their behavior diverges significantly from that of the group to which they belong. First, however, the properties of a group of 10 ohm-cm n/p cells, which were furnished as controls in shipment No. 3, will be given.

B. TEN OHM-CM n/p CELLS

Table I gives pre-irradiation and post-irradiation values for 10 ohm-cm n/p cells. The table gives values for cells irradiated to 1×10^{14}, 5×10^{14} and 3×10^{15} e/cm^2 of 1 MeV electrons, and in addition, those for cells irradiated to $\approx 8 \times 10^{14}$ e/cm^2 of ≈ 0.7 MeV electrons, and will be referred to as a basis of comparison for all lithium cells in this section. The values averaged over the fourteen n/p cells were: $I_o = 69.5$ mA, $P_o = 28.1$ mW, and $V_o = 553$ mV.

TABLE I. PRE- AND POST-IRRADIATION PHOTOVOLTAIC PERFORMANCE OF n/p CONTROL CELLS

Control Cell	(e/cm^2) ϕ	Pre-irradiation			Post-irradiation			Post-irradiation		
		I_o(mA)	P_o(mW)	V_o(mV)	I(mA)	P(mW)	V(mV)	I/I_o	P/P_o	V/V_o
D-1	$1x10^{14}$	68.9	28.2	553	56.0	21.1	516	0.81	0.75	0.93
D-2	$1x10^{14}$	69.5	28.0	555	56.0	21.1	520	0.81	0.76	0.94
D-3	$1x10^{14}$	71.0	28.4	552	58.3	21.7	518	0.82	0.77	0.93
D-4	$1x10^{14}$	69.1	27.7	553	57.0	21.3	518	0.83	0.77	0.93
D-5	$5x10^{14}$	69.0	28.1	557	48.6	17.7	503	0.71	0.63	0.90
D-6	$5x10^{14}$	73.0	28.2	555	50.1	17.6	500	0.69	0.62	0.90
D-7	$\approx 8x10^{14}$*	69.3	28.6	557	47.7	16.9	487	0.69	0.59	0.87
D-8	$\approx 8x10^{14}$*	71.0	28.1	550	46.5	16.2	487	0.66	0.58	0.88
D-9	$3x10^{15}$	67.3	27.9	551	39.5	13.6	471	0.59	0.49	0.85
D-10	$3x10^{15}$	69.0	28.6	551	40.6	14.0	471	0.59	0.49	0.85
D-11	$3x10^{15}$	68.1	27.7	550	40.5	13.9	471	0.59	0.50	0.86
D-12	$3x10^{15}$	72.0	29.3	555	40.8	13.9	471	0.57	0.47	0.85
D-13	$5x10^{14}$	69.2	27.3	548	50.1	17.9	497	0.72	0.66	0.91
D-14	$5x10^{14}$	67.2	27.4	554	48.4	17.6	500	0.72	0.64	0.90

* ≈0.7 MeV electron

C. CELLS OF SHIPMENT NO. 1

Shipment No. 1 contained twenty Quartz-Crucible cells: ten C1 cells made from ≈ 30 ohm-cm arsenic-doped silicon and ten H1 cells made from > 100 ohm-cm arsenic-doped silicon.

The lithium diffusion and redistribution temperatures and times, the averaged initial lithium concentrations, and the diffusion lengths for these cells are given in Table II. Both C1 and H1 cells were divided into two groups. Groups C1 (1) and H1 (1), each consisting of 8 cells, were irradiated to a fluence of 1×10^{14} e/cm^2 in November 1968; groups C1 (2) and H1 (2), each consisting of 2 cells, were irradiated to a fluence of $\approx 8 \times 10^{14}$ e/cm^2 of ≈ 0.7 MeV electrons in January 1969.

In Table II, N_{LO} is the lithium density (cm^{-3}) at the edge of the depletion region, i.e., approximately 1 μm from the junction, and dN_L/dw is the lithium density gradient (cm^{-4}) giving the increase in lithium density with distance from the depletion edge. N_{LO} is calculated from capacitance measurements taken near zero-bias, and dN_L/dw is obtained from capacitance measurements with the cell at reverse bias. Past measurements on lithium cells (Reference 7) have shown an approximately linear increase in lithium density with distance from the edge of the depletion region, i.e., constant dN_L/dw, for a region extending several microns beyond the depletion edge. This was also found to be the case in the C1 and H1 cells. It is seen from Table II that the shorter lithium diffusion time in C1 cells (5 minutes as compared to 90 minutes in H1 cells), has resulted in a very low lithium density, N_{LO}, and density gradient, dN_L/dw. The C1 cells also have a high pre-bombardment diffusion length, $L_o = 115$ μm, whereas the H1 cells have a much lower value, $L_o = 29$ μm.

TABLE II. GROUPING, IRRADIATION SCHEDULE, PROCESS PARAMETERS, AND LITHIUM CONCENTRATIONS OF C1 AND H1 CELLS

Cell Group	Number of Cells	(e/cm^2)	Li diffusion		Li redistribution		Li concentration		(μm)
		ϕ	Temp(°C)	Time(Min)	Temp(°C)	Time(Min)	N_{LO}(cm^{-3})	dN_L/dw(cm^{-4})	L_o
C1(1)	8	1×10^{14}	450	5	450	40	$<10^{14}$	1×10^{18}	110
C1(2)	2	$\approx 8\times10^{14}$*	450	5	450	40	$<10^{14}$	1×10^{18}	130
H1(1)	8	1×10^{14}	425	90	425	60	5×10^{14}	2×10^{19}	30
H1(2)	2	$\approx 8\times10^{14}$*	425	90	425	60	5×10^{14}	2×10^{19}	20

* ≈0.7 MeV electrons

The average initial output parameters for C1 cells were: I_o = 71.2 mA, P_o = 30.6 mW, and V_o = 600 mV. These are somewhat higher than the values for the n/p cells. The H1 cells have significantly lower pre-irradiation values than the n/p cells, the averages being I_o = 52.6 mA, P_o = 20.7 mW, and V_o = 561 mV. The lower values of short-circuit current are partly due to the lower minority-carrier lifetime in the H1 cells (L_o = 29 μm). However, they are also due in part to the nature of the spectrum of the tungsten light used in the tests. The tungsten source has higher relative intensity toward the red end of the spectrum than does light from the sun which is further shifted to the blue. Since red light has a lower absorption coefficient in silicon than blue light, minority carriers are generated (on the average) deeper in the base region with tungsten light than with sunlight. Thus, cell performance is much more sensitive to diffusion length under tungsten illumination than under sunlight, and the H1 cells will perform better under sunlight than the value of P_o indicates. An attempt was made to overcome this shortcoming of the measurements by calculating air-mass-zero short-circuit current of the cells applying a standard technique (Reference 10) which utilizes measurements of short-circuit current under light from a three-color filter-wheel system. Later, these filter wheel measurements were compared with I-V curves made on lot C4 cells with a solar simulator (Reference 11). The comparison showed the filter wheel value of I_o to be ~ 10 percent below the simulator value. A probable explanation of this discrepancy lies in the previous observation, by Brucker, et al (Reference 12), of a strong injection-level (or light level) dependence of the diffusion length in lithium-containing solar cells. Given the comparison with the simulator, and the fact that the light level in each filter-wheel measurement is more than a factor of 10 below the sunlight level at air-mass-zero, the filter-wheel measurements were concluded to be misleading and were discontinued.

During irradiation to 1×10^{14} e/cm^2, C1(1) cells degraded in performance to: I = 49.0 mA, P = 18.6 mW, and V = 517 mV. Since irradiation, these cells have experienced very slow recovery which has been linear with time. As of the most recent set of readings, 142 days after irradiation I = 54.6 mA, P = 20.6 mW, and V = 528 mV. Thus, after 142 days of recovery the power of C1(1) cells approximately 4 percent below the 21.4 mW averaged power for four n/p cells irradiated to 1×10^{14} e/cm^2.

Cells of group C1(2) degraded to I = 39.0 mA, P = 13.8 mW, and V = 481 mV during irradiation to a fluence of $\approx 8 \times 10^{14}$ e/cm^2 of $\approx$ 0.7 MeV electrons. Since irradiation cell performance has remained constant for 76 days; neither recovery nor redegradation has occurred. The output power of the two n/p cells after the same irradiation is 16.5 mW, substantially above that of the C1(2) cells. The slow recovery in C1(1) cells and the absence of recovery in the more heavily irradiated C1(2) cells is attributed to the low lithium density in these cells and to the high oxygen content of the cells (which lowers the lithium diffusion constant in quartz-crucible cells to a factor of ~ 1000 below that in Float-Zone cells).

The performance parameters of group H1(1) and H1(2) cells as functions of time after irradiation are shown in Figures 5 and 6, respectively. The averaged initial parameters for H1 cells were I_o = 52.6 mA, P_o = 20.9 mW, and V_o = 561 mV. On the right side of the figure the ordinate is given in milliwatts output power and the values for the appropriate n/p cells are indicated. In H1(1) cells a recovery period of ≈ 80 days during which P increases from 15.7 mW to 20.2 mW is followed by a period of stability extending to the most recent reading. The recovered power is, however, still ≈ 6 percent below the value for the 10 ohm-cm n/p cells. In H1(2) cells, recovery continues at 76 days after irradiation although the recovery rate has begun to level off. The present power for H1(2) cells is 14.4 mW, approximately 13 percent below the power of the n/p cells irradiated with them. However, it should be pointed out that the two cells of H1(2) were the lowest of the H1 cells in initial power. The rapid recovery of the H1 cells, as compared with C1 cells is concluded to be due to their heavier lithium doping.

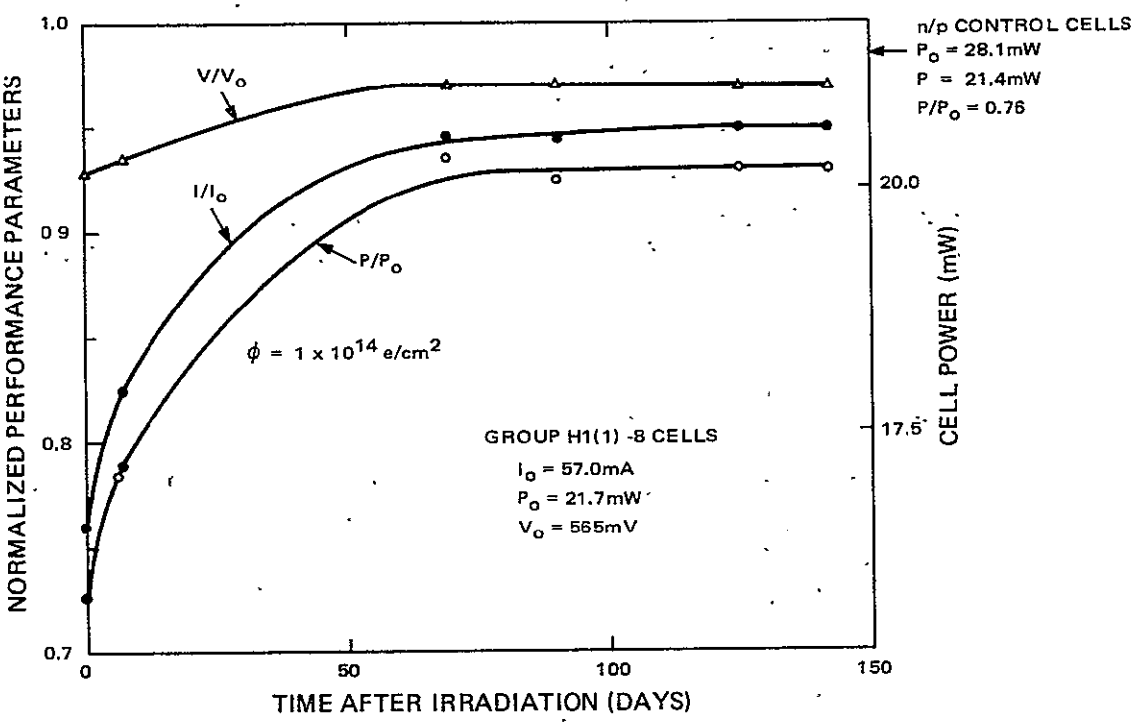

Figure 5. Cell Performance vs. Time After Irradiation to 1×10^{14} e/cm^2 (1-MeV Electrons) - H1(1) Cells

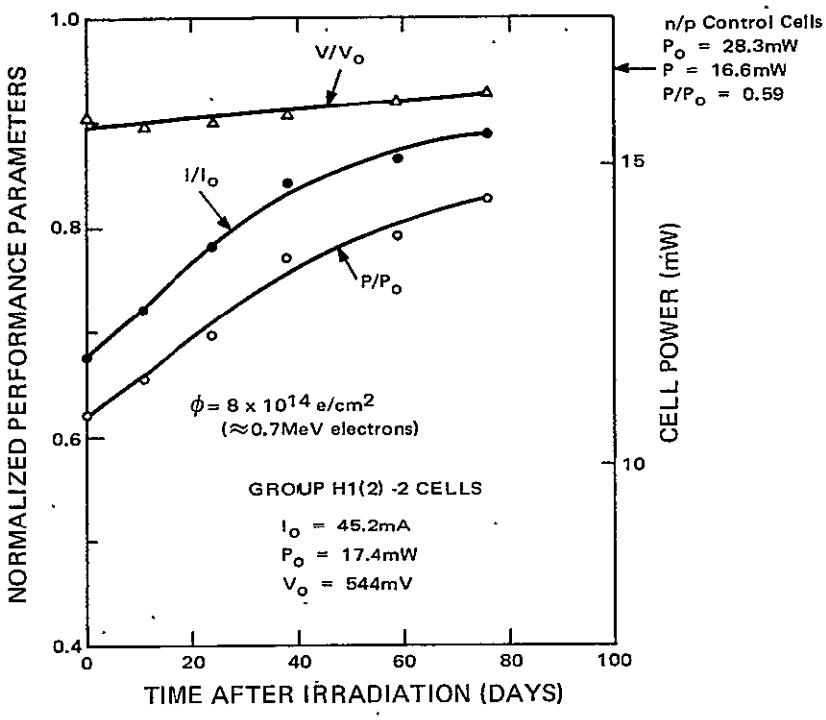

igure 6. Cell Performance vs. Time After Irradiation to 8×10^{14} e/cm^2 of ≈ 0.7 MeV Electrons - H1(2) Cells

D. CELLS OF SHIPMENT NO. 2

Shipment No. 2 contained 30 crucible-grown cells: ten C2 cells made from 5 to 10 ohm-cm, antimony doped silicon, ten H2 cells from 20 ohm-cm phosphorus doped silicon, and ten T2 cells from > 20 ohm-cm phosphorus doped silicon. The lithium diffusion and redistribution temperatures and times and the approximate initial lithium concentrations and minority-carrier diffusion lengths are given in Table III. The C2, H2, and T2 cells are each divided into three groups: (1) cells exposed to 1×10^{14} e/cm^2, (2) cells exposed to 5×10^{14} e/cm^2, and (3) cells exposed to 3×10^{15} e/cm^2.

The lithium density in the C2 cells, as determined by capacitance measurements vs. reverse bias, varied considerably from cell to cell. The cells of lot H2 had densities similar to those of H1 cells, while T2 cells had lower densitites, similar

TABLE III. GROUPING, IRRADIATION SCHEDULE, PROCESS PARAMETERS, AND LITHIUM CONCENTRATIONS OF C2, H2, AND T2 CELLS

Cell Group	Number of Cells	ø (e/cm^2)	Li Diffusion		Li Redistribution		Li Concentration		L_o (μm)
			Temp(°C)	Time(Min)	Temp(°C)	Time(Min)	$N_{LO}(cm^{-3})$	$dN_L/dw(cm^{-4})$	
C2(1)	5	$1x10^{14}$	425	90	425	120	wide range	1.4×10^{18}	80
C2(2)	2	$5x10^{14}$	425	90	425	120	wide range	1.4×10^{18}	80
C2(3)	3	$3x10^{15}$	425	90	425	120	wide range	1.4×10^{18}	80
H2(1)	5	$1x10^{14}$	425	90	425	60	$5x10^{14}$	$1x10^{19}$	40
H2(2)	2	$5x10^{14}$	425	90	425	60	$5x10^{14}$	$1x10^{19}$	40
H2(3)	3	$3x10^{15}$	425	90	425	60	$5x10^{14}$	$1x10^{19}$	40
T2(1)	6	$1x10^{14}$	400	90	400	120	$2x10^{14}$	$1x10^{18}$	90
T2(2)	2	$5x10^{14}$	400	90	400	120	$2x10^{14}$	$1x10^{18}$	90
T2(3)	2	$3x10^{15}$	400	90	400	120	$2x10^{14}$	$1x10^{18}$	90

to those of C1 cells. The average pre-bombardment diffusion lengths were: C2 cells ≈ 80 μm; H2 cells ≈40 μm; and T2 cells ≈ 90 μm.

The C2 cells had good initial parameters: I_o = 67.3 mA, P_o = 29.9 mW, and V_o = 592 mV. During irradiation to 1×10^{14} e/cm^2 cells of group C2(1) degraded to I = 45.8 mA, P = 17.4 mW, and V = 513 mV. During irradiation to 5×10^{14} e/cm^2 C2(2) cells degraded to I = 40.2 mA, P = 14.8 mW, and V = 491 mV. During irradiation to 3×10^{15} e/cm^2 C2(3) cells degraded to I = 30.5 mA, P = 10.7 mW, and V = 455 mV. Since irradiation, the photovoltaic responses of all C2 cells have remained constant and no recovery has occurred. A possible explanation for this puzzling absence of recovery was found in the donor-density profiles of the C2 cells, taken before the cells were irradiated. Such donor-density profiles are shown in Figure 7 for four cells: C3-12, C2-14, C2-15, and C2-17. It is seen that the net donor density at the edge of the depletion region differs from cell to cell, ranging from 4.1×10^{14} cm^{-3} in C2-14 to 15.2×10^{14} cm^{-3} in C2-12. However, in all four cells the density gradient is the same, namely, $1.4 \times 10^{18} cm^{-4}$. Equal gradients in cells with different densities at the junction edge is contradictory to our previous experience in lithium cells. In general, cells with high density have steep gradient, those with lower density have shallower gradient (Reference 7). For example, in H1 cells, H1-7 had $N_{LO} = 8.1 \times 10^{14}$ cm^{-3} and $dN_L/dw = 3.2 \times 10^{19}$ cm^{-4} whereas H1-26 had $N_{LO} = 4.8 \times 10^{14}$ cm^{-3} and $dN_L/dw = 0.8 \times 10^{19}$ cm^{-4}. We, therefore, suggest that the cell-to-cell variation in density in C2 cells is due rather to cell-to-cell variation in the starting antimony doping than to lithium doping and that the density gradient is due to the tail of the boron distribution from the p-doped skin. This explanation implies that very little, if any,

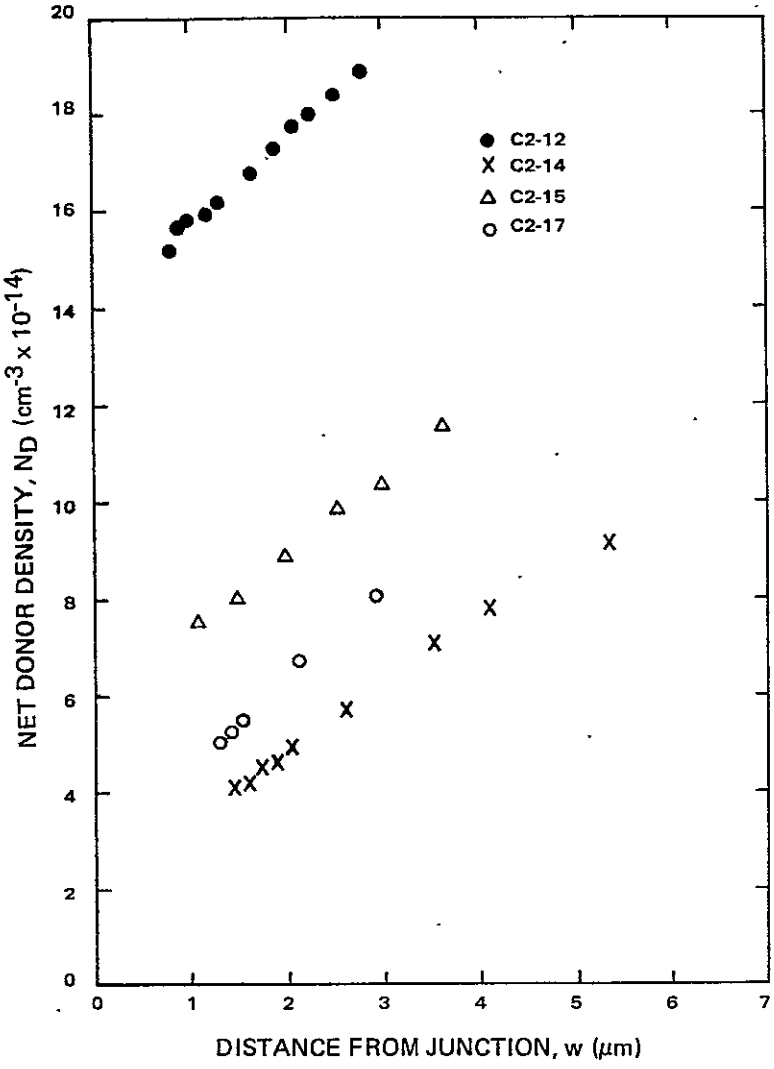

Figure 7. Net Donor-Density Profiles for Four C2 Cells

lithium is in the region measured, i.e., up to 5 μm from the junction. This would account for the failure of the cells to recover. Figure 8, which is derived from Figure 7 as the negative of the density difference between the point of measurement and the junction edge, shows clearly that the density variations from the junction edge are almost identical for all cells. The figure also shows the shape of the distribution which is hypothesized to be the tail of the boron distribution.

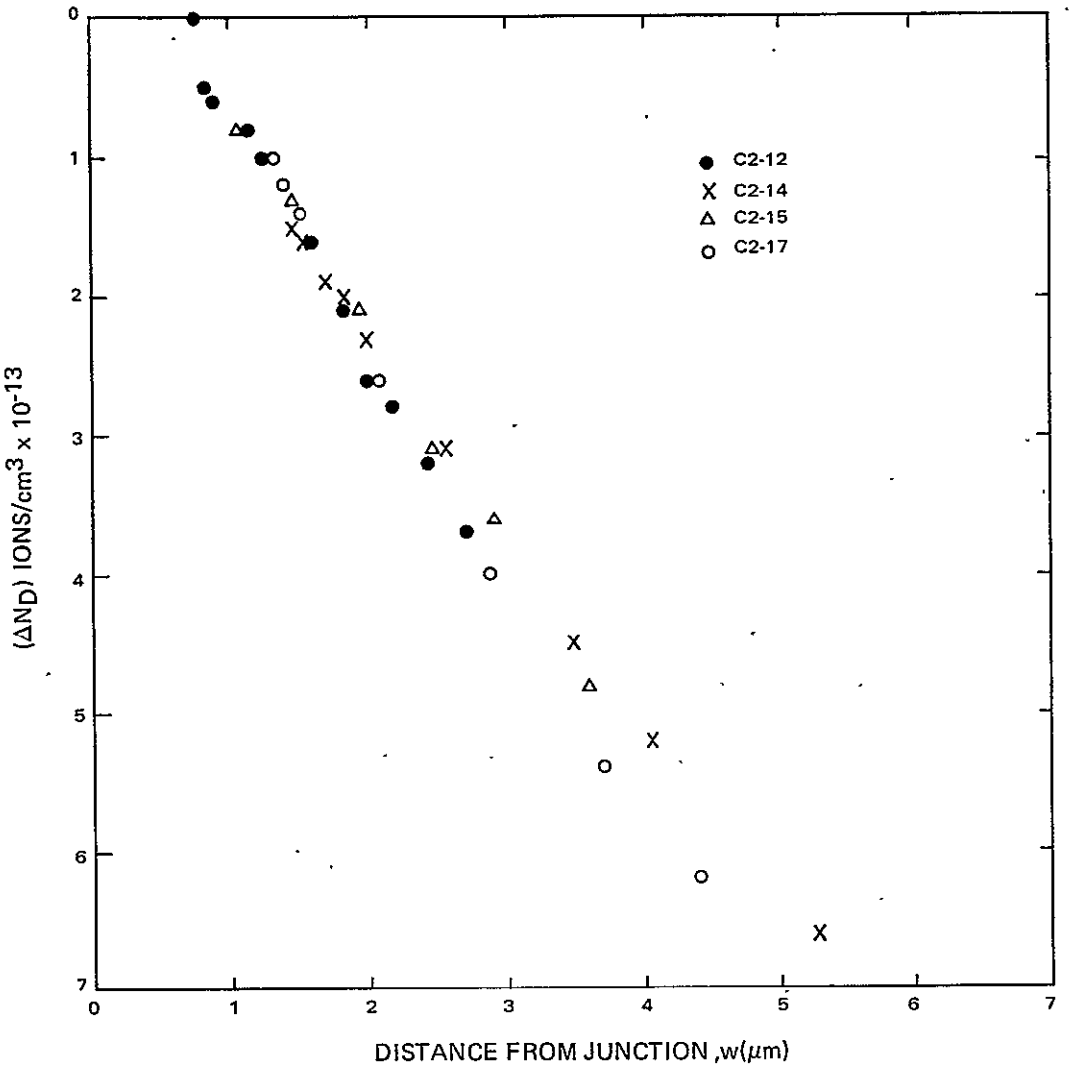

Figure 8. Net Donor Density Variation From Edge of Depletion Region for Four C2 Cells

Although this shape does not fit well with an error function, the value of boron density implied ($\sim 10^{14}$ cm^{-3} at ~ 0.7 μm from the junction) approximates the value expected there for a solar cell junction, i.e., diffusion at $\approx$ 1100°C for 15 min. with an ≈ 0.5 μm junction depth.

The post-irradiation performance of the C2 cells at all fluence levels is below that of the n/p cells so that these particular cells are not very interesting in terms of radiation hardening.

The cells of group H2(1) also had reasonably good initial performance (P_o = 26.0 mW). The recovery, shown in Figure 9, is from 0.65 P_o immediately after irradiation to 0.88 P_o sixty-nine days after irradiation, giving the H2(1) cells an averaged power of 22.9 mW, significantly above the average of two 10 ohm-cm n/p cells irradiated to the same fluence. None of the cells of this group has shown any erratic behavior over the duration of the tests which extend beyond the time shown in Figure 9 to 142 days after irradiation. Between the 69th and 142nd days after irradiation no further change in cell performance occurred.

The cells of group H2(2) had initial power of 24.3 mW. Figure 10 gives the recovery curves after 5×10^{14} e/cm^2 for these cells which show that 59 days after irradiation they have recovered to a power level equal to that of the n/p cells irradiated with them. As the recovery curve has not yet saturated, further recovery is expected from these cells.

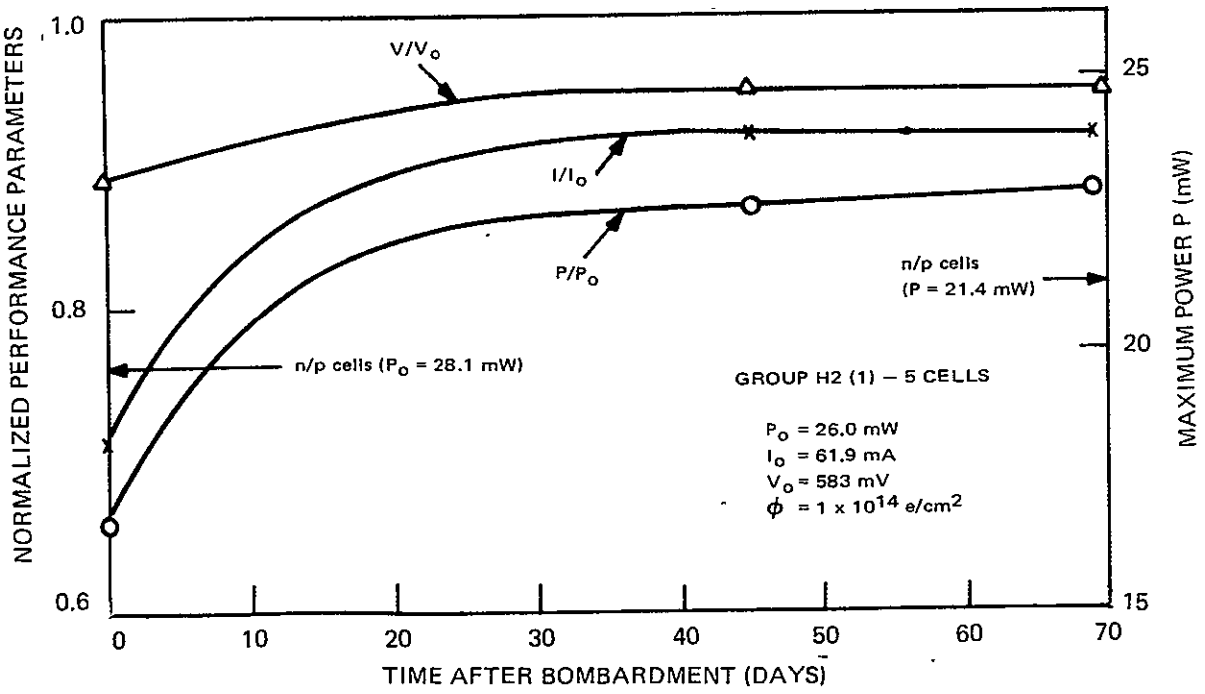

Figure 9. Cell Performance vs. Time After Irradiation to 1×10^{14} e/cm^2 (1-MeV Electrons) - H2(1) Cells

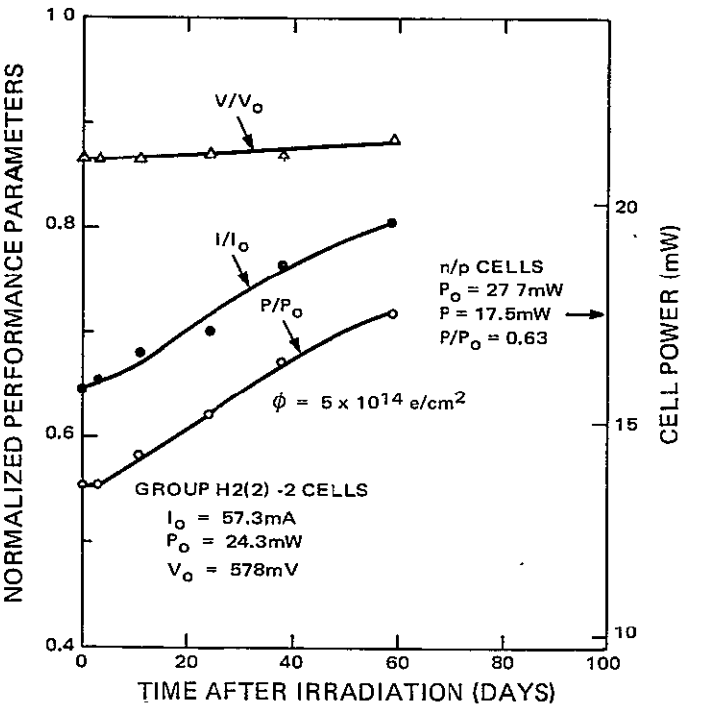

Figure 10. Cell Performance vs. Time After Irradiation to 5×10^{14} e/cm^2 (1-MeV Electrons - H2(2) Cells

The H2(3) cells had initial power of 25.2 mW. Recovery curves after irradiation to 3×10^{15} e/cm^2 are given in Figure 11. These cells show a slower recovery rate than that of the H2(2) cells, presumably due to the higher fluence and consequent depletion of lithium near the junction. Seventy-six days after irradiation the power of the H2(3) cells is $\approx$18 percent below that of n/p cells. However, experience on heavily irradiated crucible-grown cells (see Figure 3, Appendix A) indicates that significant additional recovery of these cells can be expected over the next $\approx$9 months.

An interesting feature of the recovery curves for both H2(2) and H2(3) cells is the "hesitation" which occurs after irradiation before the approximate linear increase of the performance curves. This hesitation is of $\approx$3 days duration in the case of the H2(2) cells and $\approx$25 days in the more heavily irradiated H2(3) cells. This could suggest that at least two distinct lifetime-influencing processes with different time constants are competing in the post-irradiation dynamics of the crucible-grown lithium cell. It is also interesting to compare the H2 cells with the H1 cells, since they underwent the same lithium diffusion schedules and thus the

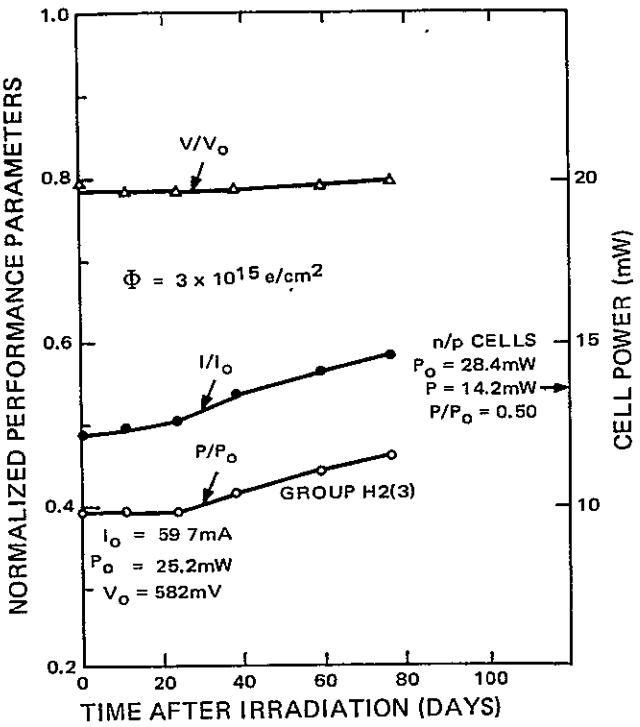

Figure 11. Cell Performance vs. Time After Irradiation to 3×10^{15} e/cm^2 (1-MeV Electrons) - H2(3) Cells

only gross difference is that H1 cells were aresenic-doped while H2 cells were phosphorus-doped. Initially the H2 cells had better performance, the average power for all H2 cells being 25.5 mW; that for all H1 cells being 20.8 mW. The initial diffusion length for H2 cells was $\approx 40\,\mu$m, significantly higher than the $\approx 29\,\mu$m for H1 cells. The post-irradiation recovery rates show gross similarity as is seen by comparison of Figures 6 and 10. Unfortunately the data of Figure 6 is insufficient to ascertain whether the "hesitation of recovery" was also experienced by H1(2) cells. However, the established difference between these two cell groups is the ≈ 20 percent performance advantage of the H2 cells. It would be valuable to ascertain whether this performance advantage was due to the use of phosphorus rather than arsenic as an initial dopant. In order to do this a controlled experiment involving simultaneous lithium diffusion of phosphorus and arsenic doped cells together with control (non-lithium) cells from both crystals would have to be performed.

The T2 cells had high short-circuit current, $I_o = 68.6$ mA, but the photovoltaic characteristics had a rather low curve power factor of 0.66. (The averaged power factors for C2 and H2 cells were 0.75 and 0.72, respectively.)

Consequently, the initial power for T2 cells was only 26.5 mW. The A factor of the cells was obtained using multi-light-level I-V characteristics (Reference 9), and was found to be close to unity in the current range of interest, 30 to 65 mA. However, the cells were found to have approximately 1-ohm series resistance (as compared with ≈ 0.3 ohm for C2(1) and H2 cells). This series resistance was largely responsible for the low curve power factor in the T2 cells.

Group T2(1) cells had initial performance parameters I_o = 68.2 mA, P_o = 26.8 mW, and V_o = 583 mV. Immediately after irradiation to 1×10^{14} e/cm^2 the values were 48.3 mA, 16.5 mW, and 506 mV. The post-irradiation behavior of these cells is remarkable in that they showed unusually fast recovery. The cells recovered to I = 60.2 mA, P = 23.2 mW, and V = 560 mV after 45 days, however most of this recovery actually occurred in the first ten days after irradiation. The swiftness of recovery is all the more surprising when it is considered that the lithium distribution in the T2 cells is very similar to that in the C1 cells. The C1(1) cells had a recovery rate (~1 percent per 20 days) only one sixtieth of that of the T2(1) cells (~30 percent in 10 days). In view of this, it is suspected that the T2 cells actually have a much lower oxygen content than is typical for crucible-grown cell, and as a consequence, the lithium-diffusion constant is correspondingly higher. The post-irradiation series resistance of the T2(1) cells is ≈1 ohm, the same as the pre-irradiation value. Since recovery, the cells have remained stable at 23.4 mW, ≈9 percent above the post-irradiation level of the n/p cells.

Cells of groups T2(2) and T2(3) had initial performance values similar to cells of group T2(1) with one exception. The exception was cell T2-14 of group T2(2) which displayed a shunt leakage of ~80 ohm. This shunt leakage persisted after irradiation. The other cell of group T2(2), cell T2-13, recovered to a power of 20.2 mW eleven days after irradiation. This power, which is ≈13 percent above the 17.5 mW for the n/p cells, has been maintained to the latest reading, 76 days after irradiation.

Both T2(3) cells developed shunt leakage (~100 ohm) and series resistance problems after irradiation. The series resistance after the high (3×10^{15} e/cm^2) fluence is probably due to carrier removal from these lightly doped cells. This series resistance increased from ~2 ohm immediately after irradiation to ~4 ohm at 1 month after irradiation. This is in agreement with results of bulk sample measurements (Appendix B) which indicate continuing carrier removal during room-temperature recovery in Quartz-Crucible silicon. The development of shunt leakage is more puzzling. In spite of these problems, the short-circuit current of these cells was monitored; 76 days after irradiation I = 44.8 mA. This compares well with the 40.3 mA obtained for the n/p cells irradiated to 3×10^{15} e/cm^2.

E. CELLS OF SHIPMENT NO. 3

In addition to the n/p cells listed in Section IV-B, the third cell shipment included fifteen T3 cells manufactured from phosphorus-doped Lopex silicon with starting resistivity > 50 Ω-cm, ten H4 cells made from phosphorus-doped Float-Zone silicon with ≈100 Ω-cm starting resistivity, and sixty C4 cells made from 100 Ω-cm Float-Zone silicon.

The process variables, approximate initial lithium concentrations, and initial diffusion lengths of T3 and H4 cells are listed in Table IV. T3 cells are seen to have very high lithium densities, $N_{LO} \sim 3 \times 10^{15}$ cm^{-3}, $dN_L/dw \sim 10^{20}$ cm^{-4}, but also high diffusion lengths ≈ 80 μm. These cells, together with Texas Instruments Lopex and Float-Zone cells received under a predecessor NASA contract (Reference 3) prove that high lithium doping and high minority-carrier lifetime are not necessarily incompatible. The cells from lot H4 also have high lithium density near the junction, a factor of ~3 below that for the T3 cells. The H4 cells, however, have low diffusion lengths, the average being approximately 30 μm.

TABLE IV. GROUPING, IRRADIATION SCHEDULE, PROCESS PARAMETERS, AND LITHIUM CONCENTRATIONS OF T3 AND H4 CELLS

Cell Group	Number of Cells	(e/cm^2)	Li Diffusion		Li Redistribution		Li Concentration		(μm)
		ϕ	Temp(°C)	Time(Min)	Temp(°C)	Time(Min)	N_{LO}(cm^{-3})	dN_L/dw(cm^{-4})	L_o
T3(1)	3	1x10^{14}	400	90	0	0	3x10^{15}	1x10^{20}	80
T3(2)	3	≈8x10^{14}*	400	90	0	0	3x10^{15}	1x10^{20}	80
T3(3)	3	3x10^{15}	400	90	0	0	3x10^{15}	1x10^{20}	80
H4(1)	2	1x10^{14}	425	90	425	60	1x10^{15}	3x10^{19}	30
H4(2)	3	≈ 8x10^{14}*	425	90	425	60	1x10^{15}	3x10^{19}	30

*Electron energy: approx. 0.7MeV

Considerable difficulty was encountered in the measurement of the properties of both T3 cells and H4 cells. The problem with T3 cells arose due to intermittent shunt leakages. Such shunt leakage was encountered during both dark and illuminated I-V measurements although, in general, it became more severe with increasing illumination. Spontaneous changes were frequently encountered during the course of a measurement. It is tentatively concluded that the cell leakage was internal. Given the high doping density of these cells, it is possible that precipitates could form in the junction region, giving rise to shunt leakage.

In any case, the leakage rendered several cells, namely T3-17, -21, -27, -28, -29, and -30, useless for testing purposes, and several others, as will be seen below, questionable as to measurements of power and open-circuit voltage.

The H4 cells presented contact problems. On many of the cells it was not possible to obtain good contact. This problem was alleviated in the case of some cells by applying solder to one of the corner darts of the top contact. However, proper contact has not been obtained to cells H4-39[6], -42, or -53.

The T3 cells were divided into three groups which were irradiated to 1×10^{14} e/cm^2, $\approx 8 \times 10^{14}$ e/cm^2 of ≈ 0.7 MeV electrons, and 3×10^{15} e/cm^2. The H4 cells were divided into 2 groups irradiated to 1×10^{14} e/cm^2 and $\approx 8 \times 10^{14}$ e/cm^2 of ≈ 0.7 MeV electrons.

The performance parameters obtained for H4 cells are given in Table V. These cells presented continuing contact problems and, thus, data beyond three days after irradiation was not obtained.

TABLE V. PRE- AND POST-IRRADIATION PHOTOVOLTAIC PERFORMANCE OF H4 CELLS

Cell Group	ϕ (e/cm^2)	Pre-irradiation			Post-irradiation			3 Days			6 Days			11 Days		
		I_o(mA)	P_o(mW)	V_o(mV)	I/I_o	P/P_o	V/V_o	I/I_o	P/P_o	V/V_o	I/I_o	P/P_o	V/V_o	I/I_o	P/P_o	V/V_o
H4(1)	1×10^{14}	47.0	18.8	545	0.91	0.88	0.97	0.97	0.93	1.00	-	-	-	-	-	-
H4(2)	$\sim 8 \times 10^{14}$	47.5	16.1	534	0.80	0.63	0.89	-	-	-	-	-	-	-	-	-

In groups T3(1) and T3(2) irradiated to 1×10^{14} e/cm^2 and $\approx 8 \times 10^{14}$ e/cm^2, respectively, the shunt leakage problem again was encountered in several cells. Cells displaying shunt leakage were omitted when computing the average powers and voltages in T3 groups. However, the short-circuit current measurement is not affected by shunt leakage and such measurements are plotted in Figure 12. Figure 12 indicates a redegradation in current amounting to approximately 5 percent of the absolute current level in both groups of cells. The similarity of the curve shapes is evident, thus indicating the same time constants for recovery

[6] Actually H4-3539. The first two digits of the four-digit number following the lot designation on H cells have been dropped.

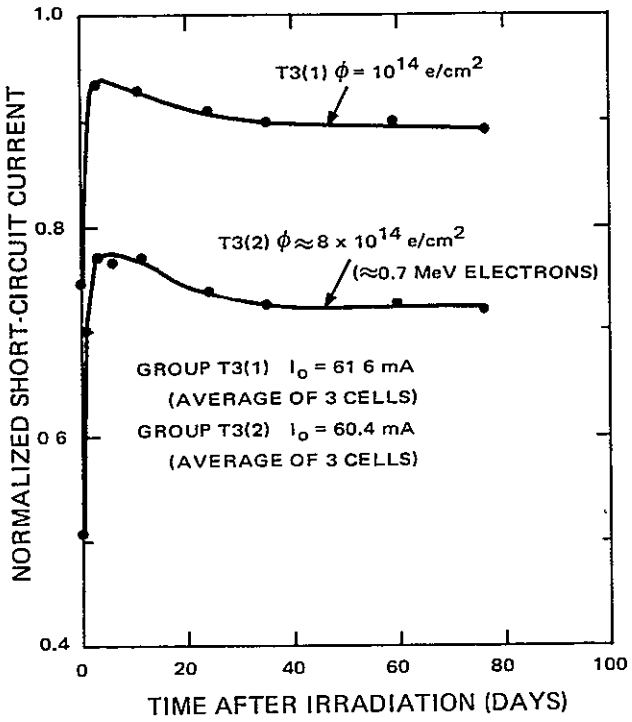

Figure 12. Short-Circuit Current for Cells of Group T3(1) and T3(2)

and redegradation in both cell groups. This is as expected given the hypothesized recovery mechanism (Section IIC). Since N_{LO} ($\approx 3 \times 10^{15}$ cm^{-3}) is much greater than the radiation-induced defects for either group T3(1) or T3(2), the recovery of these cells reduces to a first order reaction. The similar time constants for redegradation in the two groups hints at the interesting possibility that at least one mode of redegradation is independent of the defect density.

Performance curves for group T3(3) are given in Figure 13. The T3(3) cells encountered no post-irradiation shunt leakage problems. This could be due to the high irradiation fluence but may also be fortuitous. The curves of Figure 13 show the same very rapid recovery seen in short-circuit current for T3(1) and T3(2) cells. The redegradation in I (and consequently P) is again evident and has the same time constant as in the cases of T3(1) and T3(2). The T3(3) cells have P = 14.2 mW as of the latest reading, 76 days after irradiation, which is equal to the value obtained for the n/p control cells.

Sixty cells from lot C4, fabricated from 100 ohm-cm Float-Zone silicon, have been tested. These cells came under five groupings or "batches". Each batch, consisting of 12 cells, underwent a given lithium diffusion schedule. For example,

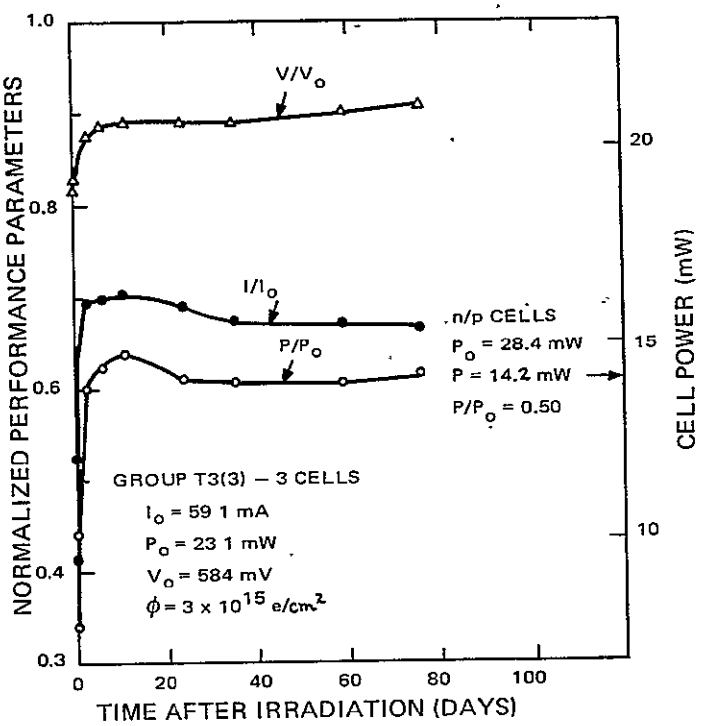

Figure 13. Cell Performance vs. Time After Irradiation to 3×10^{15} e/cm^2 (1 MeV Electrons) - T3(3) Cells

referring to Table VI, batch I consists of cells C4-1 to C4-12, all of which underwent a 90-minute lithium diffusion at 425°C with no subsequent distribution. Each batch was divided into four cell groups: a group of 4 cells irradiated to 1×10^{14} e/cm^2, a group of 3 irradiated to 5×10^{14} e/cm^2, a group of 3 irradiated to 3×10^{15} e/cm^2, and a group of 2 left unirradiated. In addition to the information noted above, Table VI lists the approximate lithium concentrations and the initial diffusion lengths for each batch. In agreement with Reference 13, it is seen that for the lithium-diffusion cycles employed, the lithium density in the base region near the junction decreases with increasing redistribution time. Thus, batch III has lower values of N_{LO} and dN_L/dw than batch II, which in turn, has lower values than batch I. Similarly, batch V has lower values than batch IV. It is also seen that in this lot of cells, the initial diffusion length increases with decreasing lithium concentration in agreement with the trend in most lithium cells. (This trend is not followed in the case of T3 cells or TI 900 series cells (Appendix A).) Unfortunately even the best batch in this regard, i.e., batch III, has a relatively low diffusion-length average of ≈ 40 μm.

TABLE VI. GROUPING, IRRADIATION SCHEDULE, PROCESS PARAMETERS, AND LITHIUM CONCENTRATIONS OF C4 CELLS

Batch	Group	Number of Cells	Cell Numbers	(e/cm^2)	Li Diffusion		Li Redistribution		Li Concentration		(μm)
				ϕ	Temp(°C)	Time(Min)	Temp(°C)	Time(Min)	$N_{LO}(cm^{-3})$	$dN_L/dw(cm^{-4})$	L_o
I	C4(1)	4	C4-1 to C4-4	$1x10^{14}$	425	90	none	none	$3x10^{15}$	$5x10^{19}$	15
	(2)	3	C4-5 to C4-7	$5x10^{14}$	425	90	none	none	$3x10^{15}$	$5x10^{19}$	15
	(3)	3	C4-8 to C4-10	$3x10^{15}$	425	90	none	none	$3x10^{15}$	$5x10^{19}$	15
	(4)	2	C4-11 & C4-12	0	425	90	none	none	$3x10^{15}$	$5x10^{19}$	15
II	(5)	4	C4-13 to C4-16	$1x10^{14}$	425	90	425	60	$2x10^{15}$	$2x10^{19}$	20
	(6)	3	C4-17 to C4-19	$5x10^{14}$	425	90	425	60	$2x10^{15}$	$2x10^{19}$	20
	(7)	3	C4-20 to C4-22	$3x10^{15}$	425	90	425	60	$2x10^{15}$	$2x10^{19}$	20
	(8)	2	C4-23 & C4-24	0	425	90	425	60	$2x10^{15}$	$2x10^{19}$	20
III	(9)	4	C4-25 to C4-28	$1x10^{14}$	425	90	425	120	$2x10^{14}$	$1x10^{18}$	40
	(10)	3	C4-29 to C4-31	$5x10^{14}$	425	90	425	120	$2x10^{14}$	$1x10^{18}$	40
	(11)	3	C4-32 to C4-34	$3x10^{15}$	425	90	425	120	$2x10^{14}$	$1x10^{18}$	40
	(12)	2	C4-35 & C4-36	0	425	90	425	120	$2x10^{14}$	$1x10^{18}$	40
IV	(13)	4	C4-37 to C4-40	$1x10^{14}$	450	40	none	none	$2x10^{15}$	$2x10^{19}$	15
	(14)	3	C4-41 to C4-43	$5x10^{14}$	450	40	none	none	$2x10^{15}$	$2x10^{19}$	15
	(15)	3	C4-44 to C4-46	$3x10^{15}$	450	40	none	none	$2x10^{15}$	$2x10^{19}$	15
	(16)	2	C4-47 & C4-48	0	450	40	none	none	$2x10^{15}$	$2x10^{19}$	15
V	(17)	4	C4-49 to C4-52	$1x10^{14}$	450	40	450	80	$3x10^{14}$	$1x10^{18}$	30
	(18)	3	C4-53 to C4-55	$5x10^{14}$	450	40	450	80	$3x10^{14}$	$1x10^{18}$	30
	(19)	3	C4-56 to C4-58	$3x10^{15}$	450	40	450	80	$3x10^{14}$	$1x10^{18}$	30
	(20)	2	C4-59 & C4-60	0	450	40	450	80	$3x10^{14}$	$1x10^{18}$	30

Table VII lists the pre-irradiation and post-irradiation photovoltaic parameters measured for these cells. The values listed are, as before, averaged over all the cells in the group unless otherwise specified. In general, cells of a given batch were similar in behavior (allowing for a ~10 percent spread between the highest and lowest value of I_0 in a given batch). One exception was found in cells C4-30 to -35 in batch III. These six cells displayed series resistances of approximately 1.5 ohms before irradiation. This series resistance had a severe influence on their post-irradiation behavior as will be discussed below.

Table VII describes cell behavior up to a time 11 days after irradiation. Subsequent to the compilation of this table, results have been obtained up to 76 days after irradiation. Many cell groups had stabilized by the 11th day after irradiation and, in these cases, the last values listed in the table are also the present values. These cases will be noted in the text. Cases where significant changes occurred after this time will be further discussed.

In discussing the recovery and stability studies, we will first consider the cells irradiated to 1×10^{14} e/cm^2, i.e., groups (1), (5), (9), (13) and (17). It is seen that the cells with the best initial performance, namely (9) and (17), suffer the greatest fractional degradation during irradiation, I/I_0 being 0.83 and 0.85, and P/P_0 being 0.79 and 0.82, respectively, for these groups. This was found to be the case at all three radiation fluences. Within 3 days after bombardment,

TABLE VII. PRE- AND POST-IRRADIATION PHOTOVOLTAIC PERFORMANCE OF C4 CELLS

Group	ϕ (e/cm^2)	Pre-irradiation			Post-irradiation			150 Min			3 Days			6 Days			11 Days		
		I_o(mA)	P_o(mW)	V_o(mV)	I/I_o	P/P_o	V/V_o	I/I_o	P/P_o	V/V_o	I/I_o	P/P_o	V/V_o	I/I_o	P/P_o	V/V_o	I/I_o	P/P_o	V/V_o
								Batch I											
C4(1)	$1x10^{14}$	39.1	15.8	537	0.92	0.90	0.98	-	-	-	0.97	0.97	0.99	0.97*	0.97*	1.00*	0.97	0.96	0.98
(2)	$5x10^{14}$	40.2	15.8	539	0.83	0.77	0.94	-	-	-	0.96	0.87	0.98	-	-	-	0.96	0.92	0.98
(3)	$3x10^{15}$	39.1	15.3	532	0.71	0.59	0.88	0.84	0.71	0.89	0.97	0.85	0.92	0.97*	0.84*	0.91*	0.97	0.86	0.93
(4)	0	40.3	15.7	539	-	-	-	-	-	-	-	-	-	-	-	-	-	-	-
								Batch II											
(5)	$1x10^{14}$	44.3	17.7	534	0.90	0.86	0.96	-	-	-	0.99	0.98	0.99	0.98*	0.98*	0.99*	0.99	0.98	0.99
(6)	$5x10^{14}$	45.4	17.5	531	0.77	0.69	0.91	-	-	-	0.99	0.95	0.98	0.99*	0.96*	0.98*	0.99	0.96	0.98
(7)	$3x10^{15}$	44.9	17.7	531	0.59	0.46	0.84	0.74	0.51	0.84	0.94	0.72	0.87	-	-	-	0.99	0.75	0.88
(8)	0	46.2	17.7	532	-	-	-	-	-	-	-	-	-	-	-	-	-	-	-
								Batch III											
(9)	$1x10^{14}$	54.5	21.1	532	0.83	0.79	0.95	-	-	-	0.96	0.97	0.99	0.98	0.98	0.99	1.00	0.98	0.99
(10)	$5x10^{14}$	55.2	20.3	538	0.69	0.60	0.86	-	-	-	0.95	0.83	0.94	0.99	0.86	0.94	1.00	0.86	0.94
**(11)	$3x10^{15}$	54.7	19.1	538	0.59	0.38	0.77	0.61	0.38	0.77	0.73	0.34	0.77	0.78	0.32	0.77	0.81	0.29	0.77
(12)	0	55.3	19.9	535	-	-	-	-	-	-	-	-	-	-	-	-	-	-	-
								Batch IV											
(13)	$1x10^{14}$	38.8	15.0	525	0.95	0.91	0.98	-	-	-	0.98	0.96	0.99	0.99*	0.90*	0.99*	0.99	0.96	0.99
(14)	$5x10^{14}$	38.9	15.3	527	0.89	0.82	0.95	-	-	-	0.98	0.93	0.99	0.97*	0.93*	0.98*	0.99	0.93	0.99
(15)	$3x10^{15}$	38.7	15.1	517	0.74	0.63	0.89	1.84	0.72	0.89	0.97	0.86	0.94	-	-	-	1.00	0.89	0.95
(16)	0	39.0	14.3	526	-	-	-	-	-	-	-	-	-	-	-	-	-	-	-
								Batch V											
(17)	$1x10^{14}$	51.7	19.6	528	0.85	0.82	0.95	-	-	-	1.00	0.99	0.99	1.00	0.99	0.99	1.00	0.99	0.99
(18)	$5x10^{14}$	53.1	20.8	535	0.70	0.61	0.88	-	-	-	0.97	0.90	0.95	0.99	0.91	0.96	1.00	0.92	0.96
(19)	$3x10^{15}$	50.5	20.0	530	0.60	0.43	0.81	0.62	0.44	0.81	0.85	0.57	0.82	0.90	0.58	0.83	0.95	0.60	0.83
(20)	0	53.4	21.4	532	-	-	-	-	-	-	-	-	-	-	-	-	-	-	-

*Only one cell measured
**High series resistance

all five groups have recovered to within 4 percent of the original power. The only change in performance since the 11th day after irradiation occurred in group C4(1). This cell group has suffered a small (2.5 percent) loss in power between the 11th and 60th day due mainly to a change in open-circuit voltage.

The cells in groups (2), (6), (10), (14), and (18) were irradiated to 5×10^{14} e/cm^2. These cells partially recovered in the first 11 days since irradiation with indications of redegradation present only in cells C4-30 and -31 of group (10), two of the cells with high initial series resistance. The redegradation experienced by these two cells is in the form of a small increase in series resistance from ≈ 1.4 ohms immediately after irradiation to ≈ 1.7 ohms six days after irradiation. During the time in which this series-resistance increase occurred, short-circuit current recovery was also taking place so that the net result was a slight increase in the output of these two cells. The other cell of group (10), C4-29, had a lower initial series resistance, 0.7 ohm. This cell also showed a slight post-irradiation resistance increase to 0.85 ohm which occurred between the first and sixth day after irradiation.

In the time since the eleventh day of the tests, all cell groups irradiated to 5×10^{14} e/cm^2 have remained constant within experimental error in power, short-circuit current and open-circuit voltage. A slight additional increase in series resistance to 1.1 Ω was noted in cell C4-29 on the thirty-fifth day. No further change was observed since that time.

The cells in groups (3), (7), (11), (15), and (19) were irradiated to 3×10^{15} e/cm^2. Group C4(11) suffered continuing degradation in power output for approximately 20 days after irradiation. Approximately twenty days after irradiation, the group's cell parameters stabilized at I = 46 mA, P = 5.5 mW, and V = 420 mV. The cells of C4(11) are C4-32 to -34 which initially had high series resistances of ≈ 1.5 ohms. Immediately after irradiation, the series resistance in these cells was ≈ 2.7 ohms, and six days after irradiation was 4.5 ohms. Thus, the degradation in power was (probably entirely) due to the increase in series resistance. The pre-irradiation photovoltaic characteristics of C4-32 are given in Figure 14 for illumination by 140 mW/cm^2 tungsten and for ~ 70 mW/cm^2 illumination. The series resistance was obtained (Reference 9) from the curves by measuring the voltage at a point offset an equal amount, in this case 6.5 mA, from the short-circuit current point on each curve. By taking the difference in this voltage between the two curves (0.038 V) and dividing by the difference in short-circuit current (25.3 mA) the resistance is found to be ≈ 1.5 ohms. Post-irradiation curves for C4-32 taken at 140 mW/cm^2 are shown in Figure 15. Curves are given for 20 minutes, 150 minutes, 3 days, and 11 days after irradiation. These curves show the effect of increasing resistance on the curve shape and power output. The series resistance was directly measured in the 20-minute, 150-minute, and 3-day curves by the method of Figure 14. By the sixth day after

irradiation, the series resistance had become sufficient to significantly effect the short-circuit current. This is shown in the 11-day curve where a significant negative slope is seen at the current intercept. In order to get accurate measurements of light-generated current and series resistance under these conditions, it would be necessary to drive the terminal voltage sufficiently negative to reduce the p/n junction bias to zero.

The cells in group C4(7), C4-20 to -22, all developed a ≈300 ohm shunt leakage immediately after irradiation. The shunt resistance has since remained at this ≈300 ohm value. The three cells from group C4(19), C4-56 to -58, developed series resistances of ≈1.5 ohms and shunt leakages of ≈150 ohms during irradiation. These resistances have also remained constant since immediately after irradiation.

Performance plots for four groups of C4 cells irradiated to 3×10^{15} are given in Figures 16 through 19. A very interesting element in the post-irradiation behavior of the cells irradiated to 3×10^{15} e/cm^2 is the almost total recovery of the short-circuit current. This is seen, in particular, in Figures 17 and 19 for groups (7) and (19). Almost all of the loss in performance of these cells with respect to the pre-irradiation performance is due to a loss in open-circuit voltage. This is quite the opposite of the situation in most lithium cells (Section III, Section IVB-D), n/p cells (Reference 14), and in lithium cells immediately after irradiation (Figures 16 to 19 at zero days) where the short-circuit current loss is the larger factor in cell degradation. The situations in groups C4(3) and C4(15) is somewhat different (Figures 16 and 18). The recovery of open-circuit voltage in these cells is much more pronounced and rapid than in the case of groups C4(7) and C4(19) and, after approximately one month, the ratios I/I_o and V/V_o are approximately equal. In contrast, 76 days after irradiation groups C4(7) and C4(19) have I/I_o values 7% and 13% above the V/V_o values, respectively. The cell group among these with the highest lithium density is C4(3), followed in order by C4(15), then C4(7), with C4(19) having the lowest density. Thus, the cells with lowest initial lithium density show the largest residual (post-recovery) degradation in open-circuit voltage 76 days after irradiation.

Attempts were made to relate this behavior to physical parameters through investigation of the equations for short-circuit current and open-circuit voltage (References 12 and 15),

$$J = 15.5 \log_{10} \left[(D_p \tau_p)^{1/2} \right] \qquad (2)$$

and

$$V = 0.0575 \log_{10} J \left[\frac{0.062 \exp (39E_g)}{\rho_n \mu_n D_p} \left(D_p \tau_p \right)^{1/2} \right] \qquad (3)$$

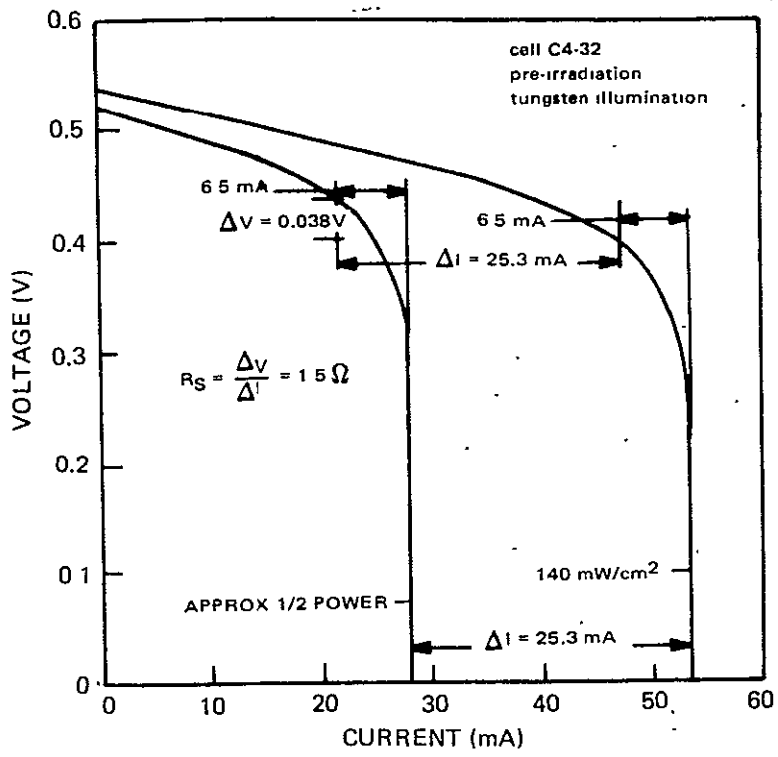

Figure 14. Pre-Irradiation I-V Curves for Cell C4-32 at Two Light Levels

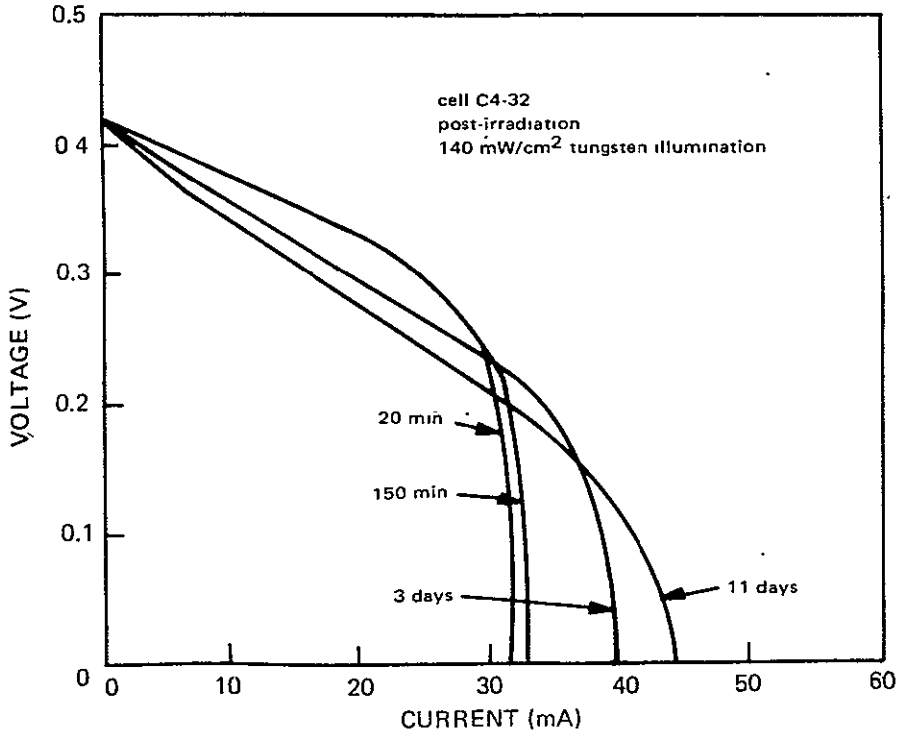

Figure 15. Post-Irradiation I-V Curves for Cell C4-32 Taken With 140 mW/cm^2 Tungsten Illumination ($\phi = 3 \times 10^{15}$ e/cm^2)

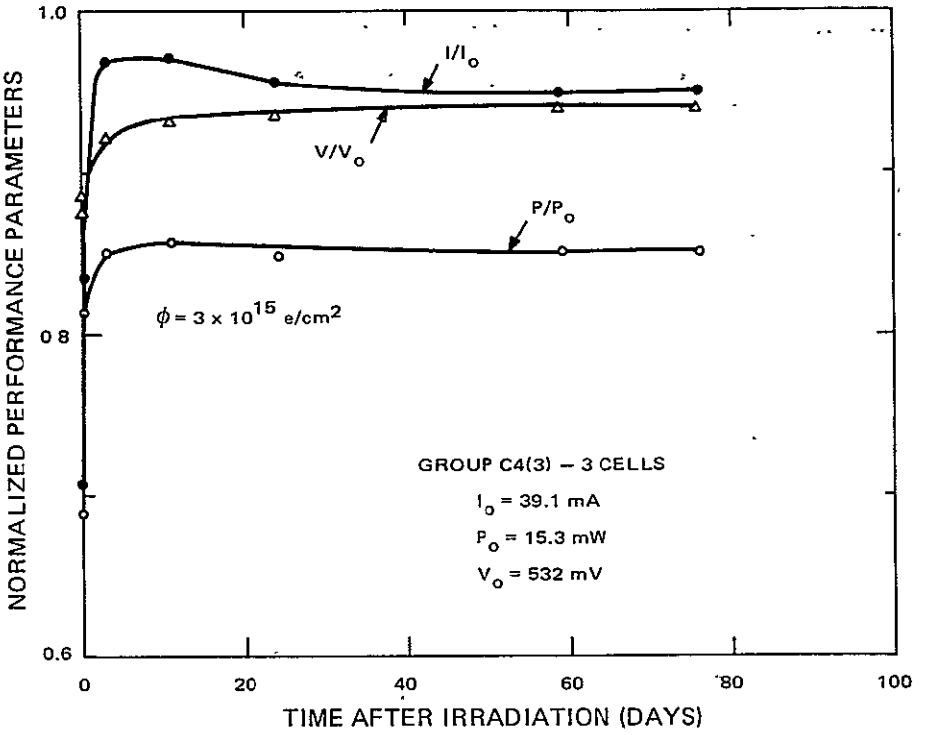

Figure 16. Cell Performance vs. Time After Irradiation to 3×10^{15} e/cm^2 (1 MeV Electrons) - C4(3) Cells

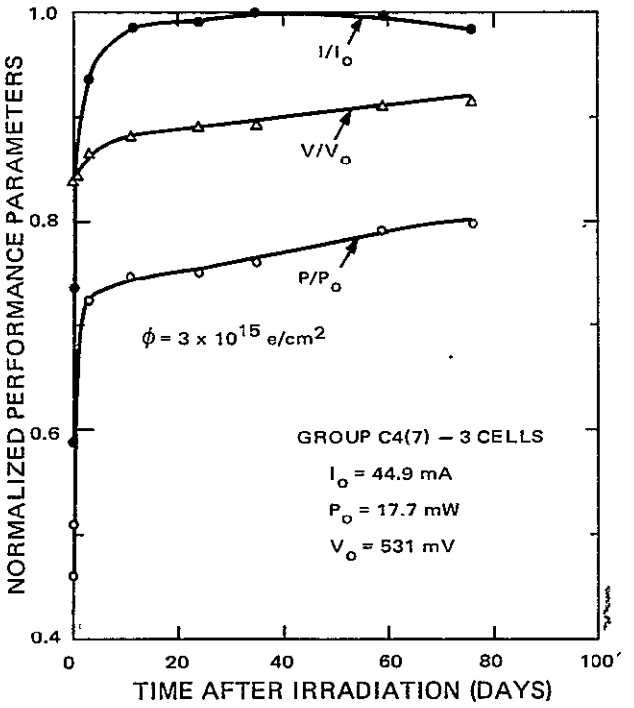

Figure 17. Cell Performance vs. Time After Irradiation to 3×10^{15} e/cm^2 (1-MeV Electrons) - C4(7) Cells

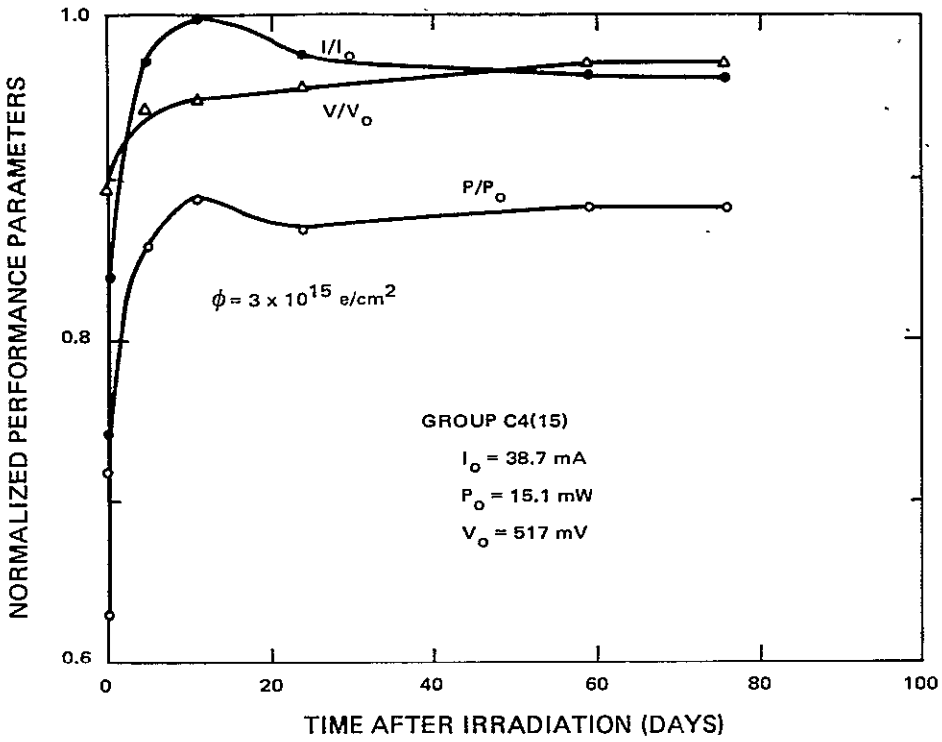

Figure 18. Cell Performance vs. Time After Irradiation to 3×10^{15} e/cm^2 (1-MeV Electrons) - C4(15) Cells

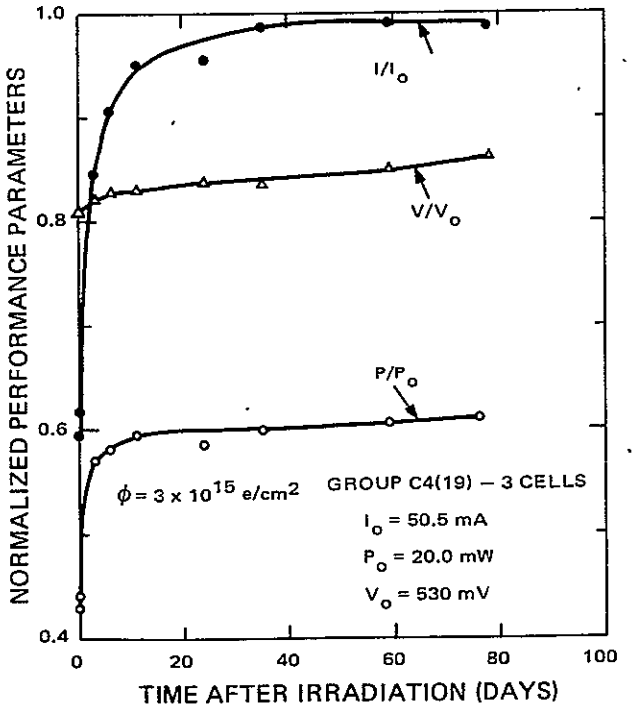

Figure 19. Cell Performance vs. Time After Irradiation to 3×10^{15} e/cm^2 (1-MeV Electrons) - C4(19) Cells

where

J is short-circuit current density,

D_p is the minority-carrier diffusion constant in the n type base,

τ_p is the minority-carrier lifetime,

E_g is the silicon band gap,

ρ_n is the resitivity of the base region, and

μ_n is the majority-carrier mobility in the base.

The equations indicate that the observed behavior of full short-circuit current recovery and persistent open-circuit voltage degradation would occur only if the product of ρ_n μ_n D_p significantly increased. Clearly, neither μ_n nor D_p increase: previous results (see Appendix B) show that μ_n remains constant at room temperature.

Thus, an effective increase in ρ_n is required for the observed changes. Such an effective increase in ρ_n is reasonable in the case of the low-density cell groups where the fluence of 3×10^{15} e/cm^2 was the same order of magnitude as the lithium density.

Further checks on the density effect were made through use of the capacitance-voltage method for measurement of donor density and through measurement of cell junction characteristics using forward biased I-V measurements and multi-level photovoltaic measurements. In Figure 20 donor-density profiles of one of the C4(19) cells, C4-56, are given before irradiation and after recovery. Although the measurements after recovery must be considered quite inaccurate due to the presence of radiation-induced traps (Reference 16) comparison with the pre-irradiation profile indicates a drop in donor density by a factor of approximately 10. In contrast, comparison of pre-irradiation and post-recovery profiles in a high density C4(3) cell (cell C4-10) indicated a decrease of only approximately 2 during the irradiation and recovery processes. Thus, the capacitance measurements confirm the density effect on degradation in open-circuit voltage.

Additional confirmation was obtained from measurement of p/n junction characteristics. The current, I_j, in a forward biased diode is given by

$$I_j = I_R \left[\exp\left(\frac{qV_j}{AkT}\right) - 1 \right] \qquad (4)$$

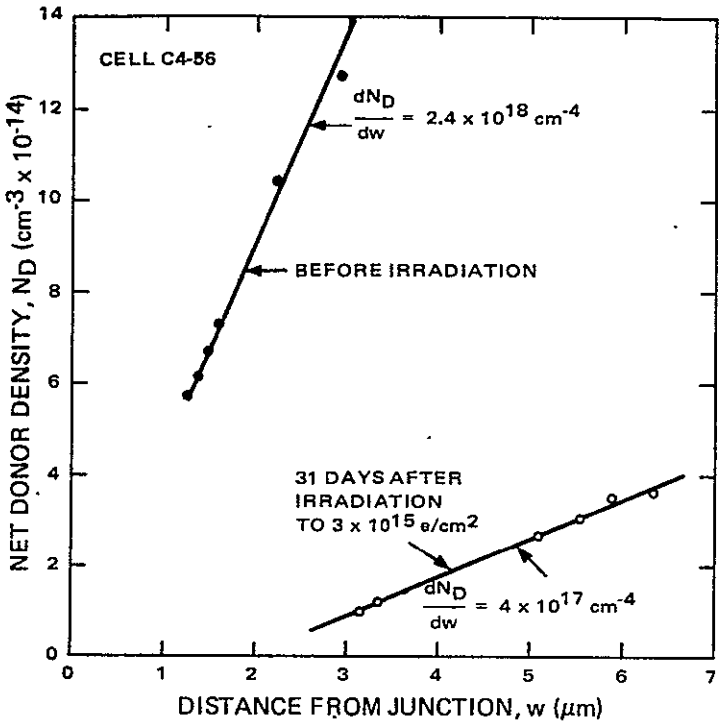

Figure 20. Donor Density Profiles for Cell C4-56 Before Irradiation to 3×10^{15} e/cm^2 (1-MeV Electrons) and After Recovery

$$I_R = \frac{qSD_p p_n}{L_p}, \qquad (5)$$

where I_R is the reverse saturation current of the diode, q is the electron charge V_j is the applied diode voltage, k is Boltzmann's constant, T is the diode temperature, S is the diode area (2 cm^2 in this case), p_n is the hole (minority-carrier) density in the n-type base, and L_p is the minority-carrier diffusion length in the base region.

Curves of diode current at low forward bias in cell C4-56 (group C4(19)) are given in Figure 21 for pre-irradiation and post-recovery conditions. The solid lines give the experimental curves, the dots indicate the curves obtained by fitting the experimental data to Eq.(4). The pre-irradiation and post-irradiation values of I_R were 7.14×10^{-7}A and 6.67×10^{-6}A, respectively. In Eq. (5) the only significant change must be in p_n since L_p was approximately 30 μm prior to irradiation and approximately 25 μm after recovery. The ratio of I_R

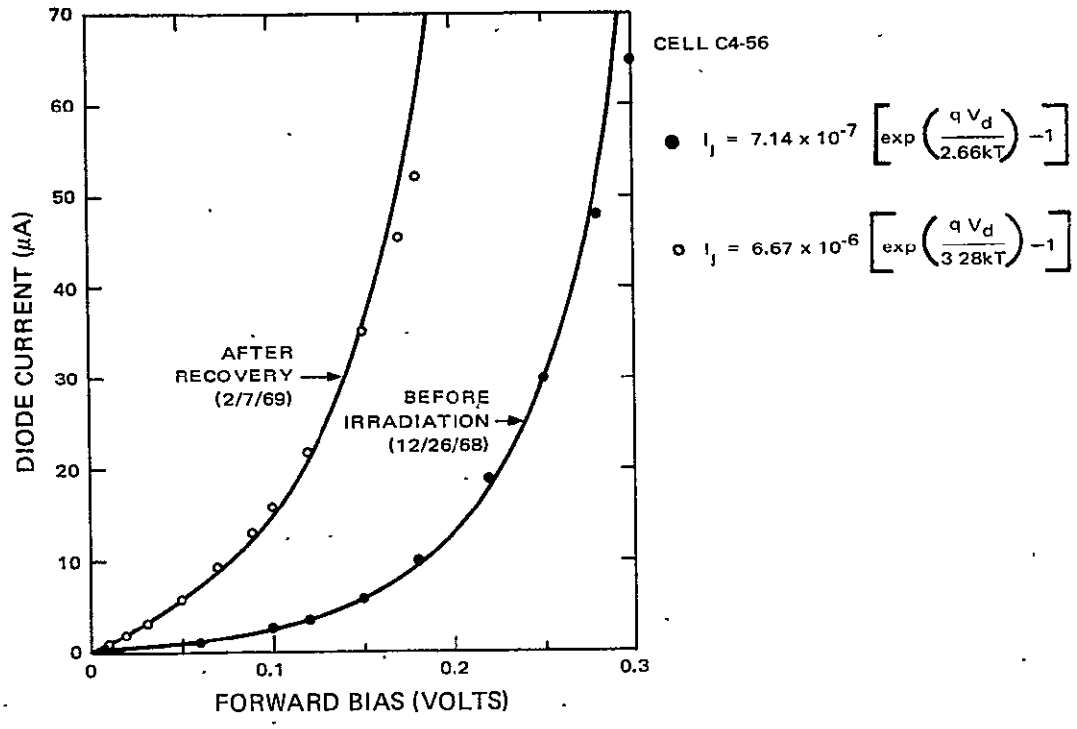

Figure 21. Experimental and Theoretical p/n Junction Characteristics of Cell C4-56 Before Irradiation and After Recovery

before irradiation to that after recovery therefore suggests a factor of ~10 increase in p_n which requires a corresponding ~10 decrease in net donor density. Similar fits were made to the curves for C4-10. The best fit to the pre-irradiation curve at low bias was obtained for $I_R = 9.15 \times 10^{-7}$A and A = 2.30. The C4-10 curve after recovery was almost identical for low biases to the pre-irradiation curve thus, indicating a very small change in the effective value of p_n.

The theoretical curves provide a good fit to the data of Figure 21 only at low biases. As the bias is increased in the C4 cells, the empirical A factor decreases as shown in Figure 22 which gives the pre-irradiation and post-recovery $I_j - V_j$ characteristics on a semi-logarithmic plot. It was suggested (Reference 17) that an apparent increase in A factor could actually be due to a high value of shunt resistance. It was determined that no single shunt resistance could cause the deviation from the high bias linear region observed in the low bias portion of Figure 22. It is worth noting, however, that the value of I_R extrapolated from the high bias (A = 1.1) region of the pre-irradiation curve is $\sim 10^{-10}$A. This is approximately the value for an ideal diode, i.e., for $p_n = 2 \times 10^5 cm^{-3}$, $D_p = 20$ cm^2/sec and $L_p = 30$ μm, Eq. (5) gives 4×10^{-10}A.

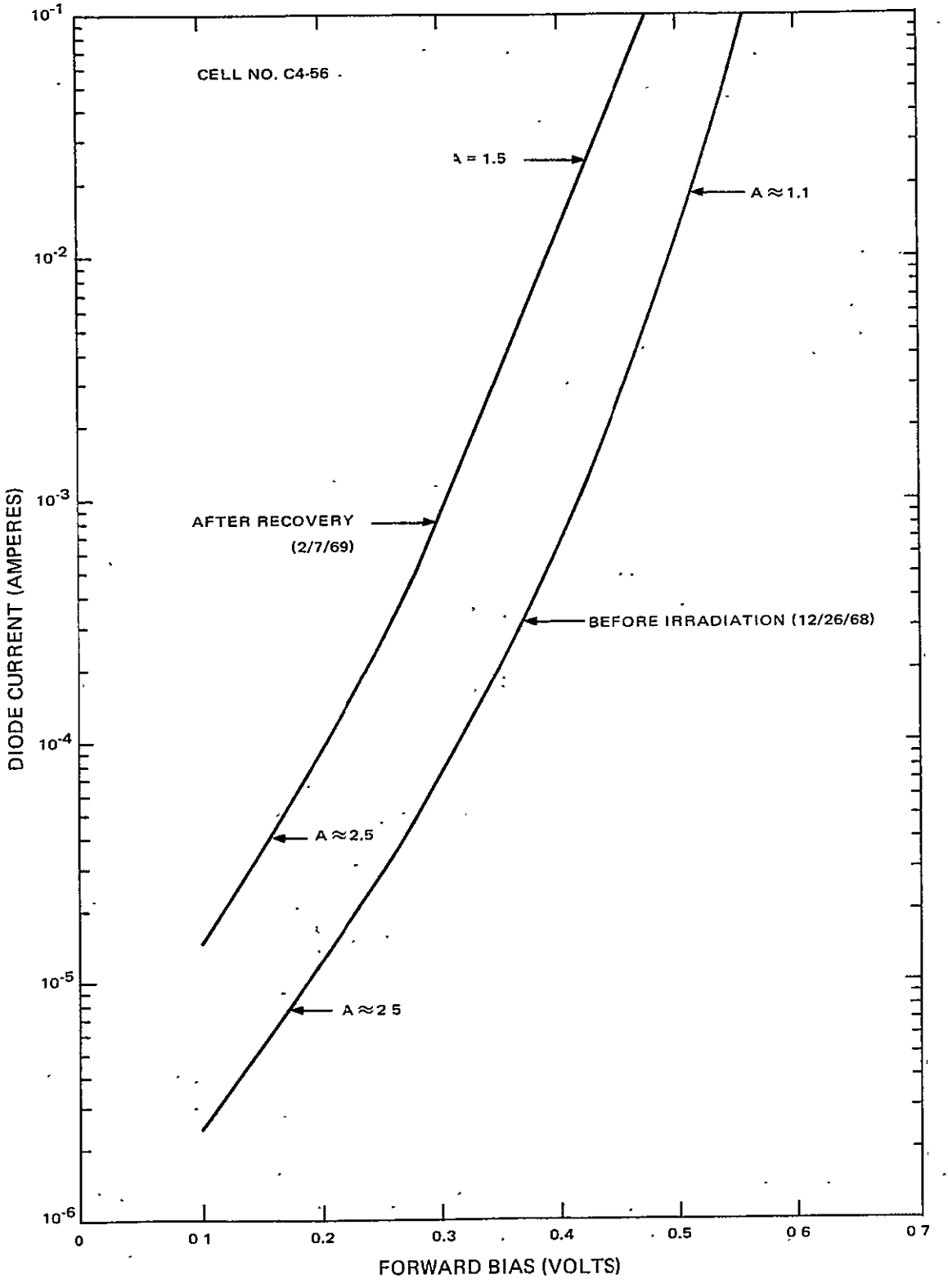

Figure 22. Experimental Semi-Logarithmic p/n Junction Plots of Cell C4-56 Before Irradiation and After Recovery

Returning to Figures 16 and 18, a slight post-recovery redegradation in cell current occurred in groups C4(3) and C4(15) between the tenth and fortieth day after irradiation. This redegradation is significant in C4(15) cells, i.e., 4 percent. The 2 percent redegradation experienced by C4(3) cells is probably real but is still within the error of the measurement.

Significant recovery is still occurring in the open-circuit voltage of C4(7) cells (Figure 17) and C4(19) cells (Figure 19) seventy-six days after irradiation. Recovery in short-circuit current was completed in these cells after approximately 40 days. This continuing voltage recovery could be due to lithium motion from the base region into the region near the junction thereby decreasing the effective resistance, ρ_n, near the junction.

F. CELLS OF SHIPMENT NO. 4

A total of 100 lithium cells were received in this shipment. They are listed in Table VIII. The initial photovoltaic characteristics of these cells have been measured. The values of short-circuit current and open-circuit voltage are given in Table IX. Cells from most of the lots display good curve power factors; two exceptions are cells from lots T6 and T7.

Three of these cells, C5-43, T4-14, and H6-21, have been irradiated to 5×10^{14} e/cm^2. Their post-irradiation performance values are: C5-43; I = 35.4 mA, V = 517 mV; T4-14, I = 32.1 mA, V = 457 mV; H6-21, I = 35.8 mA, V = 499 mV.

TABLE VIII. LIST OF CELLS RECEIVED IN SHIPMENT NO. 4

Cell I.D. No.	Quantity	Crystal Type	Diff. Time (Minutes)	Redist. Time (Minutes)	Temp. (°C)
C5-11 thru C5-20	10	Crucible	40	0	450
C5-41 thru C5-50	10	F. Z.	40	0	450
C5-71 thru C5-80	10	Crucible	90	120	425
C5-101 thru C5-110	10	F. Z.	90	120	425

Mfr.	Lot No.	Quantity	I.D. Prefix	Crystal Type	ρ (ohm-cm)	Dopant	Diff. Time (min)	Redist. Time (min.)	Temp. (°C)
T.I.	4	10	T4-	F. Z.	>50	Phos.	90	0	400
Heliotek	5	10	H5-	F. Z.	≈20	Phos.	90	60	350
Heliotek	6	10	H6-	Crucible	≈20	Phos.	90	60	450
T.I.	5	10	T5-	Lopex	≈50	Phos.	90	0	400
T.I.	6	10	T6-	Lopex	≥50	Phos.	480	0	325
T.I.	7	10	T7-	Crucible	≥20	Phos.	480	0	325

TABLE IX. INITIAL PERFORMANCE PARAMETERS OF CELLS RECEIVED IN SHIPMENT NO. 4

Cell	I (mA)	V (mV)	Cell	I (mA)	V (mV)	Cell	I (mA)	V (mV)
T4-11	55.5	585	C5-75	68.7	585	H6-24	63.5	581
12	55.2	583	76	69.0	590	H6-30	63.7	585
13	54.6	580	77	69.9	584	T6-11	70.2	588
14	56.5	570	78	71.2	588	12	69.0	600
15	55.4	585	79	70.7	592	13	68.3	592
16	56.9	583	80	71.5	593	14	69.3	595
17	57.7	570	101	56.2	545	15	70.7	573
18	53.3	575	102	57.2	535	16	68.7	596
19	564	578	103	56.0	539	17	68.4	591
20	56.4	575	104	59.4	539	18	68.8	591
C5-11	57.0	603	105	59.5	536	19	69.7	592
12	56.9	601	106	55.8	531	20	69.1	595
13	56.8	593	107	52.8	534	T7-11	70.6	580
14	57.0	594	108	53.7	542	12	73.8	591
15	59.1	599	109	59.6	540	13	68.2	590
16	58.4	600	110	60.6	537	14	68.0	583
17	58.2	596	H5-13	63.1	562	15	73.3	580
18	57.0	600	15	64.7	560	16	70.3	580
19	57.5	593	18	74.0	560	17	72.2	590
20	54 5	597	20	70.2	560	18	70.1	594
41	47.2	560	21	73.4	557	19	69.3	578
42	44.2	560	00	73.3	552	20	70.0	584
43	44.4	552	01	72.7	560	T5-11	60.7	594
44	38.7	538	02	77.4	555	12	57.5	601
45	41.0	542	04	78.0	555	13	58.5	596
46	46.3	560	11	73.3	557	14	56 1	591
47	39.4	539	H6-21	48.0	544	15	55.1	596
48	43.2	560	22	49.0	546	16	54.2	601
49	44.8	553	28	49.4	542	17	54.9	590
50	44.7	561	30	48.5	550	18	57 9	596
71	70.0	593	36	50.1	548	19	55.8	600
72	72.1	596	27	57.4	566	20	55.3	595
73	73.4	597	19	52.3	560			
74	64.7	577	43	63.4	589			

SECTION V

MEASUREMENTS OF LITHIUM DIFFUSION CONSTANT

A. GENERAL

Work by the present authors (Reference 7) and by Wysocki (Reference 6) leaves little doubt that the recovery of damage in lithium-doped silicon is controlled by the rate of diffusion of lithium ions. Thus, any direct measurement of diffusion properties of lithium in the devices in question may throw an important light on the recovery process and its optimization in silicon devices.

Mass transport of lithium at elevated temperatures has been observed previously in lithium drift-compensated devices and has been utilized to measure the mobility of lithium in these devices (Reference 18). These devices were very different from solar cells in that they consisted of a lightly doped p-type base into which a heavily doped, graded junction of lithium has been diffused. Lithium was the only n-type dopant present and the diffusion constant was obtained by measuring the rate of decrease in device capacitance as the lithium drifts into and compensates the boron-doped base at temperatures in the 25 to 125°C region. In such devices, the diffusion constant, D_F, of free lithium in silicon of high purity was found to be 2×10^{-14} cm^2/sec at room temperature (Reference 19). However, in less pure silicon, impurities (e.g., oxygen) were found to form chemical complexes with lithium, thereby reducing the effective lithium-diffusion constant. This effect was variable from sample to sample. When studying the properties of individual lithium-doped devices, it is therefore advantageous to obtain direct measurements of the lithium-diffusion constant for each sample used.

B. MEASUREMENT METHOD

In later stages of work on an earlier contract[7], the drift of lithium at room temperature in a junction field was observed and utilized for the first time to obtain a direct measurement of an effective lithium-diffusion constant at the edge of the p/n junction depletion region in solar cells. A brief outline of the method is as follows: An initial measurement of cell capacitance at zero bias was obtained. Then a small d-c reverse bias was applied to the cell. (The bias level was 3 V in the experiments.) This bias was maintained steadily over a period of time (~10 minutes) except at periodic (~30 second) intervals when the bias was switched off and the capacitance at zero bias was measured. The bias was then

[7] Contract No. NAS 5-10239

immediately reapplied after the time (~1 second) required for the zero-bias reading. The change in zero-bias capacitance as a function of time under reverse bias together with a knowledge of the donor-density profile in the region of the applied electric field enabled the calculation of the local lithium mobility, i.e., the mobility at the edge of the junction. The lithium-diffusion constant could then be obtained by use of the Einstein relation.

C. THEORY

The electric field, $\mathcal{E}$, at the zero-bias junction edge is obtained from the donor-density profile by

$$\mathcal{E} = \frac{e}{\epsilon} \int_{w_0}^{w_3} N_D \, dw \tag{6}$$

where

- e is electron charge
- ϵ is permittivity of silicon
- N_D is donor density
- w_0 and w_3 are depletion widths at zero and 3-volts bias, respectively.

The rate of change of w_0 is obtained by differentiation of the equation for cell capacitance:

$$\left| \frac{dw_0}{dt} \right| = \frac{\epsilon A}{C_0^2} \frac{dC_0}{dt}, \tag{7}$$

where C_0 is the capacitance of the junction at zero bias and A is the cell area. A measure of the lithium mobility, μ_{LO}, at the junction edge is obtained through the relation

$$\mu_{LO} = \frac{1}{\mathcal{E}} \left| \frac{dw_0}{dt} \right| \tag{8}$$

This method was applied to a total of twenty-five Lopex and Float-Zone test-diodes of 10 and 30 ohm-cm starting material. In fourteen Lopex cells, the values of diffusion constant ranged from 0.05 to 0.28 D_F; in eleven Float-Zone cells, the values ranged from 0.10 to 1.0 D_F. Recovery experiments after a 1-MeV electron fluence of 10^{13} e/cm^2 were made on twelve of these diodes. Unexpectedly, the recovery rates obtained yielded a value for the diffusion constant of lithium in the bulk of the collection region of the cell which was close to D_F, the value for free lithium.

Since the values measured at the junction edge were generally well below this value, it was considered possible that the diffusion constant near the junction edge had been lowered due to a high density of crystal imperfections near the surface and the boron-diffused region. Accordingly, during the present contract effort, the theory of the method has been generalized to consider the diffusion constant for larger distances into the base region. The measurement is performed as follows: a reverse bias V_a is applied briefly and the measured capacitance, C_a, gives the depletion width, w_a, for this bias. A reverse bias, V_b, where $V_b > V_a$, is then applied steadily to the cell. Periodically, the bias is reduced, and the bias voltage for which the capacitance is equal to C_a is found. This bias voltage, the measuring bias, will increase from the initial value, V_a, as a function of time at bias V_b due to the drift of lithium across the plane at w_a. When the measuring bias is found, the cell is returned to the bias V_b. This procedure is repeated until a plot of measuring bias as a function of time is obtained.

The change in cell capacitance is given by

$$dC = \frac{dQ}{V} - \frac{Q}{V^2}\, dV, \tag{9}$$

where

$$Q = e \int_{w_0}^{w_a} N_D \, dw$$

and

$$V = V_{p\text{-}n} + V_a ,$$

and V_{p-n} is the junction voltage at zero bias. Implicit in Equation (9) is the assumption that $C = Q/V$, which is strictly true only for a parallel-plate capacitor with no charge in the volume between plates. It does not apply to the general p-n junction where $C = dQ/dV$ (Reference 20). However, for simple distributions, such as the linearly graded junction, this Equation is true to within a constant factor ($C = Q/(3V)$ for a linearly graded junction). Several of the lithium cells tested previously exhibit a fairly good approximation to a linearly graded junction. Consequently, diffusion-constant probes will be limited to cells which satisfy this condition. The correction factor will drop out of the Equation when $dC = 0$.

In the measurement, $dC = 0$, therefore, Equation (4) reduces to

$$\frac{dQ}{dt} = \frac{Q}{V} \frac{dV}{dt} , \tag{10}$$

where dQ is the quantity of charge which has drifted across the plane at w_a with the cell at bias V_b. This quantity is also given by

$$\frac{dQ}{dt} = e\mu \mathcal{E} N_{La} A , \tag{11}$$

where N_{La} is the lithium density at w_a and $\mathcal{E}$ is found by integration of Equation (6) from w_a to w_b.

The lithium mobility is obtained from Equations (10) and (11) and the measured value of dV_a/dt.

D. STATUS

Some of the lithium cells have donor-density profiles approximating linear graded junctions. Three of these cells He 867, He 872, and He 887 were chosen for diffusion-constant measurements. Figure 23 gives plots of ΔV_a as a function of time at bias voltage, V_b, for cell He 887. In this cell, measurements were taken for three values of V_a, viz., 0V, -1V and -3V. The bias voltage, V_b, was -7V. The curves are linear to a good approximation for small values of ΔV, i.e., small changes in donor-density distribution. The value dV/dt in Equation (10) is obtained from the slope of these curves. In Figure 23, dV_0/dt is 8×10^{-4} V/min, dV_1/dt is 1.8×10^{-3} V/min, and dV_3/dt is 2.2×10^{-3} V/min. The other quantities in Eqs. (10) and (11), i.e., Q, $\mathcal{E}_a$ and N_{La} are obtained from the donor-density profile. The lithium mobility and diffusion constant are

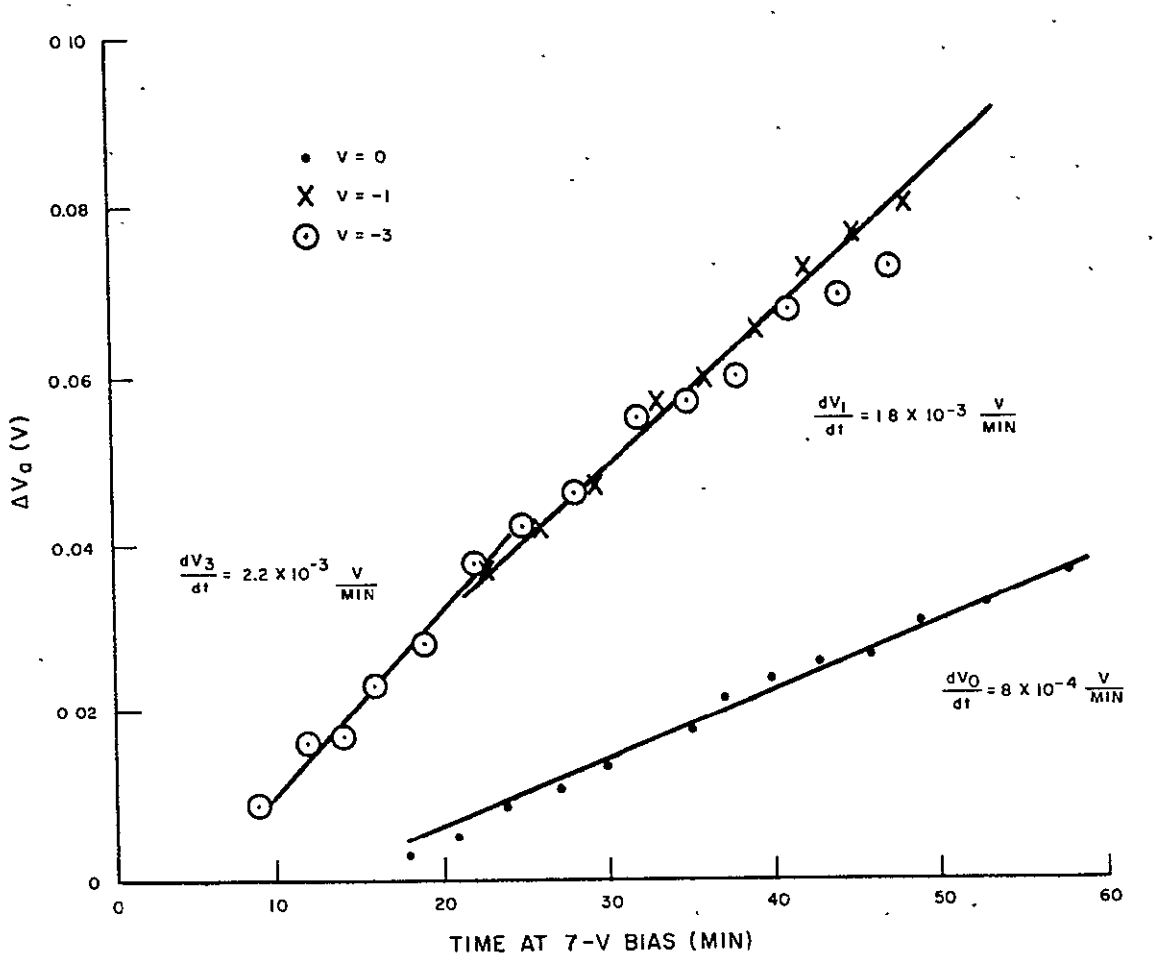

Figure 23. Plots of Change of ΔV_a Versus Time

thereby obtained as a function of distance, w_a, from the junction. The following tabulation gives the values of lithium-diffusion constant, D_{La}, (calculated from the lithium mobility by the Einstein relation) at three different values of w_a for each of the three cells tested.

Cell	V_a (Volts)	w_a (μm)	D_{La} $cm^2/sec \times 10^{15}$
He 867	0	1.30	3.9
	-2	2.30	6.5
(V_b = -10V)	-5	3.05	>8.5
He 872	0	1.24	3.3
	-2	2.12	9.5
(V_b = -8V)	-4	2.58	5.6
He 887	0	1.35	3.9
	-1	2.00	4.8
(V_b = -7V)	-3	2.75	6.8

The diffusion constant obtained at $V_a = 0$ is that at the edge of the depletion region. It is seen that in each of the cells, the diffusion constant is smallest at the depletion region edge and, that in two of the three cells, the diffusion constant increases monotonically with distance from the junction as had been hypothesized. It should be stated that the error in these measurements could be quite large since the donor-density profile is not strictly linear as was assumed in writing Eq. (10), and since donor-density variations are probably present at a given distance, w, from the junction. However, it is felt that these are less than ±30 percent; consequently, the measurements confirm the hypothesis of lowering of the lithium-diffusion constant near the junction.

SECTION VI

LOW-TEMPERATURE MEASUREMENTS

Hall-coefficient and resistivity measurements have been used to investigate the crystal-growth and irradiation-temperature dependence of the introduction rate and room-temperature annealing of carrier-removal defects in lithium-doped silicon. These studies are necessary to understand the mechanisms by which primary defects react with lithium. The reaction products (the secondary defects) are formed during the thermal reordering processes which take place after bombardment produces the primary vacancy-interstitial pair. The electrical properties of electron-irradiated silicon at moderate electron energies (E_e = 1 to 2 MeV) are dominated by these secondary defects. In general, impurities are immobile at or below room temperature, but lithium is an impurity which is highly mobile at room temperature. This mobility makes it possible for lithium to diffuse to radiation-induced defect sites. Evidence to date indicated that the interaction of lithium with the defects neutralized the degrading effect of these defects on the electrical properties of silicon solar cells.

In order to guide the production of radiation-resistant cells, it was necessary to know the ideal quantity of lithium required in the base region of the cell, and the way in which lithium interacted with phosphorous, oxygen, and radiation-induced vacancies.

The best available way of obtaining this information in its least ambiguous form is by studies of the Hall-effect and resistivity in specially prepared bars of silicon. The information obtained from such a study is recognized as being vital to the design of semiconductor devices containing lithium such as the solar cell.

The results of Hall-effect and electrical-conductivity measurements on electron-irradiated silicon doped with lithium are presented in Appendix B to this report; this is in the form of a complete scientific paper which has been approved for publication in the Physical Review. Some very important conclusions flowing from this investigation are given in the next section.

SECTION VII
CONCLUSIONS

A. GENERAL SUMMARY

The work performed on the present contract, by pursuing basic material studies and device studies in parallel, has produced significant advances in the understanding of the defect interactions, dynamics, and general prospects of lithium solar cells. The dynamics of lithium in silicon has been studied under conditions analogous to those which would be experienced in a practical lithium solar-cell array in a high-flux trapped space-radiation situation, namely in orbit near Earth, Jupiter or any other planet.

As a result of this, and the work of other contractors funded by JPL in 1968-69, the general confidence that we know what is happening in lithium cells has increased in many ways in the last year.

In the present project, the most striking new concepts have emerged from the Hall measurements of lithium-doped silicon bars, where no previous low-temperature work had been done. The work reported here has provided the first firm clues to the basic mechanisms of interaction of lithium with radiation-induced monovacancies in silicon. Further studies of these mechanisms should lead to concepts of great value in cell design. The cell measurement work has also yielded a surprising amount of novel data, especially the further development of "a capacitance probing" techniques which allow the monitoring of gross lithium motion in real time.

Another highly significant result from this work is that one case of the vitally important group of phenomena termed "redegradation" has been correlated with the gradual change in a lithium concentration gradient in the cell. Also, for the first time, a possible non-destructive measurement of the diffusion constant of lithium has been elaborated. Several other sophisticated techniques have demonstrated different facets of the behavior of lithium-doped solar cells. As a result of some experiment design work on this contract, the same techniques can shortly be applied on solar cells cooled to about -150° C. While this temperature range is very important for studies of physical mechanisms, it also simulates the thermal conditions of outer-planetary probe missions and solar planetary eclipses.

B. LITHIUM CELLS AND DIODES

During the present contract, the effort on characterization of lithium cell properties and performance has uncovered many different modes of recovery and degradation in lithium-doped diodes. The question of ultimate success depends on whether these modes can be controlled successfully, repeatably and economically. Several of the factors which have to be worked on are now clear. The work described, and previous work by the same group, on actual solar cells and model solar cells, has established that the following device parameters play a role in controlling the performance, dynamics, and stability of the cells tested: (1) density of lithium at the edge of the depletion region, (2) density gradient, of lithium near the junction, (3) resistivity of starting material, (4) gross lithium mobility, and (5) oxygen content. The possible influence of differences in n-type dopants in the starting material, and of decreases in lithium diffusion constant near the cell junction has also been noted. Clearly, not all important processing problems for lithium cells have yet been solved. It is also clear that there is at least one type of cell redegradation which is unrelated to minority-carrier lifetime redegradation. In spite of the very complex nature of lithium solar cells, revealed in the reported work, it is possible to draw from the results of this work many conclusions concerning cell performance and stability and some reasonable prospect of success in achieving control of the dynamics of lithium in the cell.

The first conclusion is that Float-Zone or Lopex cells with high lithium density at the junction ($N_{LO} \gtrsim 10^{15}$ cm^{-3}) and high density gradient ($N_{LO} \gtrsim 10^{19}$ cm^{-4}) do not give good long-term performance. Either the cells have poor initial performance, e.g., C4 cells-batches I and IV, or suffer some type of redegradation, e.g. T3 cells and cells of TI 900 series. The redegradation or degradation of this type of cell can occur either due to deterioration of junction characteristics correlated with gross motion of lithium in the junction region or by loss in short-circuit current (lifetime redegradation). In general, redegradation in these cells is less severe after high electron fluences ($\gtrsim 10^{15}$ e/cm^2) than after low fluences ($\lesssim 10^{14}$ e/cm^2). The one advantage of these cells is the very rapid recovery they undergo, even after high fluences, e.g., cells of group T3(3).

On the other end of the lithium density scale, cells with low lithium density, regardless of silicon type, have displayed good stability properties after recovery from low to moderate electron fluences ($\lesssim 10^{15}$ e/cm^2). These cells usually have good initial performance characteristics. Crucible grown cells with low lithium density usually have very slow recovery rates, e.g., C1 cells; an exception is the behavior of lot T2 cells which recovered very rapidly despite the fact that starting silicon was specified as "quartz-crucible." The one basic difficulty with these "lithium lean" cells has been the tendency to develop series resistance problems after heavy irradiations. This problem, which is clearly

due to a large increase in silicon resistivity, and is evidently aggravated by high resistivity (> 20 Ω-cm) in the starting material, occurred in T2(3) and C4(11) cells irradiated to 3×10^{15} e/cm^2 and in three Heliotek cells irradiated to 10^{16} e/cm^2 during the previous contract (see Appendix A).

The series resistance problem has indeed been correlated with a high total carrier removal in lithium-doped silicon after recovery from electron damage. This can amount to almost total carrier loss when the electron fluence is comparable to the lithium density. (See Appendix B). However, other samples of the "lean-lithium" solar cells have already shown to be competitive with the n/p solar cell in radiation resistance. After irradiation to low and moderate electron fluence values, low-density cells have been tested, e.g. T2(1) and T2(2) cells, which are 5 to 15 percent better after recovery than ≈ 10.5 percent efficiency, 10 Ω -cm n/p control cells irradiated to the same fluence value.

The best possibility for stable, high-performance, highly radiation-resistant lithium cells in the range of moderate lithium density (N_{Li} = 3 to 10×10^{14} cm^{-3} at the edge of the depletion region) and density gradient $\left(\frac{dN_{Li}}{dw} \lesssim 10^{19}\ \text{cm}^{-3}\right)$ and moderate resistivities of starting n-type silicon ($\rho \approx 10\,\Omega$ -cm, phosphorus doping).

Cells of this description, both Float-zone cells, e.g., He800 series (See Appendix A), and crucible grown cells, e.g., H2 cells, have displayed outputs after recovery greater than those from 10 Ω-cm n/p cells. These cells also have shown good long-term stability over a wide fluence range. It should be noted that, while moderate starting resistivities are good from a device point of view, the testing of lithium-doped cells and bulk material of very high purity (high initial resistivity) has been, and continues to be very valuable in uncovering the physical mechanisms of the lithium cell, since the interfering action of the dopant(s) is eliminated.

An anomaly observed during the experiments remains unexplained: The recovery rate in T2 ("crucible grown") cells which was 2 orders of magnitude higher than expected. It is possible that the starting silicon for the "crucible grown" cells was somehow made deficient in oxygen during ingot processing. It is otherwise an unusual transgression of the general rule that lithium moves more slowly in the presence of oxygen.

A second anomaly, the failure of antimony-doped C2 cells to recover, is also not fully explained. However data on the donor-density distribution in these cells leads to a strong suspicion that little or no lithium is present near the junction.

C. HALL MEASUREMENTS

Silicon Hall bars of two types of crystal growth and two lithium concentrations were bombarded at about twenty controlled temperature (T_B) levels between liquid-nitrogen (79°K) and 280°K. At all temperatures, carrier-removal rates ($\Delta n/\Delta\Phi$) were lower than for Stein's comparable irradiations of phosphorus-doped silicon. The difference was greatest at the low temperatures. Introduction rates of carrier-removal defects were exponentially dependent on the reciprocal of bombardment temperature for both types of crystal growth, but the slopes and limiting temperature values differed. The temperature dependence is not consistent with a simple charge-state-dependent probability of interstitial-vacancy dissociation and impurity-vacancy trapping.

Following bombardment, the temperature dependence of the carrier concentration and carrier mobility in the lithium-doped samples was measured periodically in the conventional manner. A characteristic pattern of reappearance of carriers (annealing of carrier removal) and disappearance of charged-scattering centers (annealing of mobility) was observed in Float-Zone refined silicon at room temperature. Such recoveries did not occur so strongly in crucible-grown silicon and a different pattern of recovery was observed in this oxygen-rich material.

It is thus clear that some processes specific to lithium as a dopant are being observed. In silicon doped with phosphorus, arsenic, boron, etc., there is no similar change of carrier concentration and mobility with time at room temperature. It is very likely, although not proven, that the interactions seen in majority-carrier removal centers are the same as those observed in recovery of minority-carrier lifetime.

A surprising feature of the behavior of Float-Zone silicon is the regeneration of of donors after the bombardment (see Figure I-3 of Appendix B. It was previously thought that, while lithium would be removed during the formation of the second complex or "recovered-damage center" of Table VII, no net change in carrier concentration would occur. The data indicates an unexpected partial dissociation of the first complex (Li-V) which, however, does not occur when oxygen is present.

Results suggest that a lithium-oxygen-vacancy (Li-O-V) complex is produced by electron bombardment in quartz-crucible silicon, and alithium-vacancy (Li-V) complex in zone-refined silicon. The mechanism of room-temperature annealing is attributed to neutralization of carrier-removal defects by lithium interaction in crucible silicon, and by both lithium interaction and defect dissociation in zone silicon. The Li-V defect is loosely bound compared to the oxygen-containing Li-O-V defect.

Thus, to fit the above new evidence, the simple schemes of damage and recovery which were proposed in previous reports require only slight modification, as follows:

- DAMAGE CENTERS FROM REACTION OF Li^+ AND $[Li\ O]^+$ WITH V

  F.Z.: $Li^+ + V^- + e \rightarrow [Li\text{-}V]^-$ [CARRIER REMOVAL CENTER]

  Q.C.: $[Li\ O]^+ + V^- + e \rightarrow [Li\ O\text{-}V]^-$ [CARRIER REMOVAL CENTER]

- ROOM-TEMP RECOVERY IS COMPLEXING OF Li WITH DAMAGE CENTERS

  F.Z.: $[Li - V]^- + Li^+ \rightarrow Li\text{-}V\text{-}Li$ [ANNEALED CENTER]

  Q.C.: $[Li\ O\text{-}V]^- + Li^+ \rightarrow Li\ O\text{-}V\text{-}Li$ [ANNEALED CENTER]

- IF OXYGEN IS NOT INVOLVED IN THE INITIAL DAMAGE CENTER, THE CENTER IS UNSTABLE AND DISSOCIATES

  $[Li - V]^- \rightarrow Li^+ + V^- + e$

- OTHER RECOVERY CENTERS

  (1) 0.08 eV - A COMPLEX DEFECT CENTER CONSISTING OF O, V, AND Li IN AN UNKNOWN ARRANGEMENT

  (2) ANNEALED A-CENTER

Based on the working assumption that the carrier-removal centers observed in this experiment also act as the dominant recombination-centers in irradiated lithium-doped silicon solar cells, several possible mechanisms for the minority-carrier lifetime degradation, annealing, and redegradation processes can be postulated. Thus, it can be postulated that the charged LiOV and Li-V complexes reduce the minority-carrier lifetime. Then lithium atoms complex with radiation-induced defects, and thereby anneal the initial decrease of minority-carrier lifetime caused by these defects. A second annealing process is the dissociation of defects such as the Li-V complex which does not contain oxygen. The fate of these slowly-generated free vacancies is not known. Lifetime redegradation in the annealed-solar cells could then be attributed to the instability of annealed defect complexes (e.g., Li-V-Li), which do not contain oxygen. In this scheme, the degree of redegradation observed in the post-recovery period of irradiated cells would then depend on the relative number of annealed centers containing oxygen compared to those not containing oxygen.

Further work on analogous experiments involving minority-carrier lifetime measurements will be needed before these models can be confirmed. However, the new evidence of the participation of lithium in slow changes in majority-carrier removal and majority-carrier mobility has put this study of models,

for the first time on a firm quantitative basis and for the first time, indicated the concentrations, charge states, and energy levels of the defects involved.

The results of this experiment provide important information required in the design of radiation-hardened solar cells. For example, silicon solar cells intended for use on a spacecraft in a radiation environment of low intensity should be fabricated from silicon containing sufficient oxygen to stabilize the radiation damage, and lower the carrier-removal rate. The increase of the annealing time constant with oxygen concentration would be limited to a value consistent with the damage rate. In contrast to this design, a spacecraft operating in a radiation environment of high intensity would require solar cells fabricated from oxygen-lean silicon. Thus float-zone silicon would be used since the experimental results show that the time constant of annealing is very short in this type of silicon. The disadvantage of higher carrier-removal rates in this type of silicon is partially compensated by the dissociation of carrier-removal defects during the annealing process, with the resultant increase of carrier density. It is clear that trade-offs in speed of annealing, carrier-removal rate, and stability can be made to meet the requirements of a mission in space.

D. FUTURE WORK

The technical approach to a future program is to perform and analyze particle irradiations and physical measurements on special test-diodes, government-furnished solar cells, and bulk silicon samples. The test-diodes will be made from material of the highest possible purity, having accurately known, but carefully varied, defect concentrations. Samples of similar materials used in the fabrication of test-diodes will also be used in making Hall-bars and lifetime bars for use in the bulk silicon studies. Characterization of the silicon used in this program with respect to the oxygen concentration, lithium concentration and distribution, and dislocation density will be accomplished to ensure the determination of the influence of these impurities on the damage and annealing mechanisms in lithium-containing solar cells.

The main experimental tactics of the exploration of lithium cell recovery and redegradation phenomena will be: (1) to furhter elucidate carrier-removal phenomena in Hall-bar experiments; (2) to predict, for these data, the probable corresponding effect in a p-on-n (Li) diode structure as regards both carrier removal and minority-carrier transport in the cell; and (3) to attempt to verify this prediction in an experimental p-on-n (Li) structure (this being either a lithium solar cell supplied by a cell manufacturer or an RCA-fabricated lithium-containing "Test-Diode," depending on the suitability of those available for the experiment).

One predictable major contingency exists. It is still a question for some debate whether the silicon defect centers producing resistivity change under irradiation are the same structures as those producing minority-carrier lifetime change. Until this is answered, it is not possible to transfer findings on bulk silicon to cell design with 100-percent confidence. If the above solar-cell measurements do not allow a suitable correlation of carrier-removal defects with minority-carrier removal centers, some effort may be diverted, as necessary, to perform more unambiguous minority-carrier lifetime measurements by photoconductive decay in lithium-doped silicon bars.

LIST OF REFERENCES

1. J. J. Wysocki, P. Rappaport, E. Davison, R. Hand, and J. J. Loferski, Appl. Phys. Letters 9, 44 (1966).
2. T. R. Waite, Phys. Rev. 107, 463 (1957).
3. G. Brucker, T. Faith, and A. G. Holmes-Siedle, Final Report on Contract No. NAS 5-10239, prepared by RCA and issued March 8, 1968.
4. L. Valdes, Proc. IRE 42, 420 (1954).
5. W. Rosenzweig, Bell Sys. Tech. Journ. 41, 1573 (1962).
6. J. J. Wysocki, IEEE Trans. on Nuclear Sci., NS-14 (December 1967).
7. T. J. Faith, G. J. Brucker, A. G. Holmes-Siedle, and R. S. Neadle, IEEE Trans. on Nuclear Sci. NS 15, 61 (1968).
8. T. J. Faith, G. J. Brucker, A. G. Holmes-Siedle and J. Wysocki, Conf. Record of the Seventh Photovoltaic Spec. Conf. IEEE Catalog No. 68C63ED, 131 (1968).
9. M. Wolf and H. Rauschenbach, Adv. Energy Conversion 3, 455 (1963).
10. H. Gummel and F. Smits, Bell Syst. Tech. Journ. 43, 1103 (1964).
11. Properties of Solar Cells C4-1 to C4-60, private communication from P. Berman.
12. G. Brucker, T. Faith, and A. Holmes-Siedle, Conf. Record of the Seventh Photovoltaic Spec. Conf. IEEE Catalog No. 68C63ED, 146 (1968).
13. P. A. Iles, Conf. Record of the Seventh Photovoltaic Specialists Conf. IEEE Catalog No. 68C63ED, 117 (1968).
14. W. R. Cherry and R. L. Statler, GSFC Report X-716-68-204 (April 1968).
15. M. B. Prince, J. Appl. Phys., 26, 534, (1955).
16. C. Sah and V. Reddi, IEEE Trans. on Electron Devices ED 11, 345, 1964.
17. J. J. Loferski Private Communication.
18. E. M. Pell, J. Appl, Phys. 31, 291 (1960).
19. E. M. Pell, Phys. Rev. 119, 12222 (1960).
20. A. K. Jonscher, Principles of Semiconductor Device Operation, Wiley, New York (1960).

APPENDIX A

LONG TERM STABILITY OF LITHIUM-DOPED SOLAR CELLS IRRADIATED WITH ELECTRONS, PROTONS, OR NEUTRONS*

T. J. Faith, G. J. Brucker, A. G. Holmes-Siedle and J. Wysocki**

RCA Astro-Electronics Division, Princeton, New Jersey

SUMMARY

Stability of photovoltaic response and diffusion length in lithium-containing p/n solar cells after irradiation by 1-MeV electrons, 16.8 MeV protons, or 14 MeV neutrons was monitored for periods ranging from 7 months to 2 years. Neutron and proton irradiated cells maintained stable outputs. Stability of electron irradiated cells depended on lithium density profile measured near the junction. Results show the need for correlation of photoresponse measurements with the density and motion of lithium near the junction. Correlation between junction capacitance changes and redegradation observed in some of the cells tested will be discussed. This, together with data on more stable lithium cells, yields tentative criteria for producing stable lithium cells.

It is noted that these cells were developmental devices made under NASA direction with the purpose of defining parameters for stable and efficient cells with the aid of studies such as those reported herein.

INTRODUCTION

Lithium containing p/n silicon solar cells have been observed to recover spontaneously at room temperature from radiation damage caused by electrons, protons, and neutrons.[1] More recently, redegradation of such cells has been observed after recovery.[2,3] This paper presents a study of the long-term variations of the photo-response and minority-carrier diffusion length of lithium cells after irradiation by protons, neutrons, and electrons. These data are compared with similar data on unirradiated cells. The stability of solar cells is frequently referred to as the variable which is being studied. A stable cell is defined as one which does not redegrade.

The radiation-resistance of lithium cells to protons and neutrons is superior to that of either commercial p/n or n/p cells.[4,5] After electron bombardment, however, performance levels of recovered lithium cells and commercial n/p cells are quite similar.[6] Thus, the stability of lithium cells after recovery from electron bombardment is of prime importance if these cells are to be competitive with n/p cells. The main body of this paper will deal with electron-irradiated lithium cells. In addition to the photovoltaic characteristics, (electron-voltaic) minority-carrier diffusion length measurements[7] and reverse-bias capacitance measurements will be reported.

DESCRIPTION OF EXPERIMENT

A large group of lithium-containing p/n silicon solar cells, furnished under NASA Contract No. NAS5-10239, were irradiated by 1 MeV electrons, 16.8 MeV protons, and 14 MeV neutrons in 1966-67. Measurements of cell parameters, including photovoltaic I-V characteristics under illumination by a filtered tungsten source at 100 mW/cm^2, and minority-carrier diffusion length[7] (based on the electron-voltaic method), were made both before irradiation and at intervals of several weeks after irradiation up to the present. From these measurements and from pre-irradiation capacitance measurements[8] on the cells, information has been obtained on the degree of stability of lithium-containing cells over a wide range of cell parameters for a proton fluence of 2.4×10^{12} p/cm^2, a neutron fluence 4.5×10^{12} n/cm^2, and for electron fluences ranging from 10^{14} to 10^{16} e/cm^2. The duration of these tests range from 7 months to approximately 2 years. In addition to the experiments on irradiated cells, stability tests of 11 months' duration have been made on unirradiated cells. The cells in all the tests, both irradiated and unirradiated, were stored at room temperature, under normal room illumination (fluorescent) and were at open-circuit condition except for short periods of time (a few hours at most while photovoltaic, electron-voltaic or reverse-bias capacitance measurements were being made). The long-term reproducibility of the photovoltaic measurements from short-circuit current measurements is ±5 percent; the

* Work supported by National Aeronautics and Space Administration (Contract No. NAS5-10239) and Jet Propulsion Laboratory Contract No. 952259.

** Present address: Xerox Corporation, Rochester, New York.

Published in Conf. Record of the Seventh Photovoltaic Spec. Conf. IEEE Catalog No. 68C63ED, 131 (1968).

diffusion-length measurements have an uncertainty of ±10 percent. In all tests, the cell area used in the calculation of performance parameters was the total cell area including contact fingers and contact strips. In the 1-MeV electron experiments, the contact strip area of the NASA Furnished 1 by 2 cm Texas Instruments (TI) cells[3] was ≈0.1 cm^2; that of the 1 by 2 cm Heliotek (He) cells[4] was ≈0.05 cm^2.

PROTON-IRRADIATED CELLS

This group of eight lithium-containing cells was irradiated by 16.8 MeV protons to a fluence of 2.4 x 10^{12} p/cm^2 in 1967. The results of the experiment were reported previously.[4] After completion of the bombardment, the cells were periodically monitored to check their long-term stability. The results over a period of 2 years are shown in Figure 1. Normalized power, P/P_o, is plotted versus time after bombardment in days. Standard n/p and p/n cells irradiated at the same time as the lithium cells are also shown in Figure 1. Power output of the lithium cells recovered within a few days after the bombardment, and thus $P/P_o = 1$ at time $t \approx 0$ in Figure 1. The non-lithium cells did not recover their output power and remained constant for the period shown. Redegradation of the lithium cells amounting to 10 percent occurred after a year; however, after another year, no further degradation has occurred.

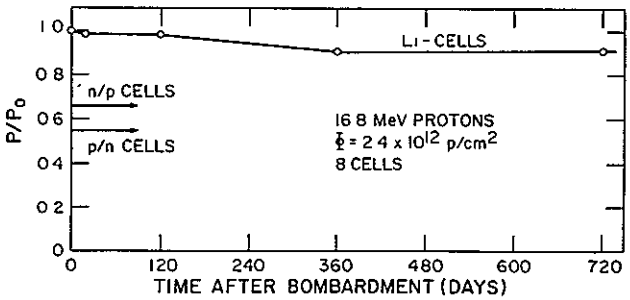

Figure 1. Stability of Power of Lithium-Doped p/n Solar Cells after Bombardment by 16.8 MeV Protons to 2.4 x 10^{12} p/cm^2

NEUTRON-IRRADIATED CELLS

This group of five cells containing lithium was irradiated by 14 MeV neutrons to a fluence of 4.5 x 10^{12} n/cm^2 in an experiment which was previously reported.[5] After completion of the experiment, the cells were periodically measured and the results are shown in Figure 2. Standard n/p and p/n cells without lithium were irradiated with the lithium cells. As shown in Figure 2, the standard cells degraded in output power and remained at this lower level for the duration of the measurements. The lithium cells continued to recover after bombardment and saturated at 80 percent of the original output power. They did not indicate any redegradation over a period of 17 months.

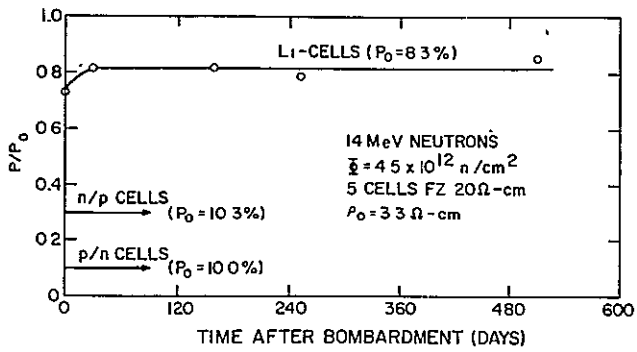

Figure 2. Stability of Power of Lithium-Doped p/n Solar Cells after Bombardment by 14 MeV Neutrons to 4.5 n/cm^2

ELECTRON-IRRADIATED CELLS

Cells Irradiated to 10^{16} e/cm^2

During February and March, 1967, a large number of government-furnished cells were irradiated to 10^{16} e/cm^2 at a flux rate of approximately 3 x 10^{15} e/cm^2/hr. These cells were manufactured by Texas Instruments Corporation[9] and Heliotek Division of Textron Electronics.[10] Periodic measurements of diffusion lengths and photo-response characteristics have been made on 17 cells with varying phosphorus background doping densities (given as resistivity, ρ_o, in the tables and figures) and lithium densities, and different growth methods.

Table I lists values of short-circuit current, J, and maximum power, P. Readings made before bombardment and approximately 1 hour, 4 days, 3 months, 8 months, 1 year, 16 months, and 19 months after bombardment are included. Pre-irradiation values of lithium concentration, N_{LI}, measured at a distance of ≈1 μm from the junction, and based on reverse-bias capacitance measurements[8] were found in early work under contract NAS5-10239,[6] and the cells were listed in order of increasing lithium concentration. In more recent work under NAS5-10239,[11] the cells were placed in three categories as to lithium concentration. Table I lists the cell performance histories according to this categorization which is as follows: the first group of six cells had initial lithium concentrations less than 2 x 10^{15} cm^{-3}; the second group of five cells had concentrations between 2 and 5 x 10^{15} cm^{-3}; the third group of four cells had concentrations between 7 and 10 x 10^{15} cm^{-3}. A fourth group of two cells, He 248P and He 249P, represent a special group of cells with a diffused heavily-doped phosphorus region near the junction.

The six cells of Group 1, although they have recovered to some extent, all have power levels below the ≈5.3 mW/cm^2 previously reported[12] for 10Ω-cm n/p cells with initial power of ≈ 11.3 mW/cm^2 after a fluence of 10^{16} ~ 1 MeV electrons/cm^2. (Reference 12

TABLE I. STABILITY OF GFE* CELLS IRRADIATED TO 10^{16} e/cm^2 IN FEBRUARY-MARCH 1967

Sample No.		ρ_o and Growth Method	Initial Measurement (December 1966)		Post-Irridation Measurements													
					1 Hour		4 Days		June 1967		November 1967		February 1968		July 1968		October 1968	
			J_o	P_o	J	P	J	P	J	P	J	P	J	P	J	P	J	P
Group 1	TI 167	20 FZ	30.8	10.8	10.8	2.3	10.9	2.2	12.9	3.0	14.5	2.9	15.4	3.2	15.1	3.2	16.0	3.3
	He 342	100 FZ	29.6	-	-	-	-	-	18.3	-	19.6	3.3	21.5	4.1	21.0	3.5	21.1	3.6
	TI 63	20 FZ	29.6	10.4	9.5	2.0	11.2	2.1	15.7	3.4	17.6	3.9	19.3	4.5	19.3	4.6	20.0	4.8
	TI 71	20 FZ	28.5	6.3	9.4	1.6	11.6	1.8	16.2	2.8	18.7	3.7	20.6	4.3	20.6	4.5	21.3	4.6
	He 341	100 FZ	28.5	-	-	-	-	-	21.0	-	20.4	2.6	22.0	3.3	20.0	2.4	20.0	2.4
	He 340	100 FZ	28.6	-	-	-	-	-	21.2	-	21.2	2.9	22.9	3.8	21.5	3.0	20.6	2.7
Group 2	TI 112	20 QC	28.0	10.5	9.5	2.5	10.2	2.7	17.4	4.0	19.7	4.9	20.6	5.6	20.7	5.9	20.8	6.0
	TI 113	20 QC	27.5	9.9	9.2	2.5	9.8	2.7	16.8	-	19.0	5.2	20.2	5.8	19.7	5.6	19.8	5.6
	TI 168	20 FZ	28.8	11.1	9.9	2.5	13.5	3.3	16.7	4.0	17.6	4.4	18.6	4.8	18.0	4.6	18.7	4.9
	TI 42	20 FZ	28.6	9.2	8.3	2.0	12.2	3.0	15.1	3.9	16.3	4.2	17.2	4.6	16.2	4.3	17.4	4.8
	TI 161	20 FZ	27.2	10.8	8.9	2.6	17.1	5.1	17.4	5.3	17.4	5.5	18.2	5.8	17.1	5.4	18.0	5.8
Group 3	TI 128	20 L	28.5	10.8	9.1	2.5	16.7	5.0	16.0	4.9	15.7	3.4	16.2	3.6	15.4	4.0	16.4	3.9
	TI 127	20 L	30.2	10.2	9.4	2.6	17.8	5.2	16.9	4.9	15.3	3.0	13.8	2.7	14.7	2.9	15.8	3.1
	TI 132	20 L	29.8	-	10.7	1.5	16.2	4.8	15.2	4.1	15.8	4.0	16.2	4.1	15.1	3.7	16.2	4.0
	TI 166	20 FZ	25.2	8.7	9.6	2.5	15.8	4.5	14.8	4.2	15.1	4.1	15.5	4.1	14.9	3.9	15.5	4.1
Group 4	He 248P	1000 FZ	24.8	8.4	16.6	3.8	22.3	6.1	22.5	5.0	22.2	6.3	23.5	7.0	23.0	6.7	23.8	6.5
	He 249P	1000 FZ	24.2	8.4	14.2	3.5	20.6	5.7	23.7	6.3	22.2	6.9	22.8	7.4	22.2	7.3	22.7	7.3

* Government Furnished Equipment

NOTES: J is measured in mA/cm^2 FZ is Float Zone L is Lopex

P is measured in mW/cm^2 QC is Quartz-Crucible

is chosen for comparison with the data reported herein, rather than, for example, the more recent Reference 13, due to the similarity in illumination conditions in Reference 12 and the present work; that is, 100 mW/cm^2 filtered tungsten light.)

The three Heliotek cells of Group 1 (He 340, 341, and 342), which were made from high-resistivity (100Ω-cm) starting material showed good recovery of minority-carrier lifetime, as seen from diffusion-length measurements and short-circuit current measurements. As of July, 1968, He 341 had the highest diffusion length (25 μm) of the cells in Group 1; cells He 340 and 342 each had a 20 μm diffusion length. From Table I, it is seen that these three cells also have high values of J relative to the other cells. In spite of this, they have three of the five lowest values of P of all the cells in Table I.

The reason for these low powers is the very low filling factor, $f = P/JV_{oc} \lesssim 0.4$, determined from the photo-response curves of these cells. This low filling factor is attributed to the high resistivity starting material, which, together with the high bombardment fluence, results in a low post-irradiation donor concentration. This could lead to problems in series resistance at the base contact or in parts of the body of the cell where lithium was heavily depleted.

Cell TI 167, which had the lowest lithium density (near the junction) of all the cells in Table I, recovered to~3 mW/cm^2. This cell has remained essentially constant at this power level since June 1967. It appears that this cell has exhausted its free lithium supply near the junction thereby excluding the possibility of further room temperature recovery. Seven TI cells with lower lithium density than TI 167 were dropped from this test soon after irradiation[6] when they displayed a very high series resistance together with a double junction. The photo-response of TI 167 indicates a high series resistance (f = 0.5) and also a significant shunt leakage of $\approx 80\Omega$.

The other two cells of Group 1, TI 63 and 71, continued to show significant recovery 11 months after irradiation. Over the past 8 months, the cells have

remained essentially stable with a slight trend toward further recovery. As of the latest reading, TI 63 has the highest power of Group 1 cells, namely 4.8 mW/cm^2. Both of these cells have low filling-factors; $f \approx 0.6$ in TI 63, and ≈ 0.5, in TI 71. The shunt resistance in both cells is $\approx 200\ \Omega$. The filling factors in the (ρ_o = 20 Ω-cm) TI cells were, however, significantly higher than those in the (ρ_o = 100 Ω-cm) He cells, suggesting that problems such as series resistance can be adequately dealt with by judicious choice of silicon growth method, initial silicon resistivity and lithium doping level. This observation, which goes far in answering some objections to the lithium cell,[14] is corroborated by the behavior of the Group 2 cells which will now be discussed.

The cells of Group 2 had initial lithium densities, N_{Li}, at $\approx 1\ \mu$m from the junction ranging from 2 to 5 x 10^{15} cm^{-3}. The common characteristic of the five Group 2 cells, together with He 248P and He 249P (1000 Ω-cm FZ) is a power level either close to or greater than the 5.3 mW/cm^2 of the 10 Ω-cm n/p cells of Reference 12. Figure 3 gives the maximum power, P, as a function of time, in days, after bombardment. The cells fall into three categories: (a) 20 Ω-cm Quartz-Crucible grown (QC) cells, TI 112 and 113; (b) 20 Ω-cm Float-Zone refined (FZ) cells, TI 42, 161, and 168; and (c) 1000 Ω-cm FZ cells with heavily doped (diffused) phosphorus layer near the junction, He 248P and 249P. No lithium-density data near the junction was obtainable on these last two cells due to the high phosphorus background.

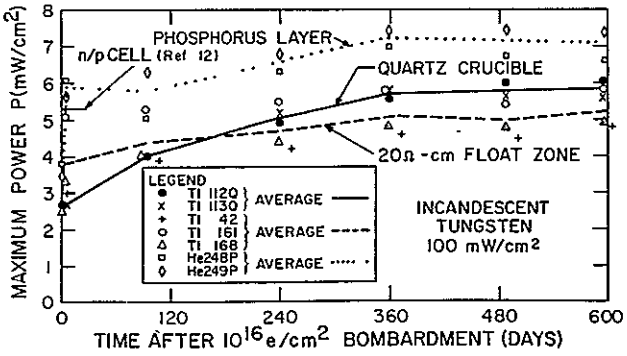

Figure 3. Annealing and Stability of Two-Quartz-Crucible Cells, Three 20Ω-cm Float-Zone Cells, and Two 1000Ω-cm Float-Zone Cells with Diffused Phosphorus Layer after Bombardment by 1 MeV Electron to 10^{16} e/cm^2

The curves for the average values for categories (a), (b), and (c) are represented in Figure 3 by dashed, solid, and dotted lines, respectively. It is seen that the 20 Ω-cm FZ and phosphorus-layer (b and c) cells recover rapidly over a period of several days then undergo an additional but very slow recovery for approximately 1 year. This slow long-term recovery in FZ cells could be explained in two different ways. First, the rapid initial flow of lithium to defects could cause local depletion of lithium near the junction,* leaving some recombination centers after the initial fast recovery unsatisfied in their demand for lithium. Lithium would have to diffuse across large distances to satisfy these centers. A second possible explanation is that, over the long-term, recovery has to compete with some redegradation mechanism; that is, recovery and redegradation mechanisms may be occurring simultaneously. Post-recovery redegradation of performance in lithium-doped cells has been observed here (e.g., Group 3 of the cells in Table I) and elsewhere[2,3] and its cause, although not well understood, has been suggested[15] to be the precipitation of lithium from the supersaturated solution that exists in these lithium-doped p/n silicon cells. (The solubility of lithium at room temperature in n-type silicon is $\sim 10^{13}$ cm^{-3}.) The precipitation of lithium in silicon is very much dependent on the heat-treatment history of the silicon after lithium doping,[16] as well as on the initial lithium doping level and silicon growth method.[17] In any case, in the 7-month period since the end of the first year after bombardment, the power output of these cells has remained constant within experimental uncertainty throughout the past 11 months, as have the other photovoltaic parameters, V_{oc} and J. Thus, if any redegradation has taken place, it has been counterbalanced by additional recovery. In this regard, it is interesting to note that a slight increase in minority-carrier diffusion length has been observed during these last 11 months. Thus, the minority-carrier lifetime in the n-type base region is still slowly increasing, suggesting a small additional recovery.

In contrast to the FZ cells, the QC cells recovered much more slowly at first due to the lowering of the effective lithium diffusion-constant caused by $(Li\text{-}O)^+$ complexing,[17] but continued to recover at a significant rate over the span of a year. At approximately a year after irradiation, the power became stabilized (as did J and V_{oc}). The average powers for each category as of the latest readings were: (a) 5.8 mW/cm^2 for the QC cells; (b) 5.2 mW/cm^2 for the 20 Ω-cm FZ cells; and (c) 6.9 mW/cm^2 for the phosphorus-layer cells. The present (October 1968) series resistance in the QC (category a) cells has been compared with that in the initial measurements made before bombardment. This comparison is shown in Figure 4 which gives the October 1968 I-V curves superimposed on the initial curves through a translation of the axes of the October 1968 curves. The knees of the October 1968 curves are sharper than the initial curves indicating that little, if any, series resistance increase has occurred since the initial measurements. Similar comparisons on the 20 Ω-cm FZ cells (b) show on the average a slight increase in series resistance. In the case of TI 161, the initial and translated October 1968 curves coincide exactly at the knee. In TI 168, the knee of the October 1968 curve being slightly below that of the initial curve ($\Delta V \approx 0.012$ volt, $\Delta J \approx 0.8$ mA/cm^2 near maximum power point). In the case of TI 42,

*Lithium concentration is lowest near the junction.[11]

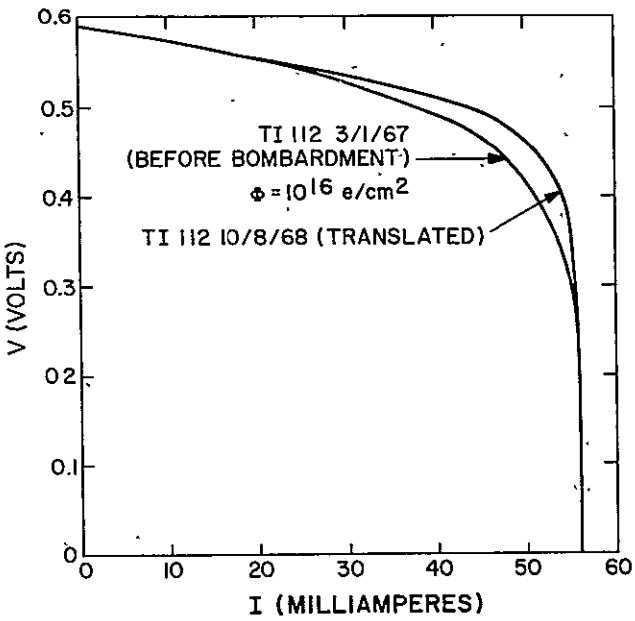

Figure 4. Comparison of Photovoltaic Characteristics of Quartz-Crucible Cell TI 112 Before Bombardment and 19 Months After Bombardment to 10^{16} e/cm^2

the knee of the October 1968 curve is significantly sharper than that of the initial curve, which itself indicated a high series resistance. Comparison of filling of He 248P and He 249P[6] gives (an already low) f = 0.64 initially for both cells. As of October, 1968, f = 0.64 and 0.55 for He 249P and He 248P, respectively. Thus, a filling factor decrease has occurred in He 248P. It is not clear whether this decrease occurred during or after irradiation.

The shunt resistances of the Group 2 cells as of October 1968 were:

TI 112 - 700 Ω;
TI 113 - 500 Ω;
TI 168 - 250 Ω;
TI 42 - 200 Ω;
TI 161 - 1000 Ω;
He 248P - 1000 Ω; and
He 249P - 1000 Ω.

It should be mentioned that, of category (b), cell TI 161 with a lithium density of 5 x 10^{15} cm^{-3} measured at ≈1 μm from the junction recovered to the n/p level of 5.3 mW/cm^2 within 3 months after bombardment. This is significant, since the radiation fluence of 10^{16} e/cm^2 of 1 MeV electrons is much greater than several years' dose in a particularly high-radiation Earth orbit, and in most orbits used, cells will not incur more than 10^{15} e/cm^2. Cells TI 42 and 168, more lightly lithium doped at ≈2 x 10^{15} cm^{-3}, show slower recovery and stabilize at powers slightly below the n/p value (see Table I).

Cells He 248P and 249P have displayed particularly good behavior after irradiation. Though pre-irradiation power values (8.4 mW/cm^2 in each cell) were low, the resistance of the cells to irradiation was high, as seen from the values 1 hour after bombardment. Recovery continued steadily with time. As of the latest reading, approximately 19 months after bombardment, the cells had values of 6.5 and 7.3 mW/cm^2 for P_{max}; that is, ≈30 percent above the value for 10 Ω-cm n/p cells after bombardment at 10^{16} e/cm^2.

All four of the Group 3 cells in Table I (that is, those with a lithium density measured at ≈1 μm from the junction > 7 x 10^{15} cm^{-3}) showed significant redegradation between the fourth day after bombardment (March 10, 1967) and the 240th day (November, 1967). In cell TI 127, this redegradation continued between the 240th and the 360th day to the extent that the value of P on the 360th day approximated that obtained 1 hour after bombardment. The values of P for the other Group 3 cells have remained constant within experimental error since the 240th day. It is noted that three of the four cells in Group 3 were Lopex* cells and that the cell suffering the least severe degradation was the FZ cell, TI 166. The number of cells in this test is too small, however, to make any firm judgments on the relative merits of Lopex and Float-Zone cells. Since November 1967, the cells have stabilized. Averaging over the four cells of Group 3, the initial (pre-irradiation) power was $\bar{P}_o$ = 9.9 mW/cm^2, that 1 hour after bombardment was 2.3 mW/cm^2, that at approximately maximum recovery 4 days after bombardment was 4.9 mW/cm^2 and that, as of the October 1968 reading, 22 months after bombardment, was 3.8 mW/cm^2. Thus, on the average, these heavily-doped lithium cells did recover to a power slightly below the 5.3 mW/cm^2 level found for n/p cells, but subsequently redegraded, then stabilized at a power level approximately 25 percent below that at maximum recovery and 65 percent above the level 1 hour after bombardment. The values of J dropped slightly (less than 10 percent) in these cells during the redegradation process; however, the major factor in the redegradation was the change in the shape of the I-V curves.[18] The (already low) average filling factor, $\bar{f}$, for these cells was ≈0.65 initially. As of the most recent readings, $\bar{f}$ ≈ 0.50. The shunt resistances were ≈70 Ω in TI 127 and TI 166, ≈250 Ω in TI 128 and ≈500 Ω in TI 132.

Cells Irradiated to ≈1.4 x 10^{15} e/cm^2

On November 1, 1968, three TI cells made from 20 Ω-cm FZ silicon with lithium densities from 2 to 3 x 10^{15} cm^{-3} measured at ≈1 μm from the junction, were irradiated to an incremental fluence of 10^{15} e/cm^2 in preparation for an injection-level experiment reported on in this conference.[19] During the injection-level tests, an additional ≈0.4 x 10^{15} e/cm^2 was applied for a fluence of ≈1.4 x 10^{15} e/cm^2. These three cells, which have displayed similar behavior are represented in Figure 5.

*Trademark of Texas Instruments Inc.

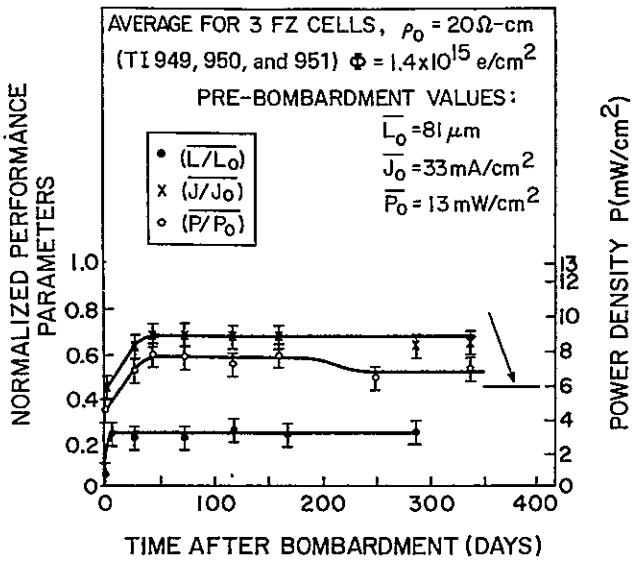

Figure 5. Stability of Performance Parameters in Three 20Ω-cm Float-Zone Cells After Bombardment to 1.4 x 10^{15} e/cm^2

This figure gives plots of the average minority-carrier diffusion length,[7] short-circuit current density and maximum power for the three cells, each normallized to the pre-bombardment values L_o, J_o and P_o, as functions of time (in days) after bombardment. The power density scale is indicated on the right side of the figure together with the power density found for 10 Ω-cm n/p cells after irradiation to 1.4 x 10^{15} e/cm^2.[12] The first diffusion length was taken soon (~5 minutes) after bombardment to 10^{15} e/cm^2. The first $(\overline{J/J_o})$ and $(\overline{P/P_o})$ values, however, were taken 70 minutes after bombardment and therefore reflect the recovery during these 70 minutes; that is, they are higher than the values immediately after bombardment. The initial, rising portions of the curves represent cell recovery. It is interesting to note that the time constant for recovery of the diffusion length, a parameter which is much more sensitive to electron irradiation than either the power or the short-circuit current, is approximately an order of magnitude shorter than that for recovery of power and short-circuit current. This suggests that the bulk lifetime is recovering at a more rapid rate than are the damage effects near the junction. The constant straightline portions of the curves represent least square best fits (in this case a simple average) to a straight line with zero slope. It is seen that $(\overline{L/L_o})$ has remained constant within experimental uncertainty (since recovery) for the 11-month duration of the experiment. However, the normallized power, $(\overline{P/P_o})$, suffered significant redegradation (broken line), from 0.59 to ≈0.50 between ≈5 and 8 months after bombardment, respectively. The normallized power has since stabilized over a 3-month period at ≈0.52, a level of ≈6.8 mW/cm^2 which is significantly above the ≈6.0 mW/cm^2 for 10 Ω-cm n/p cells. Clearly, data over a longer period of time is required to establish whether these cells will remain stable at the present levels.

The stability of $(\overline{J/J_o})$ is questionable. Although all the data points, except the one at ≈250 days, remain constant within experimental uncertainty, there is a noticeable downward trend after the 44-day reading. Decrease in open-circuit voltage, $\overline{V_{oc}}$, from 0.515 to 0.500, and filling factor, $\overline{f}$, from 0.67 to 0.65 were also encountered from the 44-day reading to the present reading. Therefore, the redegradation observed here is due to the combined effect of three parameters: short-circuit current, open-circuit voltage, and possibly series resistance. The shunt resistance in each of these cells was well above 1000Ω.

The stability of the minority-carrier diffusion length suggests that the redegradation problems are localized in the junction area where the p-skin acts as a sink for the mobile lithium ions.

Cells Irradiated to 10^{14} e/cm^2

This section is presented in three parts: (a) four FZ cells irradiated in December 1966; (b) three Lopex cells and one FZ cell irradiated on November 8, 1967; and (c) seven FZ cells irradiated on March 12, 1968.

Cells Irradiated to 10^{14} e/cm^2 in December 1966: Four Float-Zone cells of various starting resistivities have been under investigation since December 1966. These are represented in Table II, where pre-irradiation of initial values are listed, followed by a running account of measurements to date. The cells prefixed with "Ho" were manufactured by Hoffman Electronics Corporation.[20] It may be seen that Sample No. He 55-1 had significantly higher initial values than the other cells and that all cells showed practically complete recovery in photo-response. The photo-response parameters after recovery remained constant within 10 percent from December 1966 through June 1967. Severe post-recovery redegradation in power (approximately 50 percent) in cell 55-1, which was observed in the November 1967 reading, occurred between 6 and 11 months after recovery, and was accompanied by only slight decreases in short-circuit current and open-circuit voltage, and no decrease in diffusion length. A decrease in filling factor, P/JV_{oc}, was responsible for this power drop. The Hoffman cells have remained stable at the post-recovery values for over 18 months, with a slight upward trend evident in Samples No. Ho 5-1 and Ho 6-1. It is noted that reverse-bias capacitance measurements[2] gave values of N_{LI} equal to: 1.7 x 10^{15} cm^{-3} in He 55-1; 1.5 x 10^{14} cm^{-3} in Ho 33-2; 2.4 x 10^{14} cm^{-3} in Ho 5-1; and 4.3 x 10^{14} cm^{-3} in Ho 6-1. Thus, the cells with good long-term stability after a fluence of 10^{14} e/cm^2 were very lightly doped near the junction.

Cells Irradiated to 10^{14} e/cm^2 on November 8, 1967: Four TI cells, three made from 200 Ω-cm Lopex silicon, one from 20 Ω-cm FZ silicon, were irradiated to a fluence of 10^{14} e/cm^2 at a rate of ≈2 x 10^{13} e/cm^2/min. These cells had very high initial performance parameters, P_o and J_o, as shown in Table III, which

TABLE II. STABILITY OF GFE CELLS IRRADIATED IN DECEMBER 1966

Sample No.	ρ_o and Growth Method	Initial Performance 12/66		After Recovery											
				December 1966		January-February 1967		June 1967		November 1967		March 1968		July 1968	
		J_o (mA/cm^2)	P_o (mW/cm^2)	J	P	J	P	J	P	J	P	J	P	J	P
He55-1	20 FZ	29.2	9.2	26.4	9.0	26.5	8.3	25.0	8.3	24.9	4.4	26.2	4.9	26.0	4.4
Ho33-2	10 FZ	24.4	6.6	23.1	6.2	24.6	6.3	22.8	6.6	23.4	6.2	25.0	6.9	25.0	6.7
Ho5-1	100 FZ	24.7	7.7	25.0	8.0	24.7	7.6	25.0	7.7	24.0	8.0	26.6	8.5	26.8	8.5
Ho6-1	1000 FZ	23.3	6.4	23.3	8.0	23.1	7.5	24.5	8.4	24.9	8.6	26.2	9.1	26.0	8.8

NOTE: FZ is Float Zone

TABLE III. STABILITY OF GFE CELLS IRRADIATED TO 10^{14} e/cm^2 IN NOVEMBER 1967

Sample No.	ρ_o (Ω-cm) and Growth Method	October 1967		November 1967		December 1967		March 1968		April 1968		July 1968		October 1968	
		J_o	P_o	J	P	J	P	J	P	J	P	J	P	J	P
TI 952	20 FZ	33.0	12.6	[28.2]	[10.3]	30.0	11.1	28.9	10.2	30.4	10.4	27.7	8.5	28.3	7.8
TI 977	200 L	34.3	12.0	[28.4]	[9.5]	30.2	10.4	28.6	8.9	30.2	9.0	28.5	7.3	28.5	7.1
TI 978	200 L	34.5	13.4	[28.8]	[10.0]	30.6	10.3	29.2	8.5	30.7	8.5	27.0	6.5	28.6	6.7
TI 981	200 L	35.5	12.4	[29.5]	[10.0]	31.5	10.5	30.2	10.3	32.0	11.0	28.5	9.2	30.0	9.3

NOTES: [ ] values 8 days after bombardment L is Lopex

also gives the values of P and J taken at six different times after irradiation. All of these cells have displayed significant post-recovery redegradation. However, the degree of redegradation varies significantly from cell to cell.

TI 977 and 978 both have suffered severe redegredation since ≈100 days after bombardment. This is clearly seen in Figure 6 which gives plots of L, J, P, and V, normallized to the pre-irradiation values, as functions of the time after irradiation. These values are the averages for TI 977 and 978 which have displayed similar behavior. The values of J, P, and V immediately after irradiation were not obtained because diffusion length recovery experiments[21] were made (on all four cells) after irradiation. It is clear, however, that the (electron-voltaic) diffusion length is much more sensitive to irradiation than is the photovoltaic characteristic. The diffusion length ≈5 minutes after bombardment was 0.16 of its original value. Recovery to 0.63 L_o occurred at room temperature in less than 2 hours. In the ensuing ≈240 days, a decrease to 0.50 L_o has occurred. This represents a small fractional change (within the ±10 percent uncertainty in the diffusion length measurement) which would not be expected to significantly affect the photovoltaic parameters since the latter are insensitive to small minority-carrier lifetime changes (varying logarithmically with lifetime). This is verified by the stability of the normalized short-circuit current, J/J_o, shown in Figure 6. All short-circuit current values are constant after recovery within the (±5 percent) experimental uncertainty of the measurements. Nevertheless the cell output has suffered

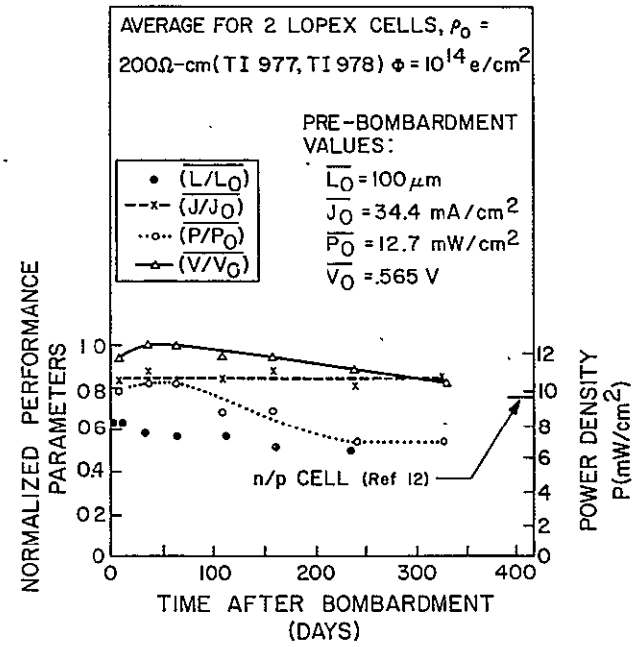

Figure 6. Stability of Performance Parameters in Two 200 Ω-cm Lopex Cells After Bombardment to 10^{14} e/cm^2

redegradation from 0.82 P_o at maximum recovery to 0.54 P_o as of the most recent measurement, a drop of ≈35 percent. In addition, the open-circuit voltage has redegraded from 1.0 V_o to 0.82 V_o, a highly significant decrease.

Figure 7 shows the photovoltaic characteristics of TI 978 taken at three different times; (a) before bombardment, (b) at the time of maximum power after recovery, and (c) as of the latest reading, 331 days after bombardment. The shape of the curve taken 331 days after bombardment indicates a severe redegradation due to a ≈15 percent drop in filling factor in addition to the redegradation caused by the ≈20 percent drop in open-circuit voltage. By comparison, the decrease in short-circuit current is only 6 percent; that is, within experimental uncertainty. Figure 7 clearly demonstrates that the stability of short-circuit current is not a sufficient criterion for lithium cell stability. A sufficient stability criterion is obtained only through examination of the entire photovoltaic response characteristic.

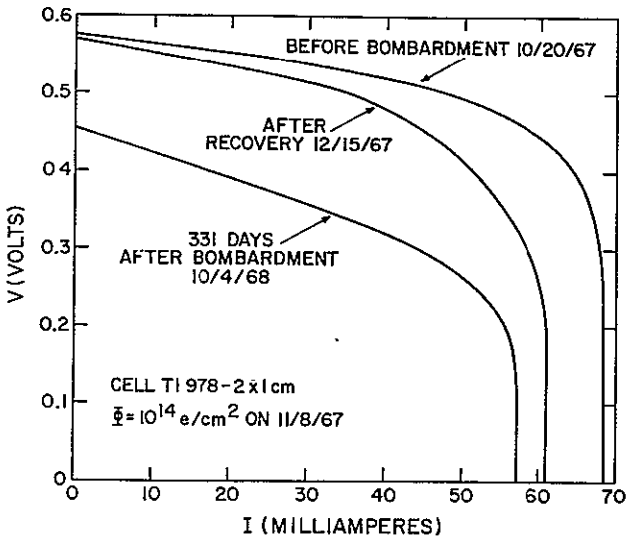

Figure 7. Comparison of Photovoltaic Characteristics of Lopex Cell TI 978 Before Bombardment, After Recovery Following Bombardment to 10^{14} e/cm^2 and After Redegradation

In comparison to the other two Lopex cells, TI 981 shows only a slight redegradation as shown in Figure 8, which is a plot similar to Figure 6 but with the open-circuit voltage omitted. In addition to suffering less redegradation, the stability time of TI 981 after recovery, i.e., ≳160 days, is somewhat greater than that for TI 977 and 978; that is, ≈100 days. The causes of redegradation, however, are the same, namely, a ≈6 percent decrease in open-circuit voltage and a change in filling factor from 0.63 after recovery to 0.59 after redegradation. It is noted that a 6-percent decrease in V is significant. This is due to the logarithmic variation in V with I_L, the light generated current, which causes the experimental uncertainty to be less than that in J and P.

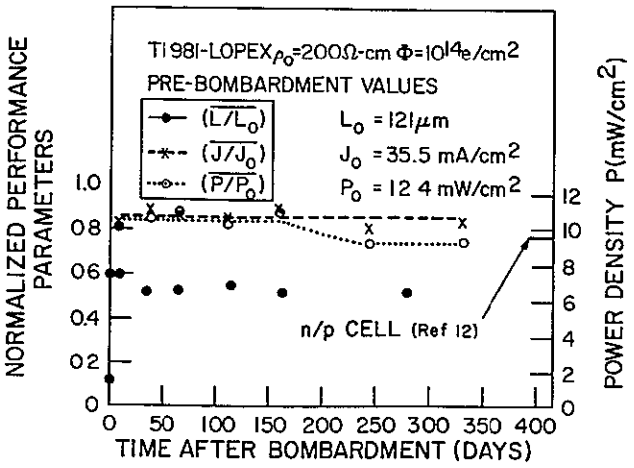

Figure 8. Stability of Performance Parameters in a 200Ω-cm Lopex Cell After Bombardment to 10^{14} e/cm^2

TI 952, the Float-Zone cell irradiated to 10^{14} e/cm^2, displayed post-irradiation behavior similar to that of the Lopex cells just discussed. The performance parameters versus time after bombardment are given for this cell in Figure 9. Power redegradation was from 0.88 P_o to 0.62 P_o; open-circuit voltage, from 0.570 to 0.521 V; filling factor, from 0.66 to 0.53.

The power after recovery in these cells ranged from ≈5 to 12 percent above that found for 10 Ω-cm n/p cells[12] after 10^{14} e/cm^2 (see Figures 6, 8, and 9). The powers after redegradation range from ≈2 to 22 percent below the n/p level.

Cells Irradiated to 10^{14} e/cm^2 on March 12, 1967: A total of nine Heliotek cells were irradiated to 10^{14} e/cm^2 at a rate of ≈2 x 10^{13} e/cm^2/min on March 12, 1968. Eight of these cells were made from 20 Ω-cm Float-Zone silicon, one from 20 Ω-cm Lopex silicon. The performance histories of these nine cells is given in Table IV. The initial performance levels of the cells

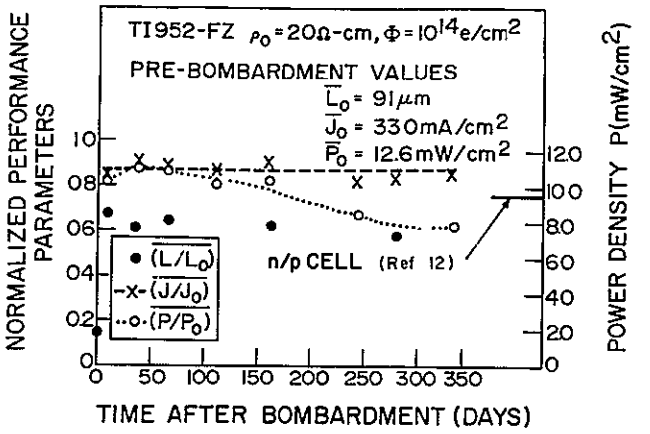

Figure 9. Stability of Performance Parameters in a 20Ω-cm Float-Zone Cell After Bombardment to 10^{14} e/cm^2

TABLE IV. STABILITY OF GFE CELLS IRRADIATED TO 10^{14} e/cm^2 IN MARCH 1968

Sample No.	ρ_o (Ω-cm) and Growth Method	November 1967		March 1968*		March 1968†		April 1968		July 1968		October 1968	
		J_o	P_o	J	P	J	P	J	P	J	P	J	P
He 651	20 FZ	26.3	9.8	27.2	10.3	23.9	8.9	27.4	10.2	23.4	6.8	25.7	9.1
He 670	20 L	27.7	10.8	28.6	10.6	24.7	9.5	28.1	6.6	25.6	8.9	26.6	10.0
He 798	20 FZ	27.6	10.4	28.6	11.1	23.4	8.5	28.5	10.8	26.3	9.8	27.3	10.1
He 810	20 FZ	28.9	10.0	28.9	10.0	24.1	8.1	28.9	10.2	26.9	9.2	27.7	9.5
He 879	20 FZ	30.1	11.9	30.9	12.3	25.0	9.2	31.0	12.0	29.1	10.9	29.4	11.1
He 881	20 FZ	29.6	11.2	30.4	10.1	25.5	8.4	30.3	9.5	28.2	9.4	28.7	8.4
He 882	20 FZ	29.6	11.4	30.5	11.9	25.1	9.0	30.5	11.6	28.5	10.6	28.8	10.6
He 884	20 FZ	30.2	10.8	31.2	11.3	25.1	8.6	30.9	11.1	28.9	10.4	29.0	10.1
He 885	20 FZ	28.9	10.9	29.8	11.3	24.6	8.8	30.0	11.3	28.2	10.5	28.3	10.3

NOTES: * before bombardment
† ≈40 minutes after bombardment

was somewhat below that of the TI cells discussed in the previous section. The post-recovery performance of the first two cells in Table IV, He 651 and 670, has been erratic. The reason for this is not understood, so that no further discussion of these two cells will be attempted. It is noted, however, that the most recent power readings are only ≈8 percent below the initial (pre-irradiation) powers.

The remaining seven cells are very similar. All underwent the same lithium diffusion cycle, namely, diffusion from the back surface for 60 minutes followed by a 90-minute redistribution, all done at 350°C.[22] The initial performance parameters were also similar and their post-irradiation properties have been reasonably similar. They will therefore be discussed as a group except where comments on individual cells are deemed appropriate.

Figure 10 gives performance histories as a function of time after bombardment averaged over the seven cells: He 798, 810, 879, 881, 882, 884, and 885. The pre-bombardment values of $\overline{P}_o = 11.1$ mW/cm^2 and $\overline{J}_o = 30.0$ mA/cm^2 were reasonably high.

The first post-bombardment value of $\overline{(L/L_o)}$, taken ≈5 minutes after bombardment, was 0.24. This is significantly higher than that averaged over the four TI cells, namely 0.15. The first values of $\overline{(J/J_o)}$ and $\overline{(P/P_o)}$ in Figure 10 were taken ≈40 minutes after bombardment. These normalized values are remarkably high, 0.87 and 0.78, respectively. This indicates a higher resistance to radiation damage than was found in

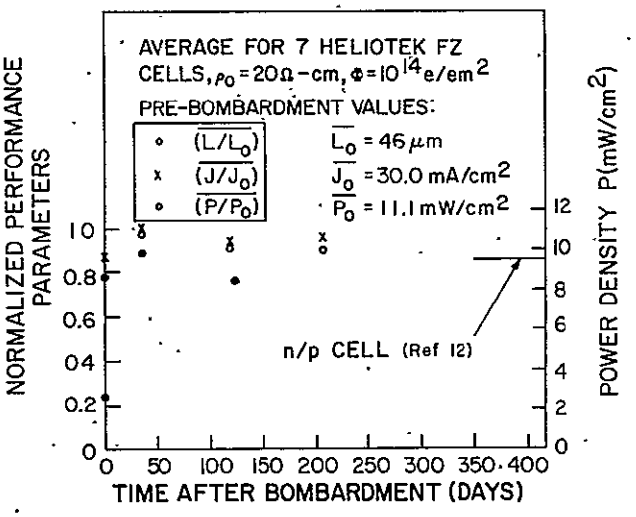

Figure 10. Stability of Performance Parameters in Seven 20Ω-cm Float-Zone Cells After Bombardment to 10^{14} e/cm^2

the TI cells irradiated to 10^{14} e/cm^2, as would be expected given the higher initial performance of the TI cells. The next readings, taken 35 days after bombardment, indicate practically complete recovery of photovoltaic response. The readings taken on this day, however, were approximately 5 percent higher on all cells than those taken on other days. It is felt, then, that the light intensity at the cells' surfaces was actually ≈105 mW/cm^2 and thus the true values of $\overline{(J/J_o)}$ and $\overline{(P/P_o)}$ should be ≈0.95 and ≈0.92, respectively, rather than the 1.0 and 0.97 readings shown in Figure 10.

Subsequent readings given $(\overline{J/J_o}) = 0.93$, and $(\overline{P/P_o}) = 0.91$ on the 119th day after bombardment; and $(\overline{J/J_o}) = 0.95$ and $(\overline{P/P_o}) = 0.90$ on the 206th day after bombardment. A set of photovoltaic characteristics for one of the cells, He 810, taken (a) before bombardment, (b) 35 days after bombardment, and (c) 206 days after bombardment is shown in Figure 11. The characteristics of He 810 are representative of six of the seven cells of this group. No sensible redegradation was evident in these six cells. (Note in Figure 11 that the characteristic taken 35 days after bombardment is believed to have been taken at ≈5 percent higher intensity than the other two curves and should therefore be translated to the left by that amount.) One of the seven cells, TI 881, did display a significant power redegradation. The series resistance of this cell after redegradation, as measured by the technique of Wolf and Rauschenbach,[23] was 2.8 Ω. Thus, the redegradation was presumably due to a series resistance increase. The filling factor decreased from 0.63 to 0.56, and the power from 9.4 to 8.4 mW/cm^2 during this time. The short-circuit current and open-circuit voltage remained constant during this time; thus the redegradation in this cell was due solely to an increase in the series resistance of the cell.

Although the duration of the post-irradiation stability tests on these Heliotek cells has been shorter (206 days) than those on the Texas Instruments cells after 10^{14} e/cm^2 (331 days), sufficient data exists to indicate better long-term stability in the Heliotek cells. It should be stated that the initial values of N_{L1} in all the Heliotek and TI cells placed them in either Group 1 or 2; that is, lithium densities less than 5×10^{15} cm^{-3}.

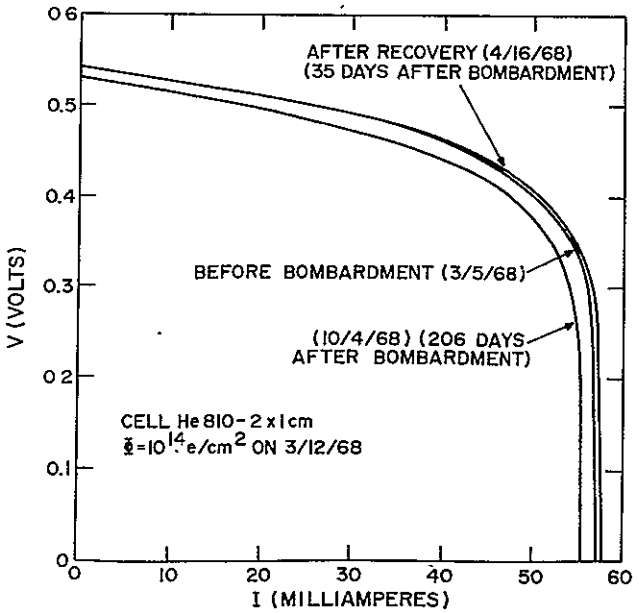

Figure 11. Comparison of Photovoltaic Characteristics of Float-Zone Cell He 810 Before Bombardment, After Recovery Following Bombardment to 10^{14} e/cm^2, and 206 Days After Bombardment

The effect of lithium density distribution on cell stability after various radiation levels is discussed more thoroughly in a later section.

All of the cells irradiated to 10^{14} e/cm^2 had, as of October, 1968, shunt resistances greater than 1000 Ω. Thus, shunt leakage has not been a factor in the performance of these cells.

Unirradiated Cells

Table V presents a performance history for 19 Heliotek (He) cells and 2 Texas Instruments (TI) cells covering approximately 11 months and beginning with the first measurement on the cells. A negligibly small electron fluence was applied to each cell during minority-carrier diffusion-length measurements. This fluence is calculated to be less than 10^{10} e/cm^2. All of the Heliotek cells shown in Table V were fabricated from 20 Ω-cm starting material. The two TI cells were fabricated from 200 Ω-cm Lopex silicon. Three of the Heliotek cells were fabricated from Lopex silicon, the remaining 16 were from Float-Zone silicon.

It is seen from Table V that, of all the cells tested, only He 867 and TI 979 have suffered degradation in power output. (The March power measurement on He 815 is considered in error, probably due to faulty contacts.) In He 867 the power degradation amounted to ≈15 percent and occurred only after 8 months. The main cause of the degradation was a series resistance increase, f decreasing from 0.79 in July 1968 to 0.65 in October 1968. In contrast, TI979 showed significant degradation between 4 and 8 months after the first measurement and as of the latest measurement was ≈35 percent below the initial value obtained in November 1967. This 35 percent is the same as the amount of redegradation suffered by two similar TI cells (977 and 978) after irradiation to 10^{14} e/cm^2 in November, 1967. In fact, as Figure 12 shows, the changes in I-V characteristic in TI 979 are approximately the same as were the changes in I-V characteristic in TI 977 and 978 (of Figure 7). Figure 12 gives photovoltaic characteristics for TI 979 as of November 1967 and October 1968. A decrease in open circuit voltage from 0.570 V to 0.510 has occurred in addition to a severe drop in filling factor, as seen from Figure 12, f = 0.64 in November 1967 to f = 0.48 in October 1968. During the same time period, the short-circuit current has remained constant within experimental uncertainty.

The degradation in power of these two unirradiated cells, He 867 and TI 979, and the stability in the short-circuit current in the same cells, again points out the insufficiency of the latter as the stability criterion in lithium-doped cells.

The initial values of N_{L1} in the unirradiated cells placed them in either Group 1 or 2; that is, lithium densities less than 5×10^{15} cm^{-3} measured at ≈1 μm from the junction. It will be seen in the discussion which follows that, while being a useful index of the effect of

TABLE V. PERFORMANCE HISTORY OF UNIRRADIATED CELLS

Sample No.	ρ_o and Growth Method	November 1967		March 1968		July 1968		October 1968	
		J_o (mA/cm^2)	P_o (mW/cm^2)	J (mA/cm^2)	P (mW/cm^2)	J (mA/cm^2)	P (mW/cm^2)	J (mA/cm^2)	P (mW/cm^2)
He 673	20 L	24.3	8.8	25.0	9.4	23.1	8.5	24.5	8.9
He 676	20 L	25.9	9.1	26.6	9.7	24.7	8.9	26.0	9.2
He 694	20 L	25.8	9.4	26.8	9.7	24.9	9.3	26.3	9.7
He 796	20 FZ	26.0	9.5	26.9	10.3	25.2	9.4	26.1	9.7
He 808	20 FZ	26.4	9.6	27.2	10.0	25.8	9.5	26.6	9.7
He 815	20 FZ	28.3	11.0	29.1	8.5	27.7	11.0	28.7	11.3
He 866	20 FZ	29.0	10.8	30.2	11.5	29.0	11.0	29.3	11.2
He 867	20 FZ	28.6	10.7	29.9	11.8	28.5	10.8	28.9	9.7
He 868	20 FZ	26.5	9.9	28.0	10.7	26.6	10.0	26.9	10.2
He 870	20 FZ	28.0	10.5	29.6	11.2	28.5	10.8	29.0	10.9
He 871	20 FZ	29.6	11.2	31.6	12.4	30.5	12.0	30.9	12.0
He 872	20 FZ	-	-	28.0	10.6	27.1	10.2	27.6	10.2
He 873	20 FZ	29.0	11.6	30.0	11.4	29.0	11.1	29.2	11.2
He 875	20 FZ	28.1	10.7	29.1	10.9	27.8	10.3	28.0	10.3
He 876	20 FZ	27.6	9.6	28.6	11.0	27.5	10.5	27.9	10.5
He 878	20 FZ	28.3	11.1	26.1	11.2	28.2	10.8	28.3	10.7
He 886	20 FZ	29.1	10.7	30.4	11.5	29.5	11.2	30.3	11.7
He 887	20 FZ	30.6	10.8	31.8	11.4	30.7	10.9	31.6	11.6
He 892	20 FZ	28.9	11.0	29.8	11.4	29.0	11.6	29.6	11.8
TI 976	200 L	32.0	12.1	33.8	12.9	32.5	11.8	33.2	12.8
TI 979	200 L	32.4	11.8	34.3	11.0	33.2	8.4	34.1	8.3

NOTES: L is Lopex
FZ is Float Zone

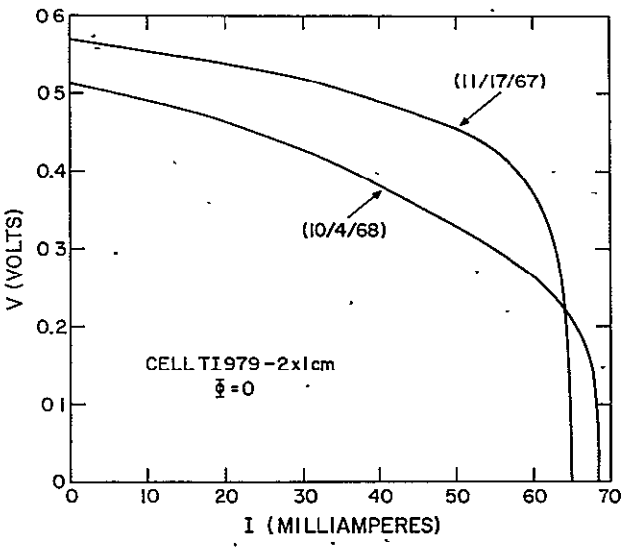

Figure 12. Comparison of Photovoltaic Characteristics of Unirradiated Lopex cell TI 981 in November, 1967, and October, 1968

lithium on cell stability, the initial lithium density value determined from capacitive measurements at a single value of reverse bias, is not sufficient for the establishment of a cell stability criterion.

Discussion of Results

Summarizing the results of the stability tests after various electron fluences, considering for the moment only FZ and Lopex cells:

- TI cells irradiated to a fluence of 10^{16} e/cm^2 have not redegraded after recovery unless the initial concentration of lithium near the junction (N_{LI}) was greater than 5×10^{15} cm^{-3}. Three He cells (He 340, 341, and 342 with $N_{LI} \lesssim 2 \times 10^{15}$ cm^{-3}) show spotty behavior, but this is attributed to a very low donor density and a consequent increase in series resistance.

- Three TI cells ($2 \times 10^{15} < N_{LI} < 3 \times 10^{15}$ cm^{-3}) have shown slight redegradation 1 year after bombardment to a fluence of $\approx 1.4 \times 10^{15}$ e/cm^2.

- Four TI cells ($1.7 \times 10^{15} < N_{LI} < 3.5 \times 10^{15}$) showed significant redegradation ~100 days after bombardment to a fluence of 10^{14} e/cm^2. Approximately 1 year after bombardment, three of these cells have redegraded to a power ≈35 percent below the maximum power achieved during recovery. On the other hand, only one of seven Heliotek cells has redegraded significantly ~200 days after bombardment to 10^{14} e/cm^2. The lithium density, N_{LI}, in these cells ranged from 1.2 to 1.7×10^{15}. He 881 ($N_{LI} = 1.7 \times 10^{15}$ cm^{-3}) has redegraded 10 percent due to an increase in series resistance.

- Eighteen of nineteen unirradiated Heliotek cells ($1 \times 10^{15} < N_{LI} < 3.6 \times 10^{15}$ cm^{-3}) have been stable over an 11-month period. The one cell which degraded was He 867 which had an initial value of $N_{LI} \approx 1.0 \times 10^{15}$ cm^{-3}. This cell degraded because of an increase in series resistance. Of the two unirradiated TI cells, TI 979, with $N_{LI} = 1.6 \times 10^{15}$ cm^{-3}, has degraded severely (≈30 percent) while TI 976, $N_{LI} = 4.1 \times 10^{15}$ cm^{-3}, has remained stable.

In light of this summary, considering only the TI cells for the moment, it is clear that (for a given value of N_{LI}) the lower the fluence, the more severe the redegradation. In addition, the higher the value of N_{LI} for a given fluence, the more severe the redegradation. This was seen to be the case for cells irradiated to 10^{16} e/cm^2. Figure 13 shows it to be true for the three Lopex cells irradiated to 10^{14} e/cm^2. Figure 13 presents plots of donor density versus distance from the junction for the three Lopex cells TI 977, 978, and 981. These plots were obtained from reverse-bias capacitance measurements[8] on the cells taken with a Boonton Model 74D capacitance bridge. As indicated in Figure 13, one set of plots was taken on October 23, 1967, before bombardment, and another on October 11, 1968 after redegradation. The cells are labelled on each plot; on the plots taken after redegradation, the percentages of redegradation in V and P are also given. Figure 13 has many noteworthy features: (1) the very great increase in lithium density near the junction in each cell; (2) the higher density gradients in higher density cells; (3) the increase in redegradation with increasing cell density; and (4) the greater increase in density at a given distance from the cell junction (over the period of 1 year) for the higher density cells. Thus, redegradation in most cases correlates with large lithium density gradients and with large changes in lithium donor profile adjacent to the junction. The significant slope of the redegraded curves near the voltage axis suggests a high series resistance in these cells. This could occur in the form of sheet resistance if enough lithium donors cross the junction to the p-skin to significantly compensate the boron acceptor content. However, a 4-point probe measurement[24] on the p-skin of TI 978 (Figure 7) indicated very high (~10^{20} cm^{-3}) remaining boron donor

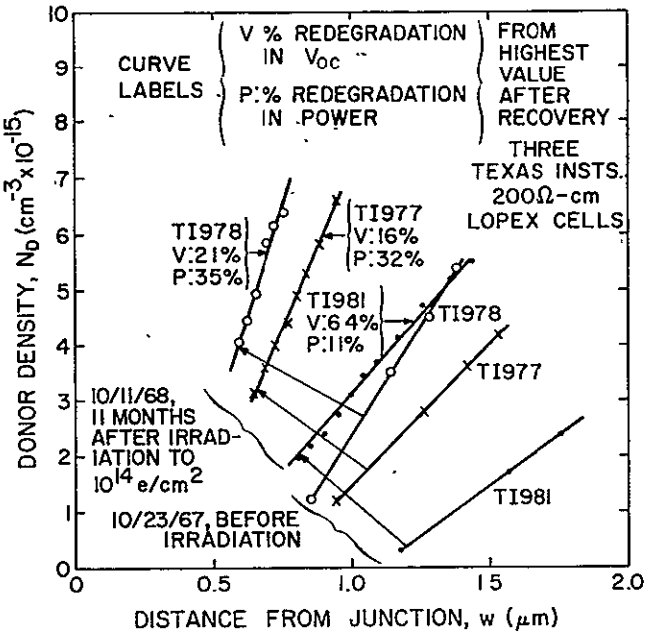

Figure 13. Comparison of Donor Density Profiles of Three Lopex Cells Before Bombardment and 11 Months After Bombardment to 10^{14}e/cm^2

density. In addition, in measurements of series resistance[23] on the TI cells showing redegradation, the values found were very low; for example, TI 952, $R_s \approx 0.60\Omega$; TI 978, $R_s \approx 0.32\Omega$. The values were in fact somewhat lower than the average for the seven Heliotek cells bombarded to 10^{14} e/cm^2, namely $\approx 1.2\Omega$. In addition, some of the He cells gave indication of sheet resistance in the form of increasing series resistance as the points of measurement move from open-circuit toward short-circuit condition on the I-V curve.[23] No such indication of sheet resistance was observed in the badly redegraded TI cells, TI 952, 977, and 978.

Thus a contradiction is evident. The redegraded (TI) cells display I-V characteristics suggesting large series resistance; however, direct measurements give low values of series resistance. In addition, the decrease in open-circuit voltage in the same TI cells is puzzling. The shunt resistances in these cells are too high ($>1000\Omega$) to significantly affect the I-V characteristic. It must be said, then, that the photovoltaic response of these cells is not understood in terms of present solar cells equivalent circuits.

Both unirradiated TI cells display spontaneous increases in lithium concentration near the junction similar to those shown in Figure 13. However, as stated before, only TI 979 degraded in output. Its series resistance was measured to be $\approx 0.68\Omega$. TI 976, which did not degrade, has a series resistance of $\approx 0.63\Omega$. It is not understood why TI 976 did not degrade.

The question also arises as to why the Heliotek cells, both those irradiated to 10^{14} e/cm^2 and those left unirradiated, have not (in most cases) redegraded (or degraded). A possible explanation for this is contained in Figure 14 which gives density profiles for two cells on two dates approximately 11 months apart. Both of the cells were fabricated from 20 Ω-cm FZ silicon and both were irradiated to 10^{14} e/cm^2. One of them, TI 952, started to redegrade ~100 days after bombardment and had redegraded ≈30 percent in power 331 days after bombardment (see Figure 9). The other, He 810, had shown no sensible redegradation 206 days after bombardment.

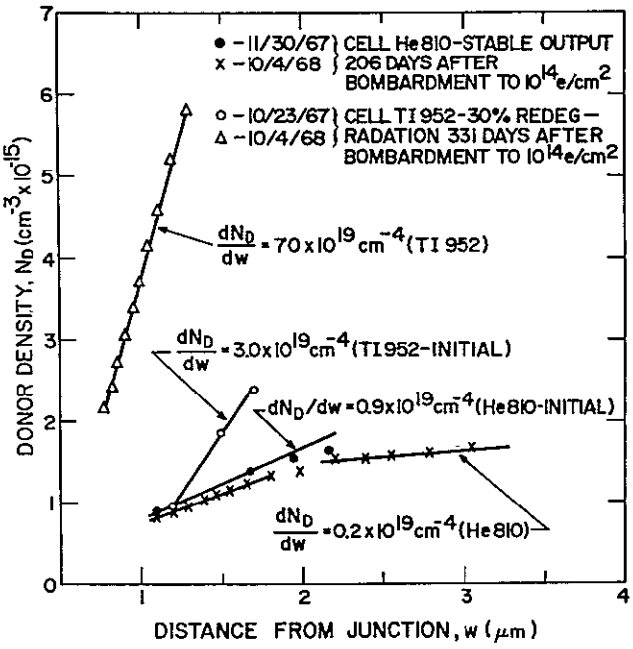

Figure 14. Comparison of Donor Density Profile Histories of a Cell which Redegraded After Recovery from 10^{14} e/cm^2 and a Cell which Maintains a Stable Output After Recovery from 10^{14} e/cm^2

The initial (10/23/67 and 11/30/67, respectively) densities of the two cells at zero bias were equal within the ≈±5 percent experimental uncertainty of the measurement; that for TI 952 was 9.5×10^{14} cm^{-3} and that for He 810 was 9.0×10^{14} cm^{-3}. However, this is where the similarity ends. The slope dN_D/dw, of the initial TI 952 profile was 3.0×10^{19} cm^{-4}, more than three times the 0.9×10^{19} cm^{-4} of He 810. The density profiles, taken approximately 11 months later on October 11, 1968, show an even more striking contrast. TI 952 displayed a large increase in density near the junction as had the other TI cells. On the other hand, He 810 had a density profile similar to the initial profile. In addition, whereas the density gradient in TI 952 was 7.0×10^{19} cm^{-4}, giving a density of 5.8×10^{15} cm^{-3} at a distance of 1.3 μm from the junction, the density gradient in He 890 decreased at ≈2 μm to 0.2×10^{19} cm^{-4}, a factor of 70 below that of TI 952. Thus, although the initial densities of the two cells at the edge of the depletion region were approximately equal, their density profiles and the subsequent behavior of these density profiles were enormously different. The behavior of He 810 was typical of all the Heliotek cells. It is therefore inferred that the lithium motion in the junction region in the Heliotek cells is much less than that in the TI cells, and that this reduced motion is responsible for the better stability of the Heliotek cells.

CONCLUSIONS

Long-term stability experiments on silicon solar cells irradiated by 16.8 MeV protons and 14 MeV neutrons show that lithium doped p/n cells have significantly higher resistance to radiation damage than either standard p/n or n/p cells. The proton and neutron fluences in the experiments were 2.4×10^{12} p/cm^2 and 4.5×10^{12} n/cm^2, respectively.

Long-term stability tests on lithium-doped p/n silicon solar cells irradiated by 1 MeV electrons to fluences from 10^{14} to 10^{16} e/cm^2 indicate that cells made from low oxygen content (Lopex or Float-Zone) silicon tend to be less stable than those made from high-oxygen silicon. However, they can be made in a stable form. They are more likely to remain stable after recovery for radiation damage if the lithium density concentration is sufficiently low; then, significant lithium movement in the region near the junction is avoided. Such cells can be made to be slightly more resistant to electron irradiation than standard n/p cells.

Several lithium cells which redegrade after irradiation to 10^{14} e/cm^2, and one which degrades spontaneously with no irradiation display post-redegradation (or post-degradation) have photovoltaic characteristics which are not explainable in terms of straightforward solar-cell equivalent circuits and simple p/n junction theory.

In most redegrading cells, the short-circuit current shows no sensible redegradation while the power and open-circuit voltage degrade. Minority-carrier diffusion length is also relatively constant during redegradation. Thus, the short-circuit current measurement does not, in general, provide a valid stability criterion in lithium-doped cells.

In Float-Zone cells with moderate lithium density and density gradient (density $\lesssim 1 \times 10^{15}$ cm^{-3} at ≈1 μm from the junction, density gradient $\lesssim 1 \times 10^{19}$ cm^{-4} near junction), stability in photovoltaic characteristic has been maintained for a period of ≈200 days after recovery from an irradiation of 10^{14} e/cm^2 1-MeV electrons. Unirradiated cells with these lithium densities also maintained stable photovoltaic characteristics over a period of approximately 11 months.

Solar cells with low oxygen content, irradiated to a higher fluence, 10^{16} e/cm^2, require higher initial

lithium densities (2 to 5 x 10^{15} cm^{-3} at ≈1 μm from the junction) to recover to a value comparable to 10 Ω-cm n/p cells; that is, ≈5.3 mW/cm^2 for 100 mW/cm^2 tungsten illumination. Cells with lower lithium density recover to lower power levels; cells with density above ≈5 x 10^{15} cm^{-3} redegrade after recovery. Cells with densities ≲5 x 10^{15} have remained stable since recovery from a fluence of 10^{16} e/cm^2, over a period covering about 1.5 years.

Two lithium-doped solar cells of high oxygen content recovered slowly to a power of ≈5.8 mW/cm^2 1 year after irradiation to 10^{16} e/cm^2. They have remained stable at this level over a period of ≈7 months. Two lithium-doped Float-Zone cells with diffused, heavily-doped phosphorus regions near the junction had power densities of ≈7 mW/cm^2 at a time 19 months after bombardment to 10^{16} e/cm^2. In both types of cell, lithium motion across the junction is retarded; in the Quartz-Crucible cells, oxygen binds lithium in $(Li\text{-}O)^+$ donor complexes; in the phosphorus-diffused cells, a potential barrier is created by the heavily-doped phosphorus region. The stability of these cells is attributed in part to this reduction in lithium motion.

ACKNOWLEDGMENTS

The authors wish to acknowledge the very helpful discussions of R. Rasmussen and M. Wolf. The photovoltaic characteristics and diffusion length measurements were made by R. Neadle.

REFERENCES

1. J. J. Wysocki, P. Rappaport, E. Davison, R. Hand, and J. J. Loferski, "Lithium Doped, Radiation Resistant Solar Cells," Appl. Phys. Lett. 9, 44, (1966).

2. J. R. Carter, "Annealing of Radiation Damage in Lithium-Doped Silicon," Proc. Sixth Photovoltaic Spec. Conf. IEEE Catalog No. 15C53, Vol. III, 145, (1967).

3. P. H. Fang, Private Communication.

4. J. J. Wysocki, "Self-Healing Radiation-Resistant Silicon Solar Cells," Proc. Sixth Photovoltaic Spec. Conf. IEEE Catalog No. 15C53, Vol. III, 96, (1967).

5. G. J. Brucker and B. Markow, "Neutron Damage in Silicon Solar Cells," Proc. Sixth Photovoltaic Spec. Conf. IEEE Catalog No. 15C53, Vol. III, 53, (1967).

6. J. J. Wysocki, G. J. Brucker, and A. G. Holmes-Siedle, RCA Annual Progress Report, Contract NAS 5-10239, (June 1967).

7. W. Rosenzweig, "Diffusion Length Measurements by Means of Ionizing Radiation," Bell Sys. Tech. Journ., 41, 1573, (1962).

8. J. Hilibrand and R. D. Gold, "Determination of the Impurity Distribution in Junction Diodes from Capacitance-Voltage Measurements," RCA Rev. XXI, 245, (1960).

9. D. L. Kendall and R. Vineyard, NASA Contract NAS 5-10274.

10. P. Payne, G. Goddelle, and E. L. Ralph, Heliotek, First Periodic Report, NASA Contract No. NAS 5-10272, 21 Aug. 66 to 24 Feb. 67.

11. G. Brucker, T. Faith, A. G. Holmes-Siedle, and R. Neadle, RCA Final Report, NASA Contract No. NAS 5-10239 (March 1968).

12. R. L. Statler, "Electron-Bombardment Damage in Silicon Solar Cells," NRL Report 6091 USNRL, Washington, D. C. (October, 1964).

13. W. R. Cherry and R. L. Statler, "Photovoltaic Properties of U.S. and European Silicon Cells under 1-MeV Electron Irradiation," GSFC Report, May, 1968.

14. J. Mandelkorn, "Comparison of Lithium Containing P on N Silicon Cells with N on P Silicon Cells," Proc. Sixth Photovoltaic Spec. Conf. Catalog No. 15C53, Vol. III, 125, (1967).

15. P. H. Fang, "Present Status of Lithium-Diffused Silicon Solar Cells," Proc. Sixth Photovoltaic Spec. Conf., IEEE Catalog No. 15C53, Vol. III, 110, (1967).

16. D. L. Kendall and R. A. Vineyard, Texas Instruments Inc., Final Report for Contract NAS 5-10274, 18 Aug. '66 to 31 Jan. '68.

17. E. M. Pell, "Interactions Between Li and O in Si," Solid State Electronics and Communications, p. 261, Eds. Desirant and Michels, Academic Press, New York, (1960).

18. M. B. Prince, "Silicon Solar Energy Converters," J. Appl. Phys. 26, 534, (1955).

19. G. J. Brucker, T. J. Faith, and A. G. Holmes-Siedle, "Injection-Level Effects in Irradiated, Lithium-Doped Solar Cells," to be published in Proc. Seventh Photovoltaic Spec. Conf., 1968.

20. P. Iles, Hoffman Electronics Corp. Semiannual Report, NASA Contract No. NAS 5-10271, 28 Aug. 66 to 28 Feb. '67.

21. T. J. Faith, G. J. Brucker, A. G. Holmes-Siedle, and R. S. Neadle, "Recovery Rate and Capacitance Measurements on Irradiated Lithium-Containing Solar Cells," IEEE Nuclear and Space Radiation Conf., Missonla, Mont., July, 1968, to be published in IEEE Trans. on Nuclear Sci. NS-15, December, 1968.

22. P. Payne, Heliotek Report No. 11, NASA Contract NAS 5-10272, 15 Aug. 67.

23. M. Wolf and H. Rauschenbach, "Series Resistance Effects on Solar Cell Measurements," Adv. Energy Conversion, 3, 455, (1963).

24. L. Valdes, "Resistivity Measurements on Germanium for Transistors," Proc. IRE 42, 420, (1954).

APPENDIX B

ELECTRICAL STUDIES OF ELECTRON-IRRADIATED LITHIUM-CONTAINING n-TYPE Si*

Hall-coefficient and resistivity measurements have been used to investigate the crystal growth and irradiation-temperature dependence of the introduction rate and room temperature annealing of carrier-removal defects in lithium-doped silicon. Initial resistivity of the quarts-crucible silicon was 30 ohm-cm and of the float-zone silicon was $\geq$1500 ohm-cm. The silicon was doped with lithium to a density of $2 \times 10^{16} cm^{-3}$. Irradiations were carried out with 1 MeV electrons at bombardment temperatures ranging from 79° K to 280° K. Specimens were annealed to 200° K thereby separating intrinsic and impurity defects. Introduction rates of carrier-removal defects were exponentially dependent on the reciprocal of temperature for both types of crystal, but the slopes and limiting temperature values differed. The slope of the carrier-removal rate versus reciprocal temperature curve is 0.055 eV in crucible silicon and 0.09 eV in zone silicon. The temperature dependence was not consistent with a simple charge-state-dependent probability of interstitial-vacancy dissociation and impurity-vacancy trapping. Carrier concentrations measured at or near room temperature were increased in zone silicon, but were decreased in crucible silicon by isothermal annealing at room temperature. Crucible-silicon samples annealed to 373° K for 10 minutes exhibited complete recovery of mobility. Complete recovery of mobility in float-zone silicon took place in an annealing time $\leq$17 hours at room temperature. The time constant of the annealing kinetics at room temperature is consistent with the smaller lithium-diffusion constant observed in oxygen-rich silicon compared to the lithium-diffusion constant in oxygen-lean silicon. The mechanism of room temperature annealing is attributed to neutralization of carrier-removal defects by lithium interaction in crucible silicon, and by both lithium interaction and defect dissociation in zone silicon. Results suggest that a lithium-oxygen-vacancy complex is produced by radiation in quartz-crucible grown silicon and a lithium-vacancy complex in float-zone refined silicon. The LiO-V defect is tightly bound compared to the oxygen free Li-V defect. Measurements of carrier density as a function of reciprocal temperature located defect-energy levels near $E_c - 0.18$ eV and $E_c - 0.13$ eV, in irradiated-crucible silicon. The first defect level is the A-center and the latter level is the reverse annealing center which is formed at a temperature of 250° K. A defect level located near $E_c - 0.08$ eV formed after crucible-silicon samples were annealed at room temperature and lithium interacted with radiation defects.

---

* This work was performed under JPL Contract No. 952249 and NASA Contract No. NAS5-10239.

A. INTRODUCTION

Bombardment of silicon crystals by high-energy particles introduces intrinsic defects in the crystal. These defects consist of interstitial-vacancy pairs which are mobile at temperatures as low as 4° K for the interstitial and 75° K for the vacancy (Ref. I-1). Studies of primary defect formation during low-temperature electron bombardment of n-type silicon crystals have been previously reported (Ref. I-2 to I-4). These studies are necessary to understand the production mechanisms of primary defects and their reaction products. The reaction products or secondary defects are formed during the thermal reordering processes which take place after completion of the bombardment. Electrical properties of electron-irradiated silicon at moderate electron energies (E = 1 to 2 MeV) are dominated by the secondary defects formed by the interaction of primary defects with impurities in the crystal. For example, the A-center is a defect-impurity complex consisting of oxygen and a vacancy. In general, impurities are immobile at or below room temperature, but lithium is an impurity which is highly mobile at room temperature. This mobility makes it possible for lithium to diffuse to radiation-induced defect sites. Interaction of lithium with the defects neutralize their degrading effect on the electrical properties of the silicon. However, at a temperature of about 250° K, lithium is virtually "frozen" in the silicon lattice, and the diffusion constant of lithium is reduced to about 1/50 the room temperature value (Ref. I-5). Thus, by irradiating samples at temperatures for which lithium is immobile and then raising the temperature, it is possible to investigate the processes by which lithium interacts with the primary and secondary defects.

The power of irradiated-solar cells decreases due to degradation of minority-carrier lifetime. However, it has been shown that electron, neutron, and proton-irradiated-silicon solar cells (Ref. I-6, I-7) containing lithium even when held at room temperature spontaneously recover much of their electrical outputs over a few hours or days following the irradiations. Thus, it appears that the mobile lithium ion moves to, and combines with the original damage center, a vacancy-impurity complex, thereby changing its minority-carrier recombination properties. The resulting new defect complex has a much smaller effect on the minority-carrier lifetime.

It is the purpose of this paper to report the results of Hall-effect and electrical-conductivity measurements on electron-irradiated silicon doped with lithium. Information concerning the damage mechanisms and properties of carrier-removal defects at bombardment temperatures ranging from 79° K to 280° K will be presented. In addition, the Hall-effect and resistivity measurements were used to monitor the isochronal annealing of defects over a temperature range of 79° K to 250° K. The

room-temperature interaction of lithium with carrier-removal defects was monitored as a function of time after irradiation by means of the aforementioned techniques.

This Appendix is divided into four major sections. The experimental techniques, apparatus, types of silicon, and electron source are discussed in paragraph B. The results of carrier-removal and mobility measurements following electron bombardment, and subsequent isochronal and isothermal annealing are presented in paragraph C. These results are discussed in paragraph D with respect to suggested mechanisms of defect formation and annealing, and previous Hall measurements and EPR results that help to identify defects found in lithium-doped silicon.

B. EXPERIMENTAL TECHNIQUES

The Hall-effect and resistivity measurements were obtained by direct current-voltage techniques on Hall bars of ≈ 0.3 ohm-cm lithium-doped n-type Quartz-Crucible and Float-Zone silicon. The resistivity of the starting material before diffusion with lithium was 30 ohm-cm phosphorus-doped Quartz-Crucible, and ≥ 1500 ohm-cm Float-Zone silicon. Lithium diffusion was carried out by heating the starting material in a 1-percent lithium-tin bath at $\approx 400°C$ for several days. After suitable cleaning processes, the silicon wafers were ultrasonically cut into the shape shown in Figure I-1a. Ohmic contacts were made to the bars by alloying with 1-percent arsenic-tin or 1-percent antimony-gold alloy. Final connection to the alloy dot was made by soldering one end of a fine wire to the dot with indium, and the other end to the indium-tinned gold pattern on a ceramic substrate which provided an insulated base for mounting the samples. The gold pattern was fixed to the ceramic substrate by the standard molybdenum silkscreen process. A thermally conductive epoxy was used to attach the Hall bar to the ceramic substrate. The metallized ceramic substrate was soldered to a copper plate. Six leads of 0.005 inch diameter formvar wire were soldered to the six contacts on the bar and a copper-constantan thermocouple was cemented to one of the arms of the bar as shown in Figure I-1b. A magnetic field strength of 1600 G and a current of 1 to 3 mA were used to make the measurements. Thicknesses of samples ranged from 0.016 inch to 0.024 inch. Four samples of each type of crystal growth were used in obtaining carrier-removal production-rates with an average lithium density of $2 \times 10^{16} \pm 10$ percent Li/cm^3 measured at room temperature (297°K) for this group of eight samples. The deviation in the carrier-removal rates obtained on Float-Zone and Quartz-Crucible samples was 12 and 15 percent, respectively. These values were computed from data obtained for a bombardment temperature at which three samples contributed values of carrier-removal rates. The initial impurity concentrations in the Quartz-Crucible silicon were a phosphorus density of $\approx 1.5 \times 10^{14}$ cm^{-3} and an oxygen density of $\approx 10^{18}$ cm^{-3}. Float-Zone silicon had an oxygen concentration of less than 10^{14} cm^{-3} as determined by the (Li-O) EPR line (Ref. I-8). Thus, the electrical behavior of the irradiated lithium-doped silicon was dominated by oxygen and lithium-defect complexes in crucible-silicon and lithium-defect complexes in zone silicon.

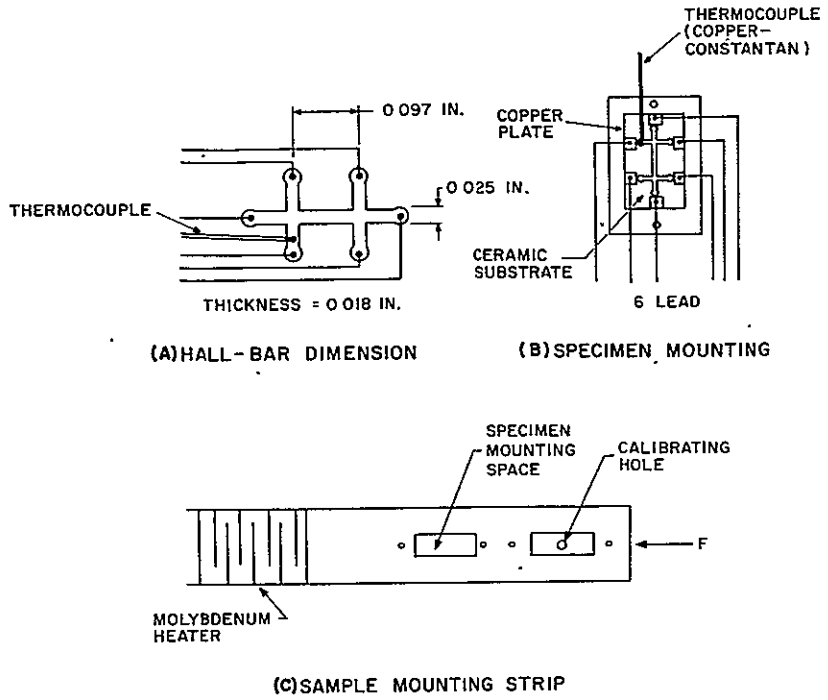

Figure I-1. Sample Geometry and Mounting Configurations

A cross section of the irradiation apparatus is shown in Figure I-2. The principle parts of the apparatus are identified by letters. Section A and B are reservoirs for the liquid nitrogen. The lower portion of the apparatus has two copper radiation shields. One extends downward from A and the other, D, surrounds the specimen. The sample mounting strip F, shown in detail in Figure I-1c, contains two holes. The specimen is mounted in one and a copper strip with a calibrated hole size, equivalent to the rectangular area which the specimen occupies, is mounted in the other. Either one of these holes can be positioned in the electron beam by means of the double bellows G and spring P. The spring is able to support the structure in its upper position when the space between the bellows is filled with air at atmospheric pressure. When this space is evacuated by a forepump, the bellows contract and lift the inner dewar, and, therefore, the sample holder, to the second position. The system can be cycled rapidly between these two positions by means of an electrically operated valve which alternately exposes the space between the bellows to the atmosphere and to the forepump vacuum. The magnetically operated shutter L is used to interrupt the beam without shutting off the machine, deflecting the beam or disturbing the setup in any way. When the beam is cut off, the sample is dropped into place by activating the three-way electrically-operated solenoid valve which exposes the bellows M to the

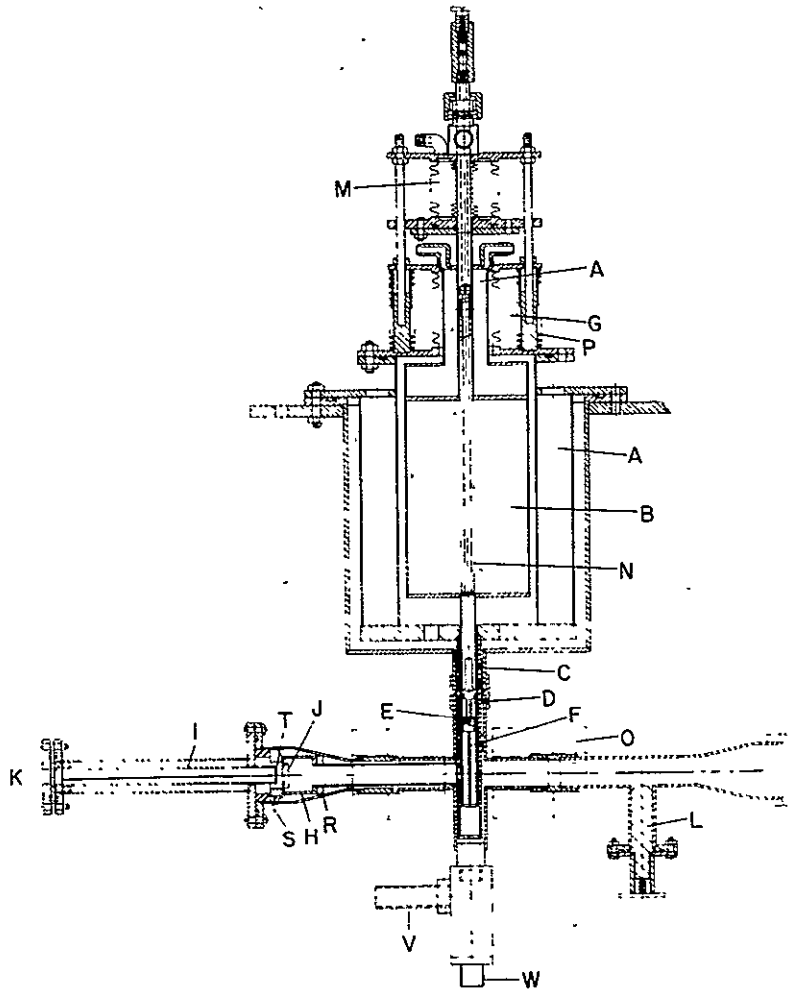

Figure I-2. Irradiation and Annealing Apparatus: (A) and (B) Liquid Nitrogen Reservoirs, (C) Dewar finger, (D) Copper Radiation Shield, (E) Molybdenum Heaters, (F) Sample Mounting Strip, (G) Bellows, (H) Faraday Cup, (I) Hollow Tube, (J) Trap Door, (K) Window, (L) Shutter, (M) Bellows, (N) Liquid Nitrogen Filling Tube, (O) Electromagnet, (P) Spring, (R) Lavite Washer, (S) Glass Seal, (T) Phosphor Screen, (V) Electrical Leads; and (W) Window.

air. An electromagnet O, whose axis is concentric with the beam, permits measurements of the Hall coefficient without any disturbance of the sample. The inside of the apparatus is evacuated by means of the vacuum pumping system of the electron accelerator through the opening where the apparatus is jointed to the beam tube.

A 1-MeV Van de Graaff accelerator was used as the electron irradiation source. The electron flux was measured by positioning the Faraday cup H directly behind the space occupied by the hole in F. The cup is insulated by a lavite washer R and has a current lead attached to it via the glass seal S. The uniformity of the beam at the specimen position was checked in the following manner. The beam current was first maximized electrically by adjusting the magnetic lens and the voltage deflection plates. At the "closed" end of the Faraday cup a trap door J was suspended across an opening. A hollow tube I which contained a thin phosphor screen T across one end could be moved through J when a soft iron washer, attached at its opposite end, was moved forward by successively switching on a set of electromagnets wound around in coil form. The phosphor screen was then moved forward until it was directly behind the position reserved for the sample. When the electrons struck the phosphor it fluoresced. The resulting pattern was viewed by a television camera which was positioned behind the window K. Any necessary focusing or deflection was made and then the tube I was withdrawn from the Faraday cup. The trap door J closed and the beam current passing through the hole in F could be measured. The sample leads were brought out of the apparatus through the side arm below the sample as shown in Figure I-2. A quartz glass window W located below the lead feed-through was used to illuminate the sample with band-gap light to check for trapping effects. The pre-irradiated or post-irradiated samples did not exhibit any significant sensitivity to light. All measurements reported here were made in the dark.

The carrier concentration and carrier mobility in the silicon samples were obtained from the Hall-coefficient and the electrical-resistivity measurements. A correction for the ratio of Hall mobility μ_H to conductivity mobility μ_c, was applied to all values of carrier density determined from Hall-coefficient measurements. The ratio μ_H/μ_c was obtained from an empirical equation (Ref. I-4) based on experimental Hall-coefficient data (Ref. I-9). Samples were sequentially bombarded from the lowest to the highest bombardment temperature in any series of irradiations. Each data point shown in the figures of this Appendix is the average of at least eight measurements obtained on each pair of Hall bar arms by reversing the magnetic field direction and by repeating the measurements. Reproducibility of the Hall and resistivity voltages was 2 and 5 percent, respectively. The carrier-removal rates measured at the higher bombardment temperatures were determined after larger changes in carrier density had taken place compared to the density changes at the lower irradiation temperatures. Therefore to check the effect of electron fluence on the results, undamaged samples were lightly bombarded at 250°K, and carrier-removal rates determined from the linear region of the carrier density versus fluence curve. The results were in agreement with the carrier-removal rates reported in this paper for this bombardment temperature. However, a sample bombarded to a fluence of 2×10^{17} e/cm^2 exhibited ≈ 94 percent change in carrier density,

and yielded a carrier-removal rate which was smaller by a factor of 5 than the value obtained on the lightly bombarded sample. This fluence dependence of carrier-removal rate occurs for very small (Ref. I-10) or very large values of fluence. To avoid these effects, the samples in this experiment were irradiated to moderate values of electron fluence which resulted in a linear dependence of carrier-density loss on fluence at all bombardment temperatures. After the completion of irradiation at selected bombardment temperatures, measurements of isochronal annealing rates, and the temperature dependence of carrier density and resistivity were made. The annealing temperature was not allowed to exceed 250° K so that the mobility of lithium ions was reduced to 1°50 of the room temperature value. By setting this temperature limit, the interaction of lithium with radiation-induced defects was reduced to a negligible amount. Following the completion of irradiations at all bombardment temperatures, the sample temperature was allowed to increase to room temperature, and the interaction of lithium with radiation-induced defects was determined from measurements of the Hall-effect and resistivity on samples which had annealed at this temperature of 290°K.

C. EXPERIMENTAL RESULTS

1. Carrier-Removal Rates

Electron irradiation of n-type silicon introduces carrier removal defects which can accept electrons from the conduction band. Thus, carriers are removed from the conduction band and charged-scattering centers are created which reduce the electron mobility. This loss of carriers and reduction of mobility cause the resistivity of the silicon to increase. The effects are separated by measuring both the resistivity and the Hall-coefficient. In these experiments measurements of carrier losses as a function of electron fluence at any bombardment temperature were used to compute a carrier-removal rate-$\Delta n/\Delta \Phi$ (CM), and the results for both crucible and zone silicon are shown in Figure I-3. These removal-rates are those rates which remain after the irradiated samples were annealed to 200° K. Therefore, these rates represent carrier-removal rates of defects which are independent of temperature and have been called ITD defects in previous studies (Ref. I-4). A carrier-removal rate of 3 cm^{-1} obtained on samples of lithium-doped zone silicon of 0.1 ohm-cm bombarded at room temperature has been reported (Ref. I-11). This value of $\Delta n/\Delta \phi$ (CM) was not a constant, but changed with time following the bombardment. It will be shown later in this Appendix that the measurement of carrier-removal rates obtained by bombardments at room temperature are influenced by the continuous loss of carriers which occurs during the annealing processes. Bombardment and measurement of carrier-removal rates at room temperature reflect the competing processes of damage and annealing. The additional defect which only occurs in oxygen-containing silicon at a bombardment temperature of $T_B = 250°K$

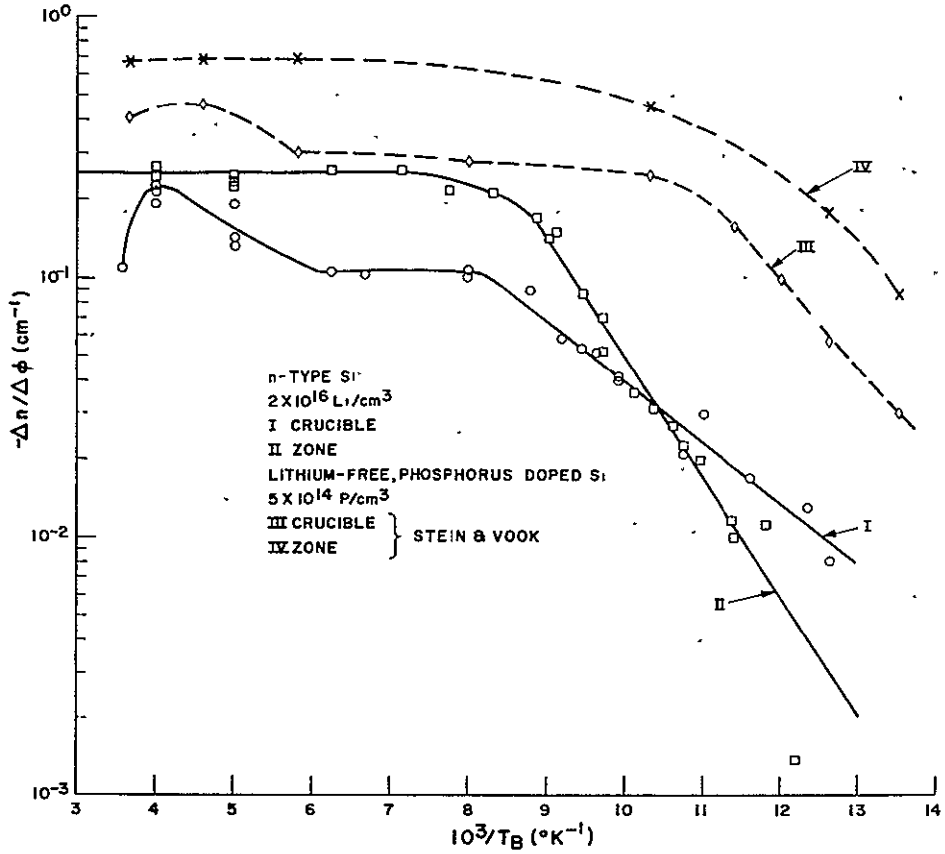

Figure I-3. Carrier-Removal Rates Versus Reciprocal Bombardment Temperature for Float-Zone and Quartz-Crucible Silicon. Measurements at 79° to 81° K after Annealing to 200° K. Results of Stein and Vook (see Ref. I-4) for 10 ohm-cm Phosphorus-Doped Zone and Crucible-Silicon shown for Comparison.

produced a peak in the $-\Delta n/\Delta\phi$ curve for crucible silicon. This defect has been attributed (Ref. I-4) to an oxygen complex since it does not occur in oxygen-lean Float-Zone-refined silicon as indicated in Figure I-3. The curve of $-\Delta n/\Delta\phi$ for zone silicon decreases with decreasing temperature at a faster rate than the curve for crucible silicon. Calculations of the slopes of these carrier-removal curves gave 0.09eV and 0.055 eV for the zone and crucible silicon curves, respectively. Apparently the defect-production mechanisms are different in these two types of silicon. Thus, this result suggests that different defects are produced in oxygen-containing silicon compared to oxygen-lean silicon. Carrier-removal rates (Ref. I-4) obtained on crucible and zone silicon doped with phosphorus to 5×10^{14} cm^{-3} are also shown in Figure I-3 for comparison. The temperature dependence of $\Delta n/\Delta\phi$ shifted to higher temperatures relative to the results obtained on the phosphorus-doped samples of higher-resistivity. This dependence on resistivity was predicted by the

charge-state-dependent theory of Reference I-4. The higher damage rates of the phosphorus-doped samples for both types of silicon are due to the higher energy electrons (E = 1.7 MeV) used to obtain these data, and also to the higher phosphorus-doping density of these samples which cause greater E-center production. It should be noted that the high temperature carrier-removal rate of zone silicon is greater than that of crucible silicon by a factor of ≈2.5. A defect complex such as the LiO-V defect is an acceptor which removes two carriers from the conduction band. In a similar way, a Li-V defect will remove two carriers in oxygen-lean silicon. In contrast to this effect, the A-center (OV) removes only a single carrier. Thus, either the production rate of Li-V defects is higher than the LiO-V defect, or more A-centers than LiO-V defects are produced in crucible silicon under the conditions of this experiment. It will be shown later that A-center production appears to be about equal to the LiO-V center production.

Sources of systematic errors in obtaining the carrier-removal rates are primarily: (1) assumed values of μ_H/μ_c for each bombardment temperature, (2) magnetic field measurement in air to represent the value of magnetic field at the sample, (3) the fluence determination, and (4) a measurement or control error of 1° K in bombardment temperature near 80°K means an error of ≈ 22 percent in the carrier-removal rate measured on zone silicon and ≈12 percent error on crucible-silicon samples based on the measured slopes of 0.09 eV for the zone-silicon and 0.55 eV for the crucible-silicon curves. The last source of error is the dominant one in both types of silicon samples.

2. Crucible Silicon

a. Carrier-Density Changes

Identification of defects can be accomplished by measuring the carrier density as a function of temperature in order to move the Fermi level through the unknown defect level. Thus, the defect level is filled and emptied of electrons, and the inflection point in the curve of carrier density versus reciprocal temperature locates the defect-energy level and its concentration. This technique is successful only when the defect level is located between the conduction band and approximately 0.2 eV below the conduction band. Curves of carrier density n, versus reciprocal temperature measured at different times before and after bombardment are shown in Figure I-4. It should be noted that the carrier-removal rates one would calculate from Figure I-4 will not correspond to any unique data point in Figure I-3. The pre-irradiation measurements of carrier densities versus temperature are

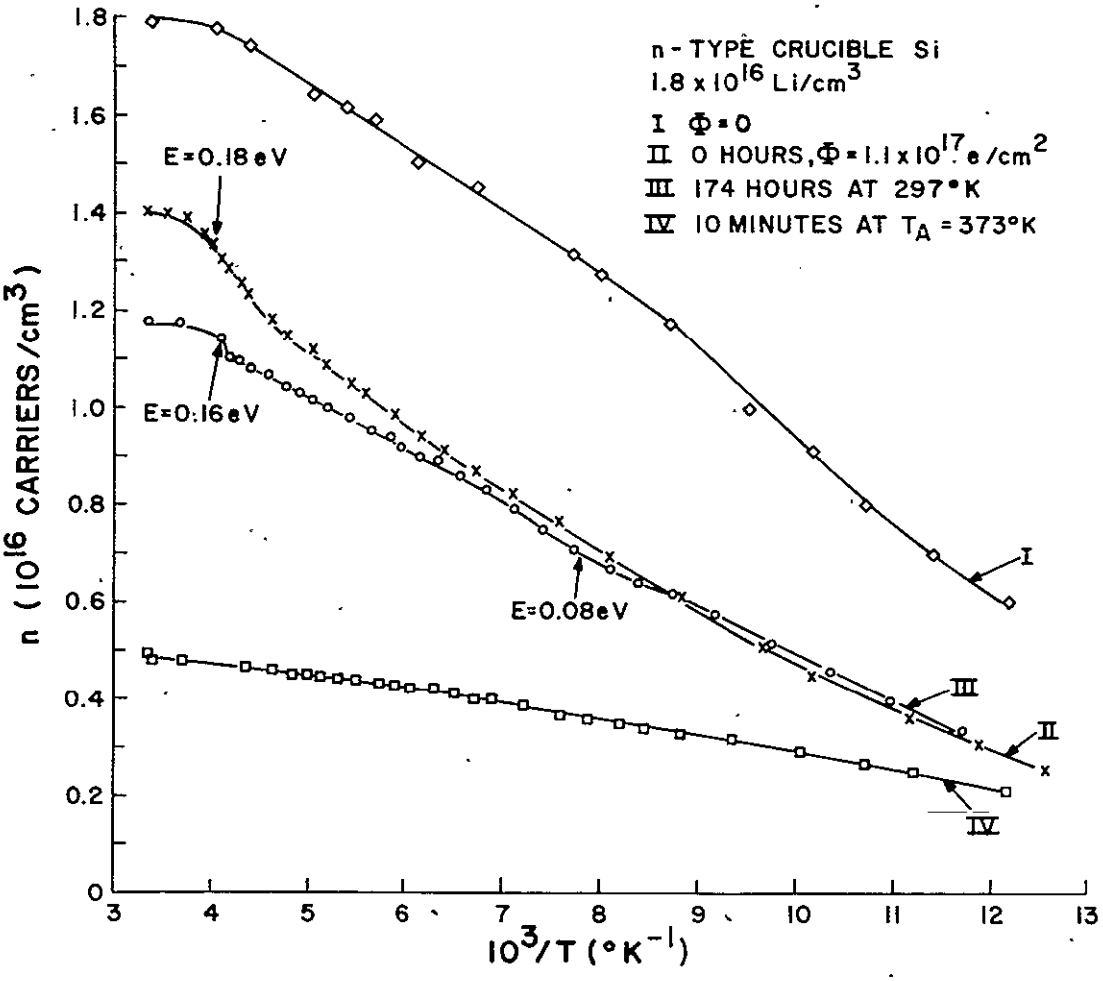

Figure I-4. Carrier Density Versus Reciprocal Temperature for Crucible Silicon (1) Before Irradiation, (2) Immediately after Irradiation, (3) Annealing to a Temperature of 297°K for 174 hours, and (4) Then Annealing for 10 min. at a temperature of 373°K.

shown in Curve I. A decrease in temperature shifted the Fermi-level towards the conduction band, and consequently the percentage of ionized donor levels decreased. Thus, the carrier density varied in accordance with the dependence of Fermi statistics on temperature. Curve III is the temperature dependence of carrier density measured immediately after the completion of all bombardments. A defect-energy level located near 0.18 eV is identified as the A-center (Ref. I-2 to I-4). The defect density is about 1×10^{15} cm^{-3} with a temperature T = 220°K

at half-filling of the defect level. This A-center concentration is about 1/3 of the total carrier-removal defects calculated from carrier-removal rates and fluences at each bombardment temperature. Since the A-center removes one electron and the LiO-V defect removes two electrons, A-center production appears to be about equal to the LiO-V defect production in the samples of this experiment. Curve III is the temperature dependence of carrier density obtained on the sample after it annealed for 174 hours at 290°K following the completion of bombardment. A decrease of carrier density at high temperature, and a slight increase of carrier density at low temperature occurred during this annealing period. The decrease of n at room temperature can be attributed either to the formation of additional deep-lying acceptor levels and/or loss of lithium due to the complexing of lithium with A-centers or LiO-V-centers. This latter possibility of a lithium loss to explain the decrease of carrier density at high temperature is strongly supported by the increase of the Hall mobility at low temperature. In the defect center previously located near 0.18 eV shifted to 0.16 eV below the conduction band. The formation of a new level located near E_c -0.08 eV is indicated by Curve III. This level also appears in irradiated-crucible silicon of low-doping density (2×10^{15} cm^{-3}) after annealing to 297°K, but the level appeared to be very distinct and measurable (see Figure I-10). The final curve shown in Figure I-4 was obtained after annealing for 10 minutes at a temperature of 373°K. The purpose of this technique was to speed up the interaction of lithium with radiation-induced defects. Curve IV shows that all defect levels have disappeared and the carrier density has decreased extensively at all temperatures. Thus, the interaction time of lithium with defects was accelerated considerably by the high temperature annealing. All defects appear to be neutralized at an annealing temperature and for a duration which is insufficient to anneal normal defect centers (e.g., A, E, C, etc.).

b. Mobility Changes

The Hall-mobility data gives strong support to the suggested annealing mechanism of lithium complexing with defects and neutralizing their electrical effect. Figure I-5 shows the Hall-mobility versus reciprocal temperature for the same sample and measured under the same conditions as in Figure I-4. Curve II is the mobility measured immediately after bombardment. Curves III and IV show the mobility progressively recovering from the state of damage after 34 and 174 hours at 297°K following bombardment. Clearly, charged-scattering centers are being neutralized since the mobility varies inversely with the number of charged centers. Curve V is the mobility measured after the sample was annealed for 10 minutes at a temperature of 373°K. These measurements showed that the mobility completely recovered to approximately the pre-irradiation values. Therefore, the scattering conditions in the sample after this annealing process are equivalent to the initial conditions before bombardment.

3. Zone Silicon

a. Carrier-Density Changes

In order to study the effect of oxygen on the results, samples fabricated from Float-Zone Silicon were irradiated and measured. The low-oxygen content ($\leq 10^{14}$ cm^{-3}) and high resistivity ($\geq$ 1500 ohm-cm) of the starting silicon prevented a significant number of impurity-defect complexes from forming except for lithium-defect complexes. Figure I-6 shows the carrier density versus reciprocal temperature measured before bombardment, immediately following bombardment, and after 17 hours at room temperature following bombardment. Irradiated float-zone silicon exhibited an increase of carrier density at all temperatures, instead of a spontaneous decrease of carrier density which occurred in crucible silicon after annealing at room temperature. Both mechanisms of dissociation of carrier-removal defects, and neutralization of these defects by lithium takes place in irradiated-float-zone silicon soon after bombardment. Studies of annealing kinetics performed on lithium-doped solar cells (Ref. I-6, I-11) indicate that the mechanism of annealing is an interaction by lithium with recombination-defect centers which neutralize their degrading effect on minority-carrier lifetime. The mechanism of solar cell annealing by the annihilation of a Li-V defect has also been proposed (Ref. I-12). The fast reaction at room temperature is due to the lack of oxygen which combines with lithium and decreases the free-lithium diffusion constant (Ref. I-5) in crucible silicon. For the concentration of lithium and oxygen in the samples used in this experiment, the diffusion constant in crucible silicon is $\approx 1/100$ the diffusion constant of lithium in zone silicon.

b. Mobility Changes

The decrease of the mobility is consistent with the introduction of charged-scattering defects in samples bombarded by electrons. Figure I-7 shows the mobility dependence on temperature for the same sample and conditions described in Figure I-6. After the 17-hour annealing period, the mobility completely recovered to slightly better than the initial values. This speed of recovery is to be contrasted with the speed of mobility-recovery in crucible silicon as shown in Figure I-5. Measurements on a crucible-silicon sample annealing at 297° K for 40 days after bombardment still showed that the mobility had not fully recovered. Thus without the necessity of annealing to a temperature of 100° C, irradiated-zone silicon exhibits neutralization and dissociation of all charged scattering centers in $\leq$ 17 hours at room temperature after completion of bombardment.

Recovery of mobility is controlled by the complexing mechanism of annealing if the assumption is made that only one lithium donor is required to neutralize a lithium-defect complex. Thus, there is no effective change in carrier density, but there is a decrease in the number of charge-scattering centers. The increase of carrier

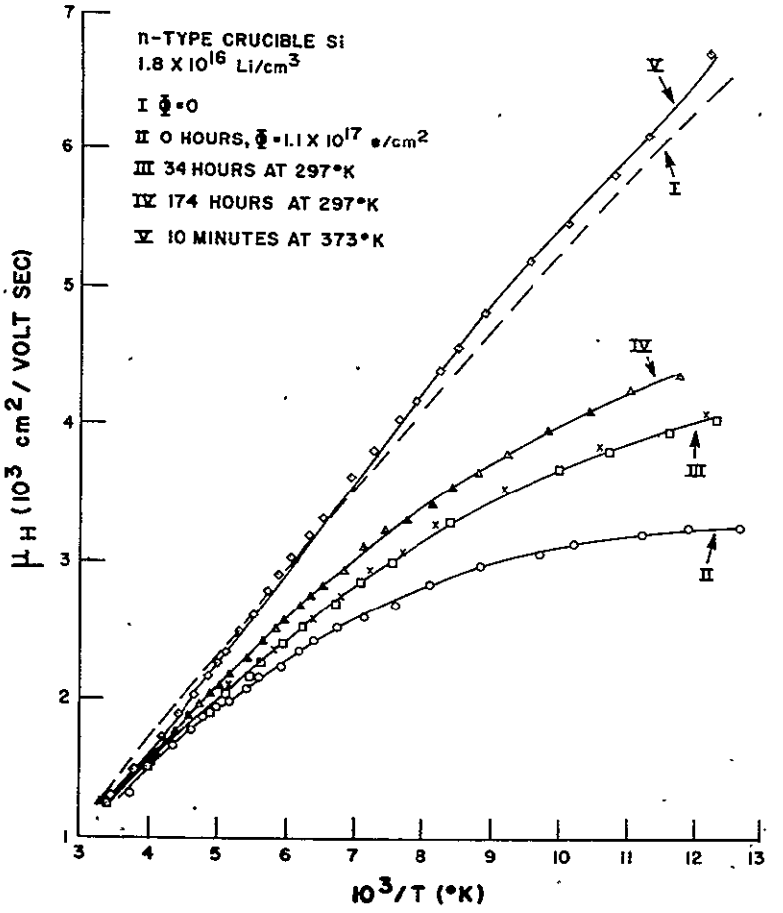

Figure I-5. Hall mobility versus reciprocal temperature for crucible silicon, (1) before irradiation, (2) immediately after irradiation, (3) annealing to a temperature of 297° K for 34 hours, (4) annealing to a temperature of 297° K for 174 hours, and (5) then annealing for 10 min. to a temperature of 373° K.

density is controlled by the mechanism of dissocation. Therefore, a measurement of recovery kinetics would indicate the existence of the two processes. Accordingly, a sample of zone silicon was irradiated to a fluence of 2×10^{15} e/cm^2 at a bombardment temperature of 250° K, and then isothermally annealed at a temperature of 297° K. Measurements of mobility and carrier density were made at temperatures of 83° K and at 297° K. The results are shown in Figure I-8 where the unannealed fraction of reciprocal mobility f_μ and of carrier density f_n are plotted versus the annealing time. The mobility recovers faster than the carrier density. It appears that recovery from radiation damage by a defect-complexing process and by a defect-dissociation process act in parallel. A surprising result was the additional annealing stage which commenced at an annealing time of 120 min. Measurements made at annealing times of 63 and 255 hours indicated that this second annealing stage was unstable since the mobility and carrier density returned to the recovery levels achieved after the first stage of recovery. The zone-silicon samples used

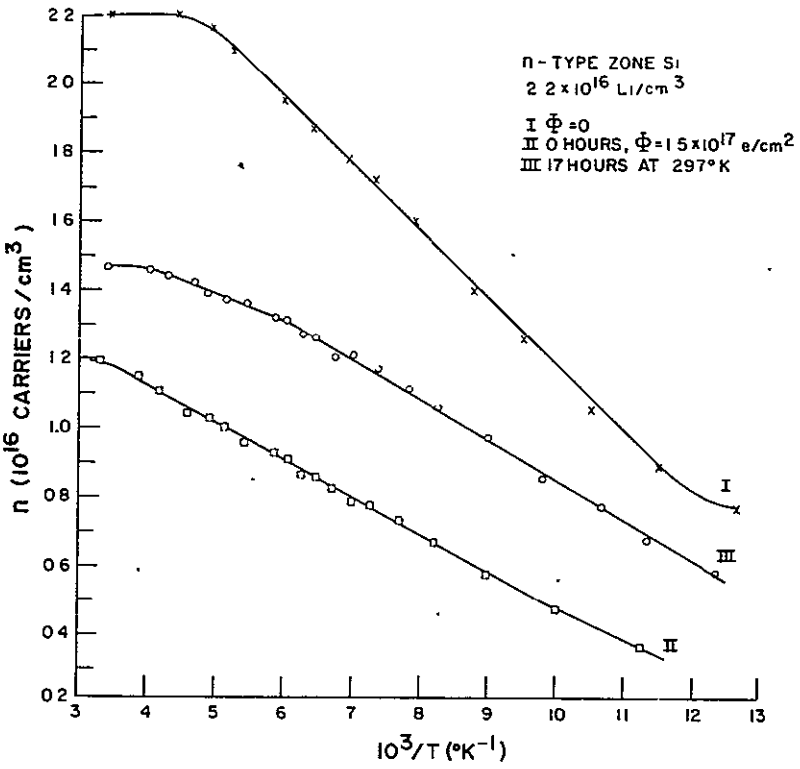

Figure I-6. Carrier density versus reciprocal temperature for zone silicon, (1) before irradiation, (2) immediately after irradiation, and (3) annealing to a temperature of 297° K for 17 hours.

in obtaining carrier-removal rates were remeasured 79 days after bombardment to check the long-term stability of the annealed samples. They did not show any significant change from the recovered-carrier density and values of mobility indicated in Figures I-6 and I-7. The carrier density measured at a temperature of 297° K increased as is shown in Figure I-8. This indicated that the free lithium density increased as a result of Li-V defects dissociating. The mobility measured at 297° K did not change since it is dominated by lattice scattering rather than charged-defect scattering at this temperature.

4. High Resistivity Crucible Silicon

a. Annealing

The purpose of this paper was to study the production mechanisms of primary and secondary defects in electron-irradiated silicon containing lithium. The high concentration of oxygen ($10^{18}cm^{-3}$) in crucible silicon prevents the formation of lithium-defect complexes in measurable quantities in samples doped with lithium to concentrations of $\approx 2 \times 10^{15}cm^{-3}$. For this reason, the major portion of the work was carried out on samples doped with lithium to a concentration of $2 \times 10^{16}cm^{-3}$. The production of A-centers dominates in crucible silicon of low doping density. This has been shown in recent EPR measurements (Ref. I-13) and also will be shown in

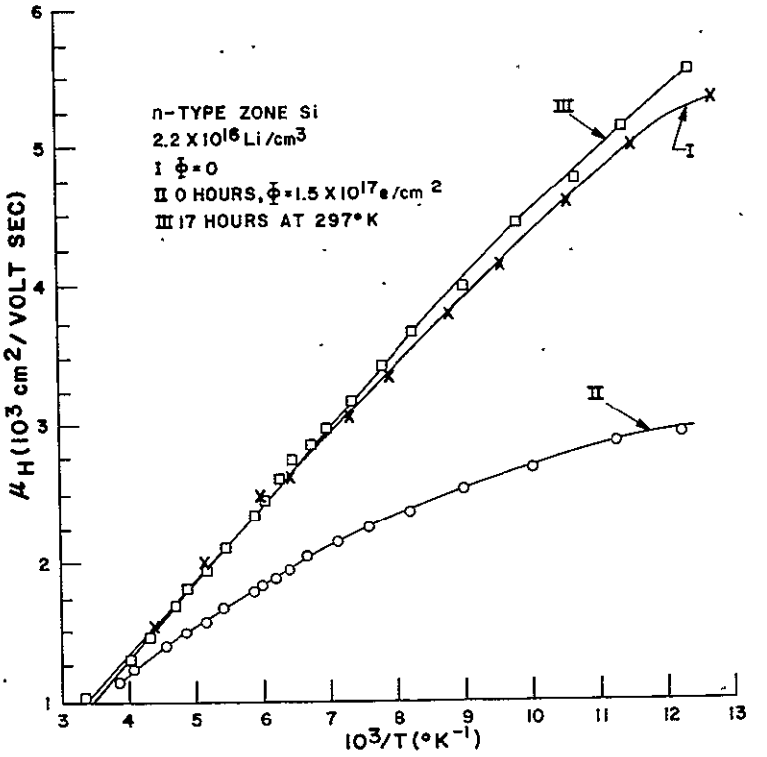

Figure I-7. Hall mobility versus reciprocal temperature for zone silicon, (1) before irradiation, (2) immediately after irradiation, and (3) annealing to a temperature of 297° K for 17 hours.

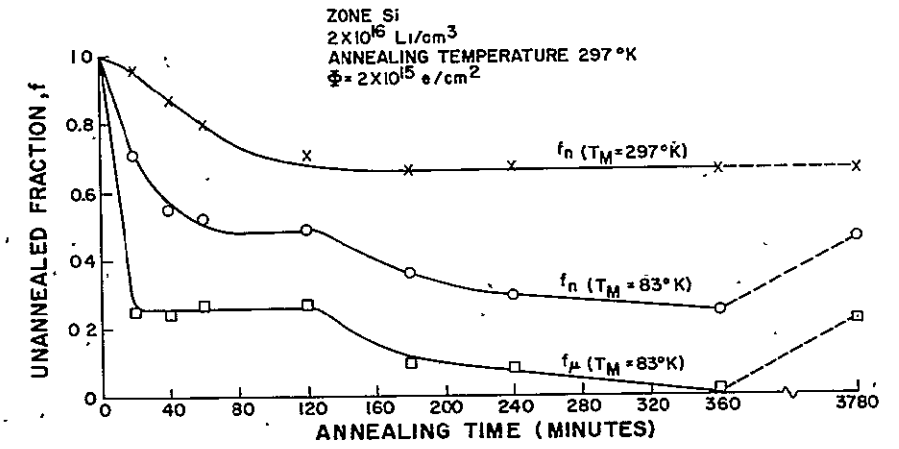

Figure I-8. Unannealed fraction of carrier density f_n and unannealed fraction of reciprocal mobility f_μ versus annealing time. Measurements made at 297° K and 83° K on zone silicon irradiated at 250° K and annealed to a temperature of 297° K

this paper. A sample of crucible silicon from the same 30 ohm-cm material used in all these measurements was doped with lithium to a concentration of $2 \times 10^{15} cm^{-3}$ and irradiated with electrons at bombardment temperatures of 79°K and 250°K.

After the completion of the low-temperature bombardments an isochronal annealing cycle of 10 min duration at each annealing temperature up to a limit of 250°K was carried out. The upper-temperature limit was set at 250°K to prevent lithium motion and interaction with defects from occurring. The product of the unannealed fraction and $-\Delta n/\Delta\Phi$ (cm) is shown in Figure I-9 together with the unannealed fraction of $1/\mu$. There appears to be two annealing stages and a reverse annealing peak at 250°K which has been observed in previous electrical experiments. Following the description of Stein and Vook (Ref. I-4), both stages are attributed to the annealing of ITI

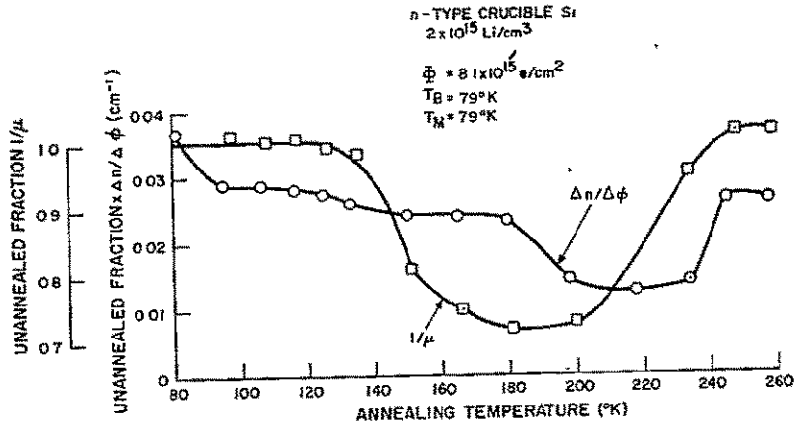

Figure I-9. Unannealed fraction of carrier-removal rate and mobility versus annealing temperature for high resistivity (2.5 ohm-cm) crucible silicon after irradiation at 79°K with measurements at 79°K

(Irradiation-Temperature Independent) defects in the temperature range of 100°K to 200°K. Stein and Vook attributed the reverse annealing peak to the formation of a defect located near an energy of 0.13 eV below the conduction band. This reverse annealing peak is not observed in oxygen-lean Float-Zone silicon, and thus the production of this defect requires the presence of oxygen. The separation of the total carrier-removal rate into the separate defect components can be deduced from the annealing cycle. Thus 0.02 cm^{-1} is attributed to ITI defects, and 0.016 cm^{-1} to ITD (Irradiation-Temperature Dependent) defects. The ITD defects are those which involve impurities such as oxygen, phosphorus or lithium. In the present case, the phosphorus background is quite low ($\approx 10^{14}$ P/cm^3), thus E-centers are not expected to occur in significant quantities. The two possibilities are the A-centers (OV) or a center involving lithium. More will be said about this latter possibility in the discussion. Correlation of mobility changes with carrier-density changes during the

annealing cycle are indicated in Figure I-9 where the unannealed fraction of $1/\mu$ is plotted versus annealing temperature. The fraction f_μ is given by Equation (I-1).

$$f_\mu = \frac{1/\mu\,(T) - 1/\mu_o}{1/\mu\,(79°K) - 1/\mu_o} \qquad \text{(I-1)}$$

where

$1/\mu\,(T)$	is the reciprocal value of mobility after annealing at temperature T and measured at T = 79° K,
$1/\mu\,(79°\,K)$	is the post-bombardment value of reciprocal mobility measured at 79° K, and
$1/\mu_o$	is the pre-bombardment value of reciprocal mobility measured at T = 79° K.

The annealing cycle of $1/\mu$ showed only a single stage of annealing, but the reverse annealing peak at T = 250° K was in agreement with the annealing cycle of the carrier-removal rate. The annealing curve agrees qualitatively with the results obtained on phosphorus-doped crucible silicon (Ref. I-4) of 10 ohm-cm resistivity, and also on lithium-doped crucible silicon of 0.3 ohm-cm. The qualitative results are independent of the dopants and their densities in these samples.

b. Carrier Density Changes

The remaining results are concerned with the temperature dependence of carrier density measured immediately after each irradiation, and then as a function of time after the last irradiation with the sample annealing at room temperature. These data are shown in Figure I-10. The most interesting results in the data of Figure I-10 are the interaction of lithium with the radiation-induced defects as demonstrated by the temporal behavior of n during the annealing process at room temperature, and the location of defect-energy levels in the carrier-density versus temperature curves. The location of defect-energy-levels can be determined from the curves of n versus reciprocal temperature. The temperature at which half filling of the defect level occurs is indicated in Figure I-10. It can be seen that two energy levels are indicated by curve II which is the data taken after completion of the annealing cycle following the irradiation at a temperature of T_B = 79° K. These levels were determined to be 0.18 eV and 0.13 eV below the conduction band which are in agreement with the results of Vook and Stein, namely 0.185 eV and 0.13 eV. The data of curve III for T_B = 250° K in Figure I-10 indicates an energy level extending over a broad temperature range with an approximate temperature $T_{1/2}$ = 208° K for the half-filling of the level. This locates the level at an energy of 0.16 eV below the conduction

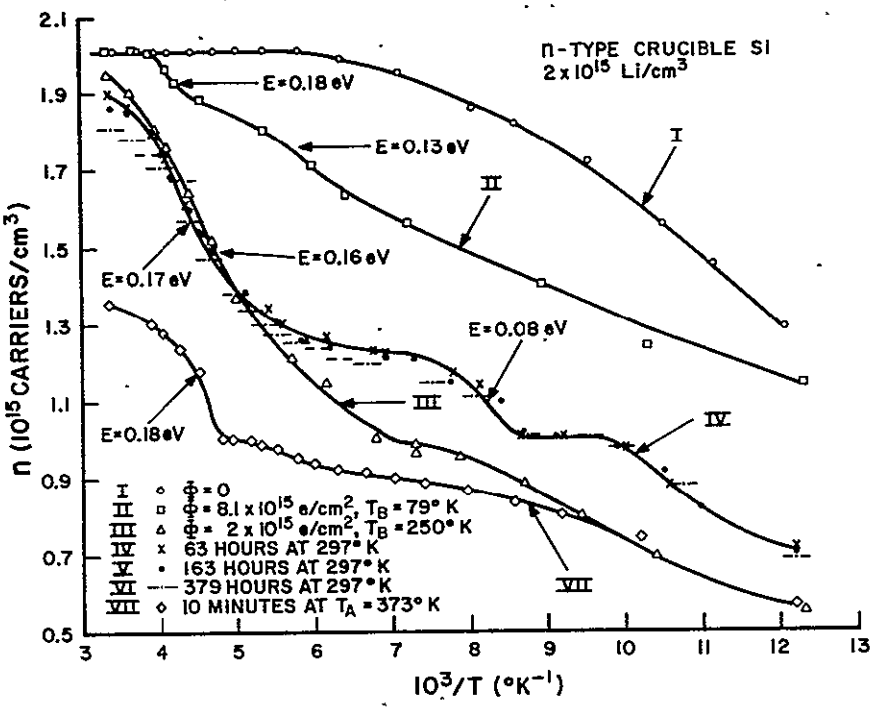

Figure I-10. Carrier-density versus reciprocal temperature for high resistivity (2.5 ohm-cm) crucible silicon, (1) before irradiation, (2) after irradiation at 79°K plus annealing to 250°K, (3) after irradiation at 250°K, (4) annealing to a temperature of 297°K for 63 hours, (5) annealing to a temperature of 297°K for 163 hours, (6) annealing to a temperature of 297°K for 379 hours, and (7) annealing to 373°K for 10 min.

band. The determination of the half-filling point is not accurate since the energy of this defect level appears perturbed or smeared out over a broad energy range. Merging of the levels at 0.18 and 0.13 eV would produce a broad energy level such as this one.

Examination of curve IV measured after 63 hours at room temperature following bombardment, shows that the level at 0.17 eV (A-center) is still present, and the 0.13 level has disappeared, however a new level at 0.085 eV has formed. Curve V and VI are measurements taken at t = 163 hrs and 379 hrs after completion of the irradiation. The 0.085 level is still present but significantly the carrier density progressively decreases at high temperature and increases at low temperature.

Loss of carrier density at high temperature and the increase of carrier density at low temperature as a function of annealing time at room temperature is similar to the behavior in the low resistivity (high-doping density) crucible silicon (see Figure I-4).

The explanation is the same as the one suggested before, namely lithium complexes with defects to neutralize their electrical effect on carrier density. However, now it is predominantly the A-center which has been affected. The number of LiO-V centers is small and unimportant. Quantitative arguments supporting this idea will be presented in the discussion. Curve VII is the result of annealing the sample at 373°K for 10 minutes, thereby accelerating the interaction of lithium with defect complexes. A defect level approximately located at 0.18 eV and distributed over a wide energy range still remains. The behavior of the mobility substantiated this fact since it did not recover to its initial value as the mobility did in the low resistivity sample. Some residual damage remained even after the high temperature annealing process. The interaction level located at 0.085 eV did not form in Float-Zone silicon and therefore it must require the presence of oxygen for it to occur.

D. DISCUSSION

1. Defect Formation

This study of primary and secondary defect formation during low temperature bombardment by 1-MeV electrons shows that two distinct types of defect dominate the electrical behavior of lithium-doped silicon. The dominant type of defect is a secondary defect formed by the complexing of vacancies with crystal impurities. Vacancies are supplied from metastable interstitial-vacancy close-pairs. The irradiation-temperature dependence of defect formation has been attributed (Ref. I-2, I-4, I-14) to an intrinsic production process of vacancy liberation. This does not appear to be the complete description of defect production mechanisms in lithium-doped silicon. The second type of defect formed during bombardment is introduced at a rate which is independent of irradiation temperature, and this defect is a primary or intrinsic defect as previously reported (Ref. I-4). These defects are called ITI (Irradiation-Temperature Independent) defects. Carrier-removal rates shown in Figure I-3 were the results obtained on the samples after annealing to 200°K. The ITI defects anneal between 100°K to 200°K as shown in Figure I-9. The carrier-removal rate of ITI defects was found to be $0.003 \pm 0.002\,cm^{-1}$ in the eight samples of zone and crucible silicon. A value of $0.02\ cm^{-1}$ for the ITI defects was obtained on the high-resistivity sample of crucible silicon. Additional measurements of high resistivity samples are required to confirm this value. Both values of carrier-removal rate due to ITI defects are small compared to the value of $0.075\ cm^{-1}$ reported in Reference I-4. If one adjusts the ITI defect production rates for the higher electron energy (1.7 MeV) used in the experiments of Reference I-4, then the values reported in this paper are still in disagreement by a factor of ≈ 12 for the 0.3 ohm-cm samples. Thus these results suggest a smaller probability of ITI formation in low resistivity lithium-doped silicon.

The irradiation-temperature dependence of the production rate of impurity-complexes in silicon has been explained by a model (Ref. I-2, I-4, I-15) based on the formation of closed-spaced interstitial-vacancy pairs by electron bombardment. This model

yields a probability of vacancy liberation from the interstitial to form vacancy-impurity defects. The probability of vacancy liberation from its corresponding interstitial is given by

$$P = \frac{P_c}{1+\gamma \exp E_b^+/kT} + \frac{(1-P_c)}{1+\gamma \exp E_b^-/kT} \qquad \text{(I-2)}$$

where

- P is the probability of defect formation,
- γ is the ratio of statistical weights for the jomp which annihilates the pair to that which liberates the vacancy from the interstitial,
- E_b^+ is the energy barrier to liberation when the close-pair is in the more positive state,
- P_c is the probability of finding the close pair in a metastable state which is more positive, and
- $(1-P_c)$ is the probability of finding the close pair in a state which is more negative.

This probability P_c is given by Equation (I-3).

$$P_c = \left[1 + g \exp \frac{E_F(n_o, T) - E_M}{kT} \right]^{-1} \qquad \text{(I-3)}$$

where

g is the ratio of the number of ways the state can be occupied to the number of ways the state can be unoccupied, $E_F(n_o, T)$ is the Fermi level for electrons which is a function of initial carrier concentration n_o and temperature T, and E_M is the energy level of the metastable interstitial-vacancy pair.

Attempts to fit the data obtained on crucible or zone silicon with the simplified form of Equation (I-2) where the terms involving the difference in barrier heights are neglected and only the P_c term is considered significant were not completely successful. Data obtained on 10 ohm-cm phosphorus-doped zone-silicon (Ref. I-4) were fitted with Equation (I-3) and parameters g = 1 and E_M = 0.07 eV were used. The theoretical fit of the data is shown in the normalized defect-production probability curves for crucible silicon in Figure I-11. Equation (I-3) was used to fit the crucible silicon results of this experiment by setting E_M = 0.08 eV and g = 0.1 and this theoretical curve is also shown in Figure I-11. However, the results obtained on zone silicon cannot be fitted with an expression of this simple form. The normalized probability curves for zone silicon are shown in Figure I-12. The slope of the curve $-\Delta n/\Delta\Phi$ versus reciprocal temperature yields an energy of 0.09 eV. The best fit to the data using the simple charge-state dependent probability of defect formation was obtained with E_M = 0.08 eV and g = 0.013. The theoretical values still disagreed with experimental data in the region of the bend-

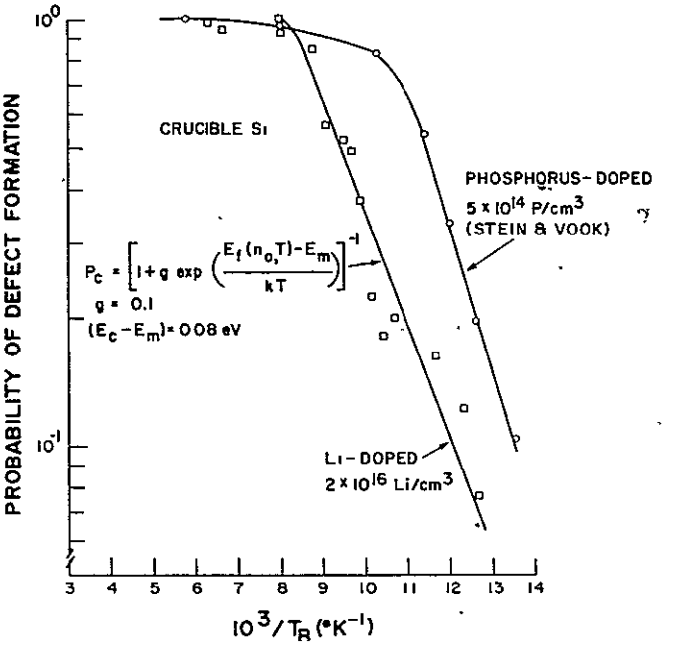

Figure 1-11. Comparison of predicted defect production probability for the charge state-limited model with measurements of defect production rates for crucible silicon. Experimental and calculated values have been normalized. Results of Stein and Vook (see Ref. 4) are shown for comparison.

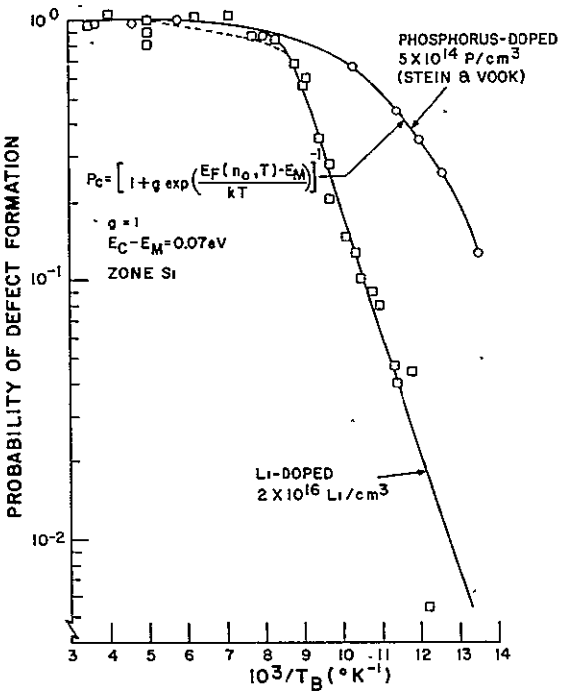

Figure 1-12. Comparison of predicted defect-production probability for the charge state-limited model with measurements of defect production rates for zone silicon. Experimental and calculated values have been normalized. Results of Stein and Vook (see Ref. 1-4) are shown for comparison.

over temperature. It should be noted that the lithium donor level is located at 0.0328 eV below the conduction band in Float-Zone silicon, and the LiO donor level at 0.0394 eV in crucible silicon (Ref. I-16). This unusual situation means that for the same donor density and temperature, the Fermi level is deeper in the forbidden energy gap in crucible silicon than in zone silicon. Thus at low temperatures, the Fermi filling factor for the metastable-close-pair energy level can be significantly different in the two types of silicon. It appears that either the complete expression given by Equation (I-2) must be used to fit the data, or the irradiation-temperature dependence does not arise solely from an intrinsic production process. The type of impurity-vacancy complex could play a part in the temperature dependence. However, the results obtained on oxygen containing silicon suggest that an intrinsic process is operative since a good fit of the data with Equation (I-3) and reasonable values of g and E_M was possible.

2. Defect Annealing

Annealing processes of defects in lithium-doped silicon are unusual since the mobility of lithium makes it possible for lithium to diffuse to and complex with defects at room temperature. High temperatures are not required to anneal large fractions of damage in bulk silicon or devices such as lithium-doped solar cells (Ref. I-6, I-7, I-11). It was shown by the data in Figure I-4 that a temperature of 100°C is sufficient to cause considerable defect annealing. Thus the range of temperatures used to anneal the samples was limited to a range of 79°K to 373°K. In the lower temperature range from 79°K to 250°K, the annealing data obtained on lithium-doped crucible and zone-silicon samples are qualitatively similar to the annealing data obtained on phosphorus-doped silicon (Ref. I-4). Irradiated-crucible and zone silicon exhibited annealing of ITI defects in the temperature range of 100° to 200°K. A reverse annealing peak amounting to a 50-percent increase of carrier-removal rate was observed at 250°K in crucible silicon. The qualitative characteristics of the annealing cycle appear to be independent of impurities other than oxygen. Spontaneous annealing of defects occurred in the irradiated lithium-doped silicon when the samples warmed up to room temperature. In this respect, the annealing behavior is unique and distinctly different from irradiated-silicon doped with impurities other than lithium. Defect annealing in crucible silicon was clearly demonstrated by the behavior of electron density versus reciprocal temperature shown in Figure I-4 and by the recovery of mobility shown in Figure I-5. It appears that lithium diffuses to and combines with defects to form defect-complexes which are neutral and electrically inactive. The loss of donors at high temperatures is attributed to the loss of LiO donors. The speed of the lithium interaction is slowed down by the oxygen which reduces the free lithium diffusion constant by $\approx 1/100$. Application of heat (100°C) accelerated the interaction of lithium with defects so that complete recovery of mobility occurred. Thus, all radiation-induced charged-scattering centers were neutralized.

In zone silicon the annealing behavior was diametrically opposite to the crucible behavior. Carrier density increased at all temperatures, and the mobility completely recovered within a short period of time at room temperature. It was observed that recovery commenced within an annealing period of 20 minutes at room temperature.

The mechanism of annealing in zone silicon is attributed to lithium complexing with defects and dissociation of loosely bound lithium-vacancy complexes. Both processes act in parallel to anneal radiation damage in zone silicon. However the recovery time constant of the complexing process appears to be faster than the time constant for the process of dissociation.

3. Defect Types and Number

The results indicate that carrier-removal centers are introduced in lithium-doped crucible and zone silicon irradiated by 1-MeV electrons. Identification of the defects responsible for carrier removal can only be inferred from these measurements since this experimental technique is an indirect method, which does not separate out, and examine specific defects as in the more powerful EPR measurement technique. B. Goldstein (Ref. I-13) has observed a four line EPR spectrum in electron-irradiated crucible-silicon, and a single line spectrum in zone-silicon doped with lithium. These damage spectra were attributed to the Li-O-V complex in crucible silicon and the Li-V complex in zone silicon. In those situations where defect energy levels are measurable (e.g., A-center see Figure I-4 and I-10), identification of defects can be made with some degree of certainty with the techniques of this experiment. Defect densities can be obtained from n versus 1/T curves, and compared with values calculated from the measured carrier-removal rates and electron fluences.

The high purity of the Float-Zone samples used in this experiment, minimized the production of E-centers and A-centers. Thus, a Li-V carrier-removal defect-complex appears to be the most probable defect responsible for carrier losses in the zone silicon. In contrast to the zone silicon, the high oxygen concentration in the crucible silicon samples means that oxygen will compete with the LiO donor for vacancies produced by electron bombardment. Lithium complexes readily with oxygen, and at least 70% of the lithium (Ref. I-8) is in the form of LiO immediately after diffusion of the crucible-silicon samples with lithium.

a. High Resistivity Crucible-Grown Silicon

One of the objectives of this investigation was to determine if the lithium-oxygen complex combines with a vacancy to form a defect similar to the E-center. Some limits can be established relative to the possibility of lithium-defect center production by the following considerations. Identification of the defects produced during the irradiations at a temperature of $T_B = 79°K$ in the high-resistivity crucible sample appears sufficiently certain so that an estimated value of lithium-center density can be made. Two energy levels can be seen in curve II of Figure I-9. The one 0.18 eV is close to the value of 0.185 eV below the conduction band reported by Vook and Stein (Ref. I-4), 0.186 eV reported by Novak (Ref. I-3), and 0.183 eV by Wertheim (Ref.

I-17). This defect level is believed to be the A-center. The second defect level in curve II is not as distinct as the A-center. It is located near 0.13 eV which agrees with the value of 0.13 eV obtained in Reference I-4 and attributed to the defect produced during the reverse-annealing peak at an annealing temperature of 250°K.

Based on a carrier-removal rate of $-\Delta n/\Delta\Phi = 0.016$ cm^{-1} plus 0.01 cm^{-1} for the defects produced during the reverse annealing peak, the total number of defects is 2.1×10^{14} cm^{-3}. The total sum of A-centers and the 0.13 eV centers from curve II is 3.6×10^{14} cm^{-3}. Since all the defects calculated on the basis of the carrier-removal rate are accounted for, there does not appear to be any lithium centers produced at $T_B = 79°K$. A further check on this conclusion can be obtained from the change in carrier density measured at room temperature after irradiation. If there are no deep centers in the band gap, then the Fermi level corresponding to room temperature should be in a position where all levels are empty and the lithium-donor density is equal to the carrier density. There was no observed loss of lithium measured at room temperature after bombardment at $T_B = 79°K$ as indicated in Figure I-10. The same calculation for the data after irradiation at $T_B = 250°K$ yields 9.5×10^{14} cm^{-3} based on data of curve III in Figure I-10. The identification of these defects is uncertain because of the diffuse nature of this level and the fact that the energy of the level is less than the value for the A-center. However the loss of lithium can be compared to the expected loss based on $-\Delta n/\Delta\Phi = 0.4$ cm^{-1} measured at $T_B = 250°K$. This calculation gives 8×10^{14} defects/cm^3. The observed loss of lithium inferred from the carrier density measured at room temperature was 6×10^{13}Li/cm^3. If lithium forms defect centers at the higher bombardment temperature, then the density is equal to or less than 6×10^{13} defects/cm^3.

After completion of the bombardment, the sample temperature was allowed to increase to 297°K. Two distinct energy levels were observed to occur at 0.17 eV and 0.085 eV below the conduction band, as shown in curve IV and V of Figure I-10. The initial number of defects before interaction by lithium took place was 8 to 9×10^{14} defects/cm^3. Curve IV yields 6.5×10^{14} defects/cm^3 associated with the energy level at 0.17 eV and 2×10^{14} defects associated with the level at 0.085 eV. Thus the total number of defects has not changed after interaction by lithium. The room temperature loss of lithium was 4×10^{13}Li/cm^3.

Curve VII of Figure I-10 shows the carrier density as a function of temperature following the annealing of the sample for 10 minutes to a temperature of 373°K. The total of 8.5×10^{14} cm^{-3} defect centers located at 0.17 eV and 0.085 eV disappeared together with 4.5×10^{14} donors/cm^3 (measured at room temperature) after this annealing process. Approximately 4.6×10^{14} centers/cm^3 located at 0.18 eV remain. Thus, a total of $\approx 4 \times 10^{14}$ defect-centers/cm^3 made up of 2.5×10^{14} A-centers/cm^3 and 2×10^{14} 0.085 eV-centers/cm^3 have been neutralized. The mobility did not recover completely as it did in the low resistivity samples. This is consistent with the residual damage due to the remaining 4.6×10^{14} defects/cm^3. Although the levels are

diffuse and the defect densities are uncertain, the quantitative considerations seem to be consistent with the idea that lithium anneals defects by complexing with them so as to neutralize their electrical effects. If lithium forms defect centers in irradiated low-doping density samples ($\approx 2 \times 10^{15}$ cm^{-3}), then the density of lithium defects after bombardment at $T_B = 250°K$ was less than or equal to 6×10^{13} cm^{-3}. This conclusion is supported by EPR experiments (Ref. I-13) which tentatively identified LiO-V and Li-V damage spectrums in irradiated crucible and zone-silicon samples fabricated from high resistivity silicon and diffused with lithium. The damage spectra were not observed in samples doped with lithium to 2×10^{15} cm^{-3}, but the spectra were observed in the samples doped to densities ranging from 2×10^{16} to 2×10^{17} cm^{-3}.

b. Low Resistivity Crucible Silicon

The total number of carrier removal defects based on the measured $-\Delta n/\Delta\Phi$, and the fluence at each bombardment temperature indicated that 3×10^{15} defects/cm^3 were introduced by the bombardment. Curve II in Figure I-4 shows that $\approx 10^{15}$ A-centers were produced, and a carrier density of $\approx 4 \times 10^{15}$ cm^{-3} measured at room temperature was loss. This implies that $\approx 10^{15}$ lithium defects (LiO-V) were also produced. Curve III indicates that after annealing at room temperature for 174 hrs, a total of $\approx 3 \times 10^{15}$ defects/cm^3 including 2×10^{15} centers/cm^3 located near 0.08 eV remain. This shallow level appears to be the same level observed in the high resistivity sample after annealing at room temperature. However, the level is not as distinct as in the high resistivity sample. The formation of this center required the presence of oxygen and the room-temperature interaction of lithium with carrier-removal centers. The annealing process at 373°K clearly neutralized all defects since the mobility completely recovered. An annealing mechanism which involves the complexing of lithium with defect centers is suggested by these results. All defect centers disappeared after the high temperature annealing. However, residual-defect centers were observed after the same treatment in the high resistivity sample. This latter effect seems to be due to the lower lithium density in this sample.

c. Zone Silicon

Curves of carrier density versus reciprocal temperature shown in Figure I-6 indicate that the energy levels of carrier-removal defects are deep in the forbidden energy gap since moving the Fermi level from close to the conduction band to ≈ 0.2 eV below the band has not revealed any defect levels. The high purity of the initial silicon insures that most of the carrier-removal defects contain lithium. The annealing kinetics of irradiated-zone silicon at room temperature are consistent with the greater lithium diffusion constant in oxygen-lean silicon. They are also consistent with annealing processes accomplished by lithium complexing with the Li-V defect and by the dissociation of Li-V defects. The dissociation of Li-V defects implies that the

oxygen-containing defects (LiO-V) in crucible silicon are more tightly bound than the Li-V defects in zone silicon (Ref. I-18), since the LiO-V complex appeared to be stable at room temperature within the time period of these measurements. A total carrier loss of 10^{16} cm^{-3} in zone silicon immediately after bombardment is indicated by the data in Figure I-6. Two carriers are removed from the conduction band by each Li-V defect. This means that 5×10^{15} LiV-defects/cm^3 were produced by the bombardment based on the assumption that the Li-V defect is the dominant carrier-removal defect. After the sample annealed at 297°K, the carrier density increased by 2.7×10^{15} cm^{-3}. If it is assumed that the number of dissociated Li-V defects is equal to 1/2 the carrier density increase, then the Li-V defect which did not dissociate is equal to 3.6×10^{15} cm^{-3}. Thus, approximately 28 percent of the carrier-removal defects annealed by dissociation and the remainder annealed by lithium interaction.

d. Mobility Changes

Mobility changes in the irradiated silicon are due to the introduction of charged defects which act as scattering centers. The mobility is proportional to the inverse second power of the charge on the scattering center. Thus, the mobility is quite sensitive to doubly charged defects and large changes in mobility are indicative of mulitply-charged defect centers. The ionized-impurity mobility can be calculated from the Brooks-Herring expression (Ref. I-18) given by

$$\mu_I = \frac{2^{7/2} K^2 (kT)^{3/2}}{\pi^{3/2} (m^*)^{1/2} e^3 N_I \left[\ln(1+b) - b/1+b\right]} \qquad \text{(I-4)}$$

where

$$b = \frac{6K m^* (kT)^2}{\pi n k^2 e^2} \qquad \text{(I-5)}$$

and K is the dielectric constant of the material, m* is the density of states effective mass, N_I is the number of ionized impurities, and n is the number of conduction electrons. The total carrier mobility is a combination of the lattice mobility and the ionized-impurity scattering mobility. Expressions have been derived for the relations between lattice, ionized impurity, and conductive mobility. A graph has been computed by Conwell (Ref. I-19) to permit an evaluation of any one of the three if the other two are known. The lattice mobility can be obtained from the work of Logan and Peters (Ref. I-20). Using these procedures, a mobility change was calculated for each zone-silicon sample, and compared to the total-experimental-mobility change. The values of mobility calculated from Equation (I-4) were consistently lower than the experimental values. Calculated values of the mobility decrease varied from 10 to 25

percent for the four samples. Measured value of the Hall-mobility decrease varied from 20 to 40 percent. Agreement would only be possible if the ratio of Hall mobility to conductivity mobility did not change during irradiation. However, the important point to note is the fact that if the centers were doubly ionized, the calculated mobilities would be considerably smaller than the measured values. This calculation indicated that the Li-V defect is a singly charged defect.

E. ACKNOWLEDGEMENTS

The writer wishes to express his indebtedness to W. Leopold for construction of special circuits and devices, to F. Kolondra who operated the Van de Graaff accelerator, to T. Faith for valuable discussions, R. Neadle who carried out the lithium diffusions, and to D. Liebowitz for fabrication of the samples.

LIST OF REFERENCES FOR APPENDIX I

I-1. G. D. Watkins, Conference Report, Toulouse Conference on Radiation Effects in Semiconductor Components, 1, A1-1 (1967).

I-2. G. K. Wertheim, Phys. Rev. 115, 568 (1959); 110, 1272 (1958).

I-3. R. L. Novak, Ph.D. Thesis, University of Pennsylvania, 1964 (unpublished).

I-4. H. J. Stein and F. L. Vook, Phys. Rev. 163, 790 (1967); "Radiation Effects in Semiconductors," Edited by F. L. Vook. (Plenum Publishing Corporation, New York, 1968) p. 115.

I-5. E. M. Pell, Phys. Rev. 119, 1222 (1960).

I-6. J. J. Wysocki, Proc. Sixth Photovoltaic Spec. Conf., IEEE Catalog No. 15C53, Vol. III, 96 (1967).

I-7. G. J. Brucker and B. Markow, 6th Photovoltaic Spec. Conf. III, 53 (1967).

I-8. B. Goldstein, Phys. Rev. Letters 17, 1 (1966).

I-9. F. J. Morin and J. P. Maita, Phys. Rev. 96, 28 (1954).

I-10. H. J. Stein and R. Gereth, J. Appl. Phys. 39, 2890 (1968).

I-11. T. Faith, G. J. Brucker, A. Holmes-Siedle and R. Neadle, IEEE Trans. on Nuclear Science NS-15, (6), (1968).

I-12. P. H. Fang, "Lattice Defects in Semiconductors," Edited by R. R. Hasiguh, (University of Tokyo Press, Tokyo, 1966) p. 155.

I-13. B. Goldstein, RCA Final Report, Contract No. F19628-68-C-0133 (1968).

I-14. G. D. Watkins, J. Corbett and R. Walker, J. Appl. Phys. 30, 1198 (1959).

I-15. R. E. Whan and F. L. Vook, Phys. Rev. 153, 814 (1967).

I-16. R. L. Aggarwal, P. Fisher, V. Mourzine, and A. K. Ramdas, Phys. Rev. 138, A882, (1965).

I-17. G. K. Wertheim, Phys. Rev., 105, p. 1730 (1957).

I-18. P. P. Debye and E. M. Conwell, Phys. Rev. 93, 693 (1954).

I-19. E. M. Conwell, Proc. IRE 40, 1327 (1952).

I-20. R. A. Logan and A. J. Peters, J. Appl. Phys. 31, 122 (1960).

APPENDIX C
PERFORMANCE PARAMETERS

PRE- AND POST-IRRADIATION PHOTOVOLTAIC PERFORMANCE OF n/p CONTROL CELLS

Control Cell	(e/cm^2) ϕ	Pre-irradiation			Post-irradiation			Post-irradiation		
		I_o(mA)	P_o(mW)	V_o(mV)	I(mA)	P(mW)	V(mV)	I/I_o	P/P_o	V/V_o
D-1	$1x10^{14}$	68.9	28.2	553	56.0	21.1	516	0.81	0.75	0.93
D-2	$1x10^{14}$	69.5	28.0	555	56.0	21.1	520	0.81	0.76	0.94
D-3	$1x10^{14}$	71.0	28.4	552	58.3	21.7	518	0 82	0.77	0.93
D-4	$1x10^{14}$	69.1	27.7	553	57.0	21.3	518	0.83	0.77	0.93
D-5	$5x10^{14}$	69.0	28.1	557	48.6	17.7	503	0.71	0.63	0.90
D-6	$5x10^{14}$	73.0	28.2	555	50.1	17.6	500	0.69	0.62	0.90
D-7	$\approx 8x10^{14}$*	69.3	28.6	557	47.7	16.9	487	0.69	0.59	0.87
D-8	$\approx 8x10^{14}$*	71.0	28.1	350	16.5	16.2	487	0.66	0.58	0.88
D-9	$3x10^{15}$	67.3	27.9	551	39.5	13.6	471	0.59	0.49	0.85
D-10	$3x10^{15}$	69.0	28.6	551	40.6	14.0	471	0.59	0.49	0.85
D-11	$3x10^{15}$	68.1	27.7	550	40.5	13.9	471	0.59	0.50	0.86
D-12	$3x10^{15}$	72.0	29.3	555	40.8	13.9	471	0.57	0.47	0.85
D-13	$5x10^{14}$	69.2	27.3	548	50 1	17.9	497	0.72	0.66	0.91
D-14	$5x10^{14}$	67.2	27.4	554	48.4	17.6	500	0.72	0.64	0.90

* ≈0.7 MeV electron

GROUPING, IRRADIATION SCHEDULE, PROCESS PARAMETERS, AND LITHIUM CONCENTRATIONS OF C1 AND H1 CELLS

Cell Group	Number of Cells	(e/cm^2) ϕ	Li diffusion		Li redistribution		Li concentration		(μ m) L_o
			Temp(°C)	Time(Min)	Temp(°C)	Time(Min)	$N_{LO}(cm^{-3})$	$dN_L/dw(cm^{-4})$	
C1(1)	8	$1x10^{14}$	450	5	450	40	$<10^{14}$	$1x10^{18}$	110
C1(2)	2	$\approx 8x10^{14}$*	450	5	450	40	$<10^{14}$	$1x10^{18}$	130
H1(1)	8	$1x10^{14}$	425	90	425	60	$5x10^{14}$	$2x10^{19}$	30
H1(2)	2	$\approx 8x10^{14}$*	425	90	425	60	$5x10^{14}$	$2x10^{19}$	20

* ≈0.7 MeV electrons

GROUPING, IRRADIATION SCHEDULE, PROCESS PARAMETERS, AND LITHIUM CONCENTRATIONS OF C2, H2, AND T2 CELLS

Cell Group	Number of Cells	ϕ (e/cm^2)	Li Diffusion		Li Redistribution		Li Concentration		L_o (μm)
			Temp(°C)	Time(Min)	Temp(°C)	Time(Min)	$N_{LO}(cm^{-3})$	$dN_L/dw(cm^{-4})$	
C2(1)	5	$1x10^{14}$	425	90	425	120	wide range	1.4×10^{18}	80
C2(2)	2	$5x10^{14}$	425	90	425	120	wide range	1.4×10^{18}	80
C2(3)	3	$3x10^{15}$	425	90	425	120	wide range	1.4×10^{18}	80
H2(1)	5	$1x10^{14}$	425	90	425	60	$5x10^{14}$	$1x10^{19}$	40
H2(2)	2	$5x10^{14}$	425	90	425	60	$5x10^{14}$	$1x10^{19}$	40
H2(3)	3	$3x10^{15}$	425	90	425	60	$5x10^{14}$	$1x10^{19}$	40
T2(1)	6	$1x10^{14}$	400	90	400	120	$2x10^{14}$	$1x10^{18}$	90
T2(2)	2	$5x10^{14}$	400	90	400	120	$2x10^{14}$	$1x10^{18}$	90
T2(3)	2	$3x10^{15}$	400	90	400	120	$2x10^{14}$	$1x10^{18}$	90

GROUPING, IRRADIATION SCHEDULE, PROCESS PARAMETERS, AND LITHIUM CONCENTRATIONS OF T3 AND H4 CELLS

Cell Group	Number of Cells	(e/cm^2) ϕ	Li Diffusion		Li Redistribution		Li Concentration		(μm) L_o
			Temp(°C)	Time(Min)	Temp(°C)	Time(Min)	$N_{LO}(cm^{-3})$	$dN_L/dw(cm^{-4})$	
T3(1)	3	$1x10^{14}$	400	90	0	0	$3x10^{15}$	$1x10^{20}$	80
T3(2)	3	$\approx 8x10^{14}$*	400	90	0	0	$3x10^{15}$	$1x10^{20}$	80
T3(3)	3	$3x10^{15}$	400	90	0	0	$3x10^{15}$	$1x10^{20}$	80
H4(1)	2	$1x10^{14}$	425	90	425	60	$1x10^{15}$	$3x10^{19}$	30
H4(2)	3	$\approx 8x10^{14}$*	425	90	425	60	$1x10^{15}$	$3x10^{19}$	30

*Electron energy: approx. 0.7MeV

PRE- AND POST-IRRADIATION PHOTOVOLTAIC PERFORMANCE OF H4 CELLS

Cell Group	ϕ (e/cm²)	Pre-irradiation			Post-irradiation			3 Days			6 Days			11 Days		
		I_o(mA)	P_o(mW)	V_o(mV)	I/I_o	P/P_o	V/V_o	I/I_o	P/P_o	V/V_o	I/I_o	P/P_o	V/V_o	I/I_o	P/P_o	V/V_o
H4(1)	$1x10^{14}$	47.0	18.8	545	0.91	0.88	0.97	0.97	0.93	1.00	-	-	-	-	-	-
H4(2)	$\sim 8x10^{14}$	47.5	16.1	534	0.80	0.63	0.89	-	-	-	-	-	-	-	-	-

GROUPING, IRRADIATION SCHEDULE, PROCESS PARAMETERS, AND LITHIUM CONCENTRATIONS OF C4 CELLS

Batch	Group	Number of Cells	Cell Numbers	(e/cm²)	Li Diffusion		Li Redistribution		Li Concentration		(μm)
				ϕ	Temp(°C)	Time(Min)	Temp(°C)	Time(Min)	$N_{LO}(cm^{-3})$	$dN_L/dw(cm^{-4})$	L_o
I	C4(1)	4	C4-1 to C4-4	$1x10^{14}$	425	90	none	none	$3x10^{15}$	$5x10^{19}$	15
	(2)	3	C4-5 to C4-7	$5x10^{14}$	425	90	none	none	$3x10^{15}$	$5x10^{19}$	15
	(3)	3	C4-8 to C4-10	$3x10^{15}$	425	90	none	none	$3x10^{15}$	$5x10^{19}$	15
	(4)	2	C4-11 & C4-12	0	425	90	none	none	$3x10^{15}$	$5x10^{19}$	15
II	(5)	4	C4-13 to C4-16	$1x10^{14}$	425	90	425	60	$2x10^{15}$	$2x10^{19}$	20
	(6)	3	C4-17 to C4-19	$5x10^{14}$	425	90	425	60	$2x10^{15}$	$2x10^{19}$	20
	(7)	3	C4-20 to C4-22	$3x10^{15}$	425	90	425	60	$2x10^{15}$	$2x10^{19}$	20
	(8)	2	C4-23 & C4-24	0	425	90	425	60	$2x10^{15}$	$2x10^{19}$	20
III	(9)	4	C4-25 to C4-28	$1x10^{14}$	425	90	425	120	$2x10^{14}$	$1x10^{18}$	40
	(10)	3	C4-29 to C4-31	$5x10^{14}$	425	90	425	120	$2x10^{14}$	$1x10^{18}$	40
	(11)	3	C4-32 to C4-34	$3x10^{15}$	425	90	425	120	$2x10^{14}$	$1x10^{18}$	40
	(12)	2	C4-35 & C4-36	0	425	90	425	120	$2x10^{14}$	$1x10^{18}$	40
IV	(13)	4	C4-37 to C4-40	$1x10^{14}$	450	40	none	none	$2x10^{15}$	$2x10^{19}$	15
	(14)	3	C4-41 to C4-43	$5x10^{14}$	450	40	none	none	$2x10^{15}$	$2x10^{19}$	15
	(15)	3	C4-44 to C4-46	$3x10^{15}$	450	40	none	none	$2x10^{15}$	$2x10^{19}$	15
	(16)	2	C4-47 & C4-48	0	450	40	none	none	$2x10^{15}$	$2x10^{19}$	15
V	(17)	4	C4-49 to C4-52	$1x10^{14}$	450	40	450	80	$3x10^{14}$	$1x10^{18}$	30
	(18)	3	C4-53 to C4-55	$5x10^{14}$	450	40	450	80	$3x10^{14}$	$1x10^{18}$	30
	(19)	3	C4-56 to C4-58	$3x10^{15}$	450	40	450	80	$3x10^{14}$	$1x10^{18}$	30
	(20)	2	C4-59 & C4-60	0	450	40	450	80	$3x10^{14}$	$1x10^{18}$	30

PRE- AND POST-IRRADIATION PHOTOVOLTAIC PERFORMANCE OF C4 CELLS

Group	ϕ (e/cm^2)	Pre-irradiation			Post-irradiation			150 Min			3 Days			6 Days			11 Days		
		I_o(mA)	P_o(mW)	V_o(mV)	I/I_o	P/P_o	V/V_o	I/I_o	P/P_o	V/V_o	I/I_o	P/P_o	V/V_o	I/I_o	P/P_o	V/V_o	I/I_o	P/P_o	V/V_o
								Batch I											
C4(1)	1×10^{14}	39.1	15.8	537	0.92	0.90	0.98	-	-	-	0.97	0.97	0.99	0.97*	0.97*	1.00*	0.97	0.96	0.98
(2)	5×10^{14}	40.2	15.8	539	0.83	0.77	0.94	-	-	-	0.96	0.87	0.98	-	-	-	0.96	0.92	0.98
(3)	3×10^{15}	39.1	15.3	532	0.71	0.59	0.88	0.84	0.71	0.89	0.97	0.85	0.92	0.97*	0.84*	0.91*	0.97	0.86	0.93
(4)	0	40.3	15.7	539	-	-	-	-	-	-	-	-	-	-	-	-	-	-	-
								Batch II											
(5)	1×10^{14}	44.3	17.7	534	0.90	0.86	0.96	-	-	-	0.99	0.98	0.99	0.98*	0.98*	0.99*	0.99	0.98	0.99
(6)	5×10^{14}	45.4	17.5	531	0.77	0.69	0.91	-	-	-	0.99	0.95	0.98	0.99*	0.96*	0.98*	0.99	0.96	0.98
(7)	3×10^{15}	44.9	17.7	531	0.59	0.46	0.84	0.74	0.51	0.84	0.94	0.72	0.87	-	-	-	0.99	0.75	0.88
(8)	0	46.2	17.7	532	-	-	-	-	-	-	-	-	-	-	-	-	-	-	-
								Batch III											
(9)	1×10^{14}	54.5	21.1	532	0.83	0.79	0.95	-	-	-	0.96	0.97	0.99	0.98	0.98	0.99	1.00	0.98	0.99
(10)	5×10^{14}	55.2	20.3	538	0.69	0.60	0.86	-	-	-	0.95	0.83	0.94	0.99	0.86	0.94	1.00	0.86	0.94
**(11)	3×10^{15}	54.7	19.1	538	0.59	0.38	0.77	0.61	0.38	0.77	0.73	0.34	0.77	0.78	0.32	0.77	0.81	0.29	0.77
(12)	0	55.3	19.9	537	-	-	-	-	-	-	-	-	-	-	-	-	-	-	-
								Batch IV											
(13)	1×10^{14}	38.8	15.0	525	0.93	0.91	0.98	-	-	-	0.98	0.96	0.99	0.99*	0.98*	0.99*	0.99	0.96	0.99
(14)	5×10^{14}	38.9	15.3	527	0.89	0.82	0.95	-	-	-	0.98	0.93	0.99	0.97*	0.93*	0.98*	0.99	0.95	0.99
(15)	3×10^{15}	38.7	15.1	517	0.74	0.63	0.89	1.84	0.72	0.89	0.97	0.86	0.94	-	-	-	1.00	0.89	0.95
(16)	0	39.0	14.3	526	-	-	-	-	-	-	-	-	-	-	-	-	-	-	-
								Batch V											
(17)	1×10^{14}	51.7	19.6	528	0.85	0.82	0.95	-	-	-	1.00	0.99	0.99	1.00	0.99	0.99	1.00	0.99	0.99
(18)	5×10^{14}	53.1	20.8	535	0.70	0.61	0.88	-	-	-	0.97	0.90	0.95	0.99	0.91	0.96	1.00	0.92	0.96
(19)	3×10^{15}	50.5	20.0	530	0.60	0.43	0.81	0.62	0.44	0.81	0.85	0.57	0.82	0.90	0.58	0.83	0.95	0.60	0.83
(20)	0	53.4	21.4	532	-	-	-	-	-	-	-	-	-	-	-	-	-	-	-

*Only one cell measured
**High series resistance

LIST OF CELLS RECEIVED IN SHIPMENT NO. 4

Cell I.D. No.	Quantity	Crystal Type	Diff. Time (Minutes)	Redist. Time (Minutes)	Temp. (°C)
C5-11 thru C5-20	10	Crucible	40	0	450
C5-41 thru C5-50	10	F Z	40	0	450
C5-71 thru C5-80	10	Crucible	90	120	425
C5-101 thru C5-110	10	F.Z.	90	120	425

Mfr.	Lot No.	Quantity	I.D. Prefix	Crystal Type	p (ohm-cm)	Dopant	Diff. Time (min)	Redist. Time (min.)	Temp. (°C)
T.I.	4	10	T4-	F. Z.	>50	Phos.	90	0	400
Heliotek	5	10	H5-	F. Z.	≈20	Phos.	90	60	350
Heliotek	6	10	H6-	Crucible	≈20	Phos.	90	60	450
T.I.	5	10	T5-	Lopex	≈50	Phos.	90	0	400
T.I.	6	10	T6-	Lopex	≥50	Phos.	480	0	325
T.I.	7	10	T7-	Crucible	≥20	Phos.	480	0	325

INITIAL PERFORMANCE PARAMETERS OF CELLS RECEIVED IN SHIPMENT NO. 4

Cell	I (mA)	V (mV)	Cell	I (mA)	V (mV)	Cell	I (mA)	V (mV)
T4-11	55.5	585	C5-75	68.7	585	H6-24	63.5	581
12	55.2	583	76	69.0	590	H6-30	63.7	585
13	54.6	580	77	69.9	584	T6-11	70.2	588
14	56.5	570	78	71.2	588	12	69.0	600
15	55.4	585	79	70.7	592	13	68.3	592
16	56.9	583	80	71.5	593	14	69.3	595
17	57.7	570	101	56.2	545	15	70.7	573
18	53.3	575	102	57.2	535	16	68 7	596
19	564	578	103	56.0	539	17	68.4	591
20	56.4	575	104	59.4	539	18	68.8	591
C5-11	57.0	603	105	59.5	536	19	69.7	592
12	56.9	601	106	55.8	531	20	69.1	595
13	56.8	593	107	52.8	534	T7-11	70.6	580
14	57.0	594	108	53.7	542	12	73.8	591
15	59.1	599	109	59.6	540	13	68.2	590
16	58.4	600	110	60.6	537	14	68.0	583
17	58.2	596	H5-13	63.1	562	15	73.3	580
18	57.0	600	15	64.7	560	16	70.3	580
19	57.5	593	18	74.0	560	17	72.2	590
20	54.5	597	20	70.2	560	18	70.1	594
41	47.2	560	21	73.4	557	19	69.3	578
42	44.2	560	00	73.3	552	20	70.0	584
43	44.4	552	01	72.7	560	T5-11	60.7	594
44	38.7	538	02	77.4	555	12	57.5	601
45	41.0	542	04	78.0	555	13	58.5	596
46	46.3	560	11	73.3	557	14	56.1	591
47	39.4	539	H6-21	48.0	544	15	55.1	596
48	43.2	560	22	49.0	546	16	54.2	601
49	44.8	553	28	49.4	542	17	54.9	590
50	44.7	561	30	48.5	550	18	57.9	596
71	70.0	593	36	50.1	548	19	55.8	600
72	72.1	596	27	57.4	566	20	55.3	595
73	73.4	597	19	52.3	560			
74	64.7	577	43	63.4	589			

INITIAL PERFORMANCE PARAMETERS FOR CELLS FABRICATED IN-HOUSE

Lopex				Float Zone				Quartz Crucible			
Sample No.	N_{LO} ($cm^{-3} \times 10^{-14}$)	N_{LB} ($cm^{-3} \times 10^{-16}$)	L_O (microns)	Sample No.	N_{LO} ($cm^{-3} \times 10^{-14}$)	N_{LB} ($cm^{-3} \times 10^{-16}$)	L_O (microns)	Sample No.	N_{LO} ($cm^{-3} \times 10^{-14}$)	N_{LB} ($cm^{-3} \times 10^{-16}$)	L_O (microns)
10 Ω-cm				1 Ω-cm				12 to 16 Ω-cm			
A-1-2	7.0	1.0	119	D-1-1		1.8	94	G-1-1	7.5	2.0	40
A-1-4	5.1	1.0	128	D-1-2		1.8	71	G-1-2	7.5	1.9	41
A-2-1	1.0	0.3	83	D-1-3		1.5	72	G-1-5	4.0	1.3	50
A-2-2	1.3	0.3	85	D-1-4		1.5	60	G-2-1	5.5	1.8	33
A-2-3	1.9	0.3	90	D-2-1		1.0	87	G-2-2	5.7	1.8	37
A-3-1	9.0	2.0	118	D-2-2		1.0	86	G-2-3	5.5	1.8	34
A-3-2		2.0	109	D-2-3		1.2	86	G-2-4	5.5	1.8	27
A-3-3	7.8	2.0	109	D-2-4		1.2	99	G-2-5	5.5	1.8	41
A-4-1	13	2.0	132	D-1-6C	0	0	66	G-1-6C	0	0	33
A-4-2	8.5	2.0	109	D-1-7CA	0	0	53	G-1-7C	0	0	33
A-4-3	7.5	2.0	112	D-1-8CA	0	0	65	G-2-6C	0	0	63
A-4-4	7.2	2.0	93	D-2-6C	0	0	50	G-2-7C	0	0	50
A-5-1	9.4	2.0	94	D-2-7CA	0	0	53				
A-5-2	10	2.0	72	D-2-8CA	0	0	46				
A-5-3	8.5	2.0	116	10 Ω-cm							
A-2-4C	0	0	47	E-1-1	5.6	1.5	100				
A-3-7CA	0	0	45	E-1-2	4.4	1.0	94				
A-4-7CA	0	0	55	E-1-3	<.5	1.5	67				
A-5-7CA	0	0	29	E-1-4		0.9	55				
1 Ω-cm				E-2-1	3.0	1.0	129				
B-1-2		1.5	105	E-2-2	1.5	1.0	96				
B-2-1		1.3	141	E-2-3	2.5	1.0	83				
B-2-2		1.3	125	E-2-4		1.0	102				
B-3-1		1.3	100	E-1-6C	.0	0	62				
B-3-2		1.5	97	E-1-7CA	0	0	42				
B-1-7CA	0	0	23	E-1-8CA	0	0	38				
B-2-7CA	0	0	30	E-2-6C	0	0	29				
30 Ω-cm				E-2-7CA	0	0	33				
C-1-5	9.0	1.5	131	E-2-8CA	0	0	33				
C-1-7	16	3.5	120	30 Ω-cm							
C-2-1	3.0	1.5	100	F-1-1	3.2	1.0	104				
C-2-2	3.2	1.1	94	F-1-2	3.5	1.0	97				
C-2-3		1.5	95	F-1-3	1.3	1.0	75				
C-2-4	3.0	1.5	97	F-1-4	3.5	1.0	97				
C-2-5		1.7	84	F-2-1	1.4	1.0	79				
C-3-2	2.3	1.5	76	F-2-2	1.0	0.9	69				
C-3-3		1.7	72	F-2-3	1.5	1.0	32				
C-3-4		1.6	83	F-2-4	2.5	1.0	68				
C-4-1	4.4	1.0	57	F-1-6C	0	0	39				
C-4-2		1.1	58	F-1-7CA	0	0	42				
C-4-3	3.0	1.1	64	F-1-8CA	0	0	47				
C-4-4	4.1	1.5	61	F-2-6C	0	0	32				
C-4-5	5.4	1.7	57	F-2-7CA	0	0	32				
C-2-6C	0	0	55	F-2-8CA	0	0	31				
C-2-7C	0	0	52								
C-2-8C	0	0	39								
C-3-6C	0	0	57								
C-3-7C	0	0	53								
C-4-6C	0	0	32								
C-4-7C	0	0	37								

INITIAL PERFORMANCE PARAMETERS FOR GFE CELLS PROVIDED DURING PRESENT YEAR

Cell	P_O (Ω-cm)	Gr. Meth.	L_o (microns)	J_{sc} (mA/cm^2)	V_{oc} (volts)	P_{max} (mW/cm^2)	N_{Lo} (cm^{-3} x 10^{-14})
TI948	20	FZ	90	33.7	.571	13.3	11
949	20	FZ	89	32.6	.569	12.9	9.5
950	20	FZ	77	32.9	.570	13.0	13
951	20	FZ	76	32.2	.568	12.7	14
952	20	FZ	91	33.0	.564	12.6	9.5
976	200	Lopex	100	32.0	.568	12.1	16
977	200	Lopex	100	34.3	.554	12.0	15
978	200	Lopex	100	34.5	.574	13.4	18
979	200	Lopex	122	32.4	.569	11.8	11
981	200	Lopex	121	35.5	.562	12.4	9.5
He651	20	Lopex	33	26.3	.535	9.8	15
670	20	Lopex	41	27.7	.545	10.8	17
673	20	Lopex	25	24.3	.522	8.8	17
676	20	Lopex	31	25.9	.519	9.1	20
694	20	Lopex	29	25.8	.525	9.4	13
796	20	FZ	29	26.0	.525	9.5	8.9
798	20	FZ	40	27.6	.518	10.4	7.7
808	20	FZ	30	26.4	.532	9.6	7.1
810	20	FZ	39	27.9	.532	9.6	7.1
815	20	FZ	42	28.3	.535	11.0	17
866	20	FZ	42	29.0	.532	10.8	7.7
867	20	FZ	39	28.6	.523	10.7	4.7
868	20	FZ	31	26.5	.527	9.9	8.3
870	20	FZ	41	28.0	.525	10.5	7.1
871	20	FZ	51	29.6	.540	11.2	7.1
872	20	FZ	31	28.0	.535	10.6	5.9
873	20	FZ	44	29.0	.544	11.6	7.1
875	20	FZ	37	28.1	.531	10.7	8.5
876	20	FZ	34	27.6	.523	9.2	8.8
878	20	FZ	36	28.3	.532	11.1	7.3
879	20	FZ	44	30.1	.542	11.9	7.0
881	20	FZ	48	29.6	.539	11.2	9.7
882	20	FZ	51	29.6	.532	11.4	8.3
884	20	FZ	53	30.2	.530	10.8	9.0
885	20	FZ	46	28.9	.530	10.9	7.5
886	20	FZ	45	29.1	.528	10.7	7.6
887	20	FZ	58	30.6	.527	10.8	5.0
890	20	FZ	34	26.4	.527	9.9	8.3
891	20	FZ	51	29.5	.535	11.3	7.5
892	20	FZ	44	28.9	.532	11.0	10

INITIAL PERFORMANCE PARAMETERS FOR GFE CELLS PROVIDED IN PREVIOUS YEAR AND MONITORED DURING PREVIOUS YEAR

Cell	P_o (Ω-cm)	Gr. Meth	L_o (microns)	J_{sc} (mA/cm^2)	V_{oc} (volts)	P_{max} (mW/cm^2)	N_{Lo} (cm^{-3} x 10^{-14})
Ho5-1	100	FZ	33	24.7	.500	7.7	
6-1	1000	FZ	39	23.3	.514	6.4	
33-2	10	FZ	26	24.4	.500	6.6	
He55-1	20	FZ	51	29.2	.553	9.2	
248P	1000	FZ	25	24.8	.530	8.4	-
249P	1000	FZ	26	24.2	.543	8.4	-
340	100	FZ	74	28.6	-	-	22
341	100	FZ	57	28.5	-	-	17
342	100	FZ	62	29.6	-	-	12
TH42	20	FZ	89	28.6	.578	9.2	22
63	20	FZ	110	29.6	.582	10.4	15
71	20	FZ	112	28.5	.534	6.3	17
112	20	Q.C.	54	28.0	.586	10.5	20
113	20	Q.C.	54	27.5	.578	9.9	20
127	20	LOPEX	72	30.2	.580	10.2	82
128	20	LOPEX	78	28.5	.594	10.8	70
132	20	LOPEX	78	29.8	-	-	92
161	20	FZ	45	27.2	.584	10.8	50
166	20	FZ	33	25.2	.570	8.7	-
167	20	FZ	84	30.8	.568	10.8	7.5
168	20	FZ	58	28.8	.580	11.1	20

RCA | Defense Electronic Products | Astro Electronics Division | Princeton, New Jersey